

Rational design, synthesis and 2D-QSAR studies of antiproliferative tropane-based compounds

Nasser S. M. Ismail,^{*a,b} Riham F. George,^c Rabah A. T. Serya,^b Fady N. Baselious,^d May El-Manawaty,^e ElSayed M. Shalaby,^f Adel S. Girgis^{*g}

^a Pharmaceutical Chemistry Department, Faculty of Pharmaceutical Sciences and Pharmaceutical Industries, Future University, Cairo 12311, Egypt.

^b Pharmaceutical Chemistry Department, Faculty of Pharmacy, Ain Shams University, Cairo, Egypt.

^c Pharmaceutical Chemistry Department, Faculty of Pharmacy, Cairo University, Cairo, Egypt.

^d Research and Development Department, Global Napi Pharmaceuticals, 6th October City, Giza, Egypt.

^e Pharmacognosy Department, National Research Centre, Dokki, Giza 12622, Egypt.

^f X-Ray Crystallography Lab., Physics Division, National Research Centre, Dokki, Giza 12622, Egypt.

^g Pesticide Chemistry Department, National Research Centre, Dokki, Giza 12622, Egypt.

* Corresponding authors, E-mail: saadnasser2003@yahoo.com (Nasser S. M. Ismail), girgisas10@yahoo.com (Adel S. Girgis).

Supporting information

Table titles

Table S1. Experimental and optimized intramolecular geometrical parameters (bond lengths, Å) of compound **14a**.

Table S2. Experimental and optimized intramolecular geometrical parameters (bond angles, °) of compound **14a**.

Table S3. Molecular descriptor values of the BMLR-QSAR model for the antitumor tropane containing-compounds (**12a–f**, **14a–i,k–o,q–s** and **16a,b**) according to the BMLR-QSAR model due to MCF7 (breast) carcinoma cell line.

Table S4. Descriptor of the BMLR-QSAR model for the subset group (A+B) against MCF7 (breast) carcinoma cell line.

Table S5. Observed and estimated/predicted activity values for the subset group (A+B) antitumor active agents according to the (A+B)-QSAR model due to MCF7 (breast) carcinoma cell line.

Table S6. Observed and estimated/predicted activity values for the subset group (C, as an external test set) according to the (A+B)-QSAR model due to MCF7 (breast) carcinoma cell line.

Table S7. Descriptor of the BMLR-QSAR model for the subset group (A+C) against MCF7 (breast) carcinoma cell line.

Table S8. Observed and estimated/predicted activity values for the subset group (A+C) antitumor active agents according to the (A+C)-QSAR model due to MCF7 (breast) carcinoma cell line.

Table S9. Observed and estimated/predicted activity values for the subset group (B, as an external test set) according to the (A+C)-QSAR model due to MCF7 (breast) carcinoma cell line.

Table S10. Descriptor of the BMLR-QSAR model for the subset group (B+C) against MCF7 (breast) carcinoma cell line.

Table S11. Observed and estimated/predicted activity values for the subset group (B+C) antitumor active agents according to the (B+C)-QSAR model due to MCF7 (breast) carcinoma cell line.

Table S12. Observed and estimated/predicted activity values for the subset group (A, as an external test set) according to the (B+C)-QSAR model due to MCF7 (breast) carcinoma cell line.

Table S13. Crystal data and structure refinement parameters of compound **14a**.

Figure captions

Fig. S1. IR spectrum of compound **12f** (KBr pellet).

Fig. S2. ^1H -NMR spectrum of compound **12f** in CDCl_3 .

Fig. S3. ^{13}C -NMR spectrum of compound **12f** in CDCl_3 .

Fig. S4. IR spectrum of compound **14a** (KBr pellet).

- Fig. S5.** ^1H -NMR spectrum of compound **14a** in CDCl_3 .
- Fig. S6.** ^1H , ^1H -COSY spectrum of compound **14a** in CDCl_3 .
- Fig. S7.** ^{13}C -NMR spectrum of compound **14a** in CDCl_3 .
- Fig. S8.** ^1H , ^{13}C -Heteronuclear Single Quantum Coherence (HSQC) spectrum of compound **14a** in CDCl_3 .
- Fig. S9.** IR spectrum of compound **14b** (KBr pellet).
- Fig. S10.** ^1H -NMR spectrum of compound **14b** in CDCl_3 .
- Fig. S11.** ^{13}C -NMR spectrum of compound **14b** in CDCl_3 .
- Fig. S12.** IR spectrum of compound **14c** (KBr pellet).
- Fig. S13.** ^1H -NMR spectrum of compound **14c** in CDCl_3 .
- Fig. S14.** ^{13}C -NMR spectrum of compound **14c** in CDCl_3 .
- Fig. S15.** IR spectrum of compound **14d** (KBr pellet).
- Fig. S16.** ^1H -NMR spectrum of compound **14d** in CDCl_3 .
- Fig. S17.** ^{13}C -NMR spectrum of compound **14d** in CDCl_3 .
- Fig. S18.** IR spectrum of compound **14e** (KBr pellet).
- Fig. S19.** ^1H -NMR spectrum of compound **14e** in CDCl_3 .
- Fig. S20.** ^{13}C -NMR spectrum of compound **14e** in CDCl_3 .
- Fig. S21.** IR spectrum of compound **14f** (KBr pellet).
- Fig. S22.** ^1H -NMR spectrum of compound **14f** in CDCl_3 .
- Fig. S23.** ^{13}C -NMR spectrum of compound **14f** in CDCl_3 .
- Fig. S24.** IR spectrum of compound **14g** (KBr pellet).
- Fig. S25.** ^1H -NMR spectrum of compound **14g** in CDCl_3 .
- Fig. S26.** ^{13}C -NMR spectrum of compound **14g** in CDCl_3 .
- Fig. S27.** IR spectrum of compound **14h** (KBr pellet).
- Fig. S28.** ^1H -NMR spectrum of compound **14h** in CDCl_3 .
- Fig. S29.** ^{13}C -NMR spectrum of compound **14h** in CDCl_3 .
- Fig. S30.** IR spectrum of compound **14i** (KBr pellet).
- Fig. S31.** ^1H -NMR spectrum of compound **14i** in CDCl_3 .
- Fig. S32.** ^{13}C -NMR spectrum of compound **14i** in CDCl_3 .
- Fig. S33.** IR spectrum of compound **14j** (KBr pellet).
- Fig. S34.** ^1H -NMR spectrum of compound **14j** in CDCl_3 .

Fig. S35. ^{13}C -NMR spectrum of compound **14j** in CDCl_3 .

Fig. S36. IR spectrum of compound **14k** (KBr pellet).

Fig. S37. ^1H -NMR spectrum of compound **14k** in CDCl_3 .

Fig. S38. ^{13}C -NMR spectrum of compound **14k** in CDCl_3 .

Fig. S39. IR spectrum of compound **14l** (KBr pellet).

Fig. S40. ^1H -NMR spectrum of compound **14l** in CDCl_3 .

Fig. S41. ^{13}C -NMR spectrum of compound **14l** in CDCl_3 .

Fig. S42. IR spectrum of compound **14m** (KBr pellet).

Fig. S43. ^1H -NMR spectrum of compound **14m** in CDCl_3 .

Fig. S44. ^{13}C -NMR spectrum of compound **14m** in CDCl_3 .

Fig. S45. IR spectrum of compound **14n** (KBr pellet).

Fig. S46. ^1H -NMR spectrum of compound **14n** in CDCl_3 .

Fig. S47. ^{13}C -NMR spectrum of compound **14n** in CDCl_3 .

Fig. S48. IR spectrum of compound **14o** (KBr pellet).

Fig. S49. ^1H -NMR spectrum of compound **14o** in CDCl_3 .

Fig. S50. ^{13}C -NMR spectrum of compound **14o** in CDCl_3 .

Fig. S51. IR spectrum of compound **14p** (KBr pellet).

Fig. S52. ^1H -NMR spectrum of compound **14p** in CDCl_3 .

Fig. S53. ^{13}C -NMR spectrum of compound **14p** in CDCl_3 .

Fig. S54. IR spectrum of compound **14q** (KBr pellet).

Fig. S55. ^1H -NMR spectrum of compound **14q** in CDCl_3 .

Fig. S56. ^{13}C -NMR spectrum of compound **14q** in CDCl_3 .

Fig. S57. IR spectrum of compound **14r** (KBr pellet).

Fig. S58. ^1H -NMR spectrum of compound **14r** in CDCl_3 .

Fig. S59. ^{13}C -NMR spectrum of compound **14r** in CDCl_3 .

Fig. S60. IR spectrum of compound **14s** (KBr pellet).

Fig. S61. ^1H -NMR spectrum of compound **14s** in CDCl_3 .

Fig. S62. ^{13}C -NMR spectrum of compound **14s** in CDCl_3 .

Fig. S63. IR spectrum of compound **16a** (KBr pellet).

Fig. S64. ^1H -NMR spectrum of compound **16a** in CDCl_3 .

Fig. S65. ^{13}C -NMR spectrum of compound **16a** in CDCl_3 .

Fig. S66. ^1H -NMR spectrum of compound **16b** in CDCl_3 .

Fig. S67. ^1H -NMR spectrum of compound **16b** in CDCl_3 .

Fig. S68. ^{13}C -NMR spectrum of compound **16b** in CDCl_3 .

Fig. S69. A projection of the optimized structure of compound **14a** by semi-empirical AM1.

Fig. S70. A projection of the optimized structure of compound **14a** by semi-empirical PM3.

Fig. S71. A projection of the optimized structure of compound **14a** by DFT/B3LYP with 6-31G(d,p) level of theory.

Fig. S72. Overlay diagram of **14a**; red (X-ray structure), green (AM1), blue (PM3) and yellow (DFT).

Fig. S73. Dose-response curve of the tropane containing-compounds against HepG2 (liver cancer) cell line.

Fig. S74. Dose-response curve of the tropane containing-compounds against MCF7 (breast cancer) cell line.

Fig. S75. BMLR-QSAR model plot of correlations representing the observed *versus* predicted $\log(\text{IC}_{50}, \mu\text{M})$ values for the subset group (A+B) against MCF7 (beast) carcinoma cell line.

Fig. S76. BMLR-QSAR model plot of correlations representing the observed *versus* predicted $\log(\text{IC}_{50}, \mu\text{M})$ values for the subset group (A+C) against MCF7 (beast) carcinoma cell line.

Fig. S77. BMLR-QSAR model plot of correlations representing the observed *versus* predicted $\log(\text{IC}_{50}, \mu\text{M})$ values for the subset group (B+C) against MCF7 (beast) carcinoma cell line (compound **16a** is an outlier).

Table S1. Experimental and optimized intramolecular geometrical parameters (bond lengths, Å) of compound **14a**.

Geometric parameters	Exp. X-ray	AM1	PM3	DFT
N1—N2	1.409	1.360	1.415	1.388
N1—C17	1.489	1.509	1.534	1.488
N1—C26	1.410	1.425	1.452	1.408
N2—C3	1.289	1.320	1.308	1.290
C3—C4	1.466	1.463	1.467	1.463
C3—C16	1.499	1.535	1.518	1.511
C4—C5	1.348	1.341	1.342	1.352
C4—C12	1.530	1.519	1.513	1.527
C5—C6	1.465	1.456	1.460	1.469
C6—C7	1.385	1.402	1.397	1.409
C6—C11	1.394	1.403	1.402	1.409
C7—C8	1.385	1.394	1.390	1.394
C8—C9	1.380	1.394	1.390	1.396
C9—C10	1.368	1.395	1.392	1.397
C10—C11	1.394	1.393	1.388	1.392
C12—N13	1.491	1.487	1.508	1.483
C12—C25	1.539	1.559	1.5490	1.564
N13—C14	1.474	1.442	1.472	1.461
N13—C15	1.479	1.490	1.509	1.479
C15—C16	1.527	1.535	1.536	1.541
C15—C24	1.527	1.554	1.541	1.559
C16—C17	1.534	1.556	1.544	1.548
C17—C18	1.513	1.498	1.498	1.518
C18—C19	1.372	1.400	1.397	1.400
C18—C23	1.380	1.400	1.396	1.401
C19—C20	1.386	1.394	1.390	1.396
C20—C21	1.363	1.395	1.391	1.395
C21—C22	1.355	1.395	1.391	1.397

C22—C23	1.407	1.394	1.390	1.394
C24—C25	1.536	1.531	1.534	1.555
C26—C27	1.382	1.412	1.399	1.408
C26—C31	1.380	1.414	1.401	1.405
C27—C28	1.387	1.392	1.390	1.390
C28—C29	1.383	1.393	1.390	1.398
C29—C30	1.385	1.394	1.391	1.393
C30—C31	1.381	1.390	1.389	1.396
RMSE	----	0.0213	0.0182	0.0178
Maximum difference	----	0.049	0.045	0.042

Table S2. Experimental and optimized intramolecular geometrical parameters (bond angles, °) of compound **14a**.

Geometric parameters	Exp. X-ray	AM1	PM3	DFT
N2—N1—C17	110.0	111.8	108.8	111.2
N2—N1—C26	115.6	120.4	116.6	116.8
C17—N1—C26	123.0	119.2	120.3	123.0
N1—N2—C3	107.8	110.3	110.7	109.0
N2—C3—C4	124.0	128.0	126.6	125.9
N2—C3—C16	113.7	113.1	113.2	113.3
C4—C3—C16	122.1	118.0	119.7	120.7
C3—C4—C5	120.9	123.0	121.7	121.7
C3—C4—C12	111.2	111.6	111.3	111.6
C5—C4—C12	127.9	125.4	127.0	126.7
C4—C5—C6	129.6	126.3	128.0	129.4
C5—C6—C7	123.0	121.5	123.2	123.8
C5—C6—C11	119.3	119.3	117.8	118.4
C7—C6—C11	117.6	119.2	119.0	117.7
C6—C7—C8	121.5	120.3	120.5	121.0
C7—C8—C9	119.7	120.2	120.2	120.4
C8—C9—C10	120.2	119.8	119.8	119.4
C9—C10—C11	120.0	120.2	120.2	120.2
C6—C11—C10	120.9	120.3	120.4	121.3
C4—C12—N13	108.3	109.2	106.7	108.8
C4—C12—C25	110.0	107.5	109.8	110.6
N13—C12—C25	105.0	105.9	105.1	104.7
C12—N13—C14	110.5	113.5	114.7	113.3
C12—N13—C15	101.6	101.5	102.1	102.8
C14—N13—C15	112.0	113.7	114.9	114.0
N13—C15—C16	104.4	105.1	104.3	103.5
N13—C15—C24	106.2	106.3	105.2	105.7
C16—C15—C24	114.2	111.2	111.8	113.9

C15—C16—C3	109.1	108.7	110.5	110.3
C15—C16—C17	120.7	118.1	116.3	121.8
C3—C16—C17	101.7	101.0	102.2	101.5
C16—C17—N1	100.3	103.3	103.4	100.8
C16—C17—C18	114.0	110.8	114.1	112.5
N1—C17—C18	113.3	116.7	115.7	114.8
C17—C18—C19	119.8	119.2	119.2	119.6
C17—C18—C23	121.0	121.3	121.5	121.4
C19—C18—C23	119.1	119.4	119.3	118.9
C18—C19—C20	120.7	120.2	120.2	120.7
C19—C20—C21	120.1	120.1	120.2	120.0
C20—C21—C22	120.2	119.8	119.9	119.6
C21—C22—C23	120.3	120.2	120.1	120.3
C22—C23—C18	119.5	120.2	120.4	120.4
C15—C24—C25	105.0	104.7	105.1	104.3
C12—C25—C24	103.8	104.1	105.4	103.8
N1—C26—C27	119.2	122.6	122.7	120.0
N1—C26—C31	121.3	118.7	117.3	121.0
C27—C26—C31	119.4	118.6	119.9	118.9
C26—C27—C28	119.7	120.1	119.6	120.1
C27—C28—C29	121.6	120.8	120.5	121.0
C28—C29—C30	117.7	119.4	119.9	118.8
C29—C30—C31	121.3	120.7	120.3	121.0
C30—C31—C26	120.2	120.3	119.8	120.1
RMSE	----	1.97	1.72	0.91
Maximum difference	----	4.8	4.4	2.8

Table S3. Molecular descriptor values of the BMLR-QSAR model for the antitumor tropane containing-compounds (**12a–f**, **14a–i,k–o,q–s** and **16a,b**) according to the BMLR-QSAR model due to MCF7 (breast) carcinoma cell line.

Entry	Compd.	Descriptors ^a				
		<i>D</i> ₁	<i>D</i> ₂	<i>D</i> ₃	<i>D</i> ₄	<i>D</i> ₅
1	12a	39.18	1.85189	2	39.4894	2.34086
2	12b	34.4	1.85545	2	39.4815	2.70299
3	12c	41.2	1.86092	2	39.49	2.46748
4	12d	38.16	1.85388	2	39.4906	1.56057
5	12e	38.62	1.85333	2	39.4905	1.9113
6	12f	37.54	1.84663	4	39.4894	2.34086
7	14a	66.08	1.85358	3	39.405	6.71167
8	14b	64.26	1.85255	3	39.389	5.37492
9	14c	65.92	1.83136	3	39.3765	5.32813
10	14d	65.1	1.8352	3	39.356	3.80648
11	14e	61.38	1.854	3	39.2777	5.22805
12	14f	63.82	1.85281	3	39.2701	5.70906
13	14g	75.52	1.85364	3	39.394	4.68172
14	14h	65.28	1.85022	3	39.3038	5.71779
15	14i	70.86	1.83777	3	39.364	2.84473
16	14k	63.72	1.85216	3	39.2734	5.70906
17	14l	69.26	1.85254	3	39.2764	3.81898
18	14m	63.76	1.8315	3	39.3917	5.05171
19	14n	65.38	1.85365	3	39.3931	5.43618
20	14o	62.88	1.84766	3	39.2991	6.29262
21	14q	69.44	1.84469	3	39.2733	5.71525
22	14r	73.66	1.85145	3	39.403	6.94013
23	14s	58.88	1.8066	5	39.3428	3.91686
24	16a	52.16	1.85135	4	39.287	5.48952
25	16b	58.56	1.85464	4	39.3782	3.99749

^a D_1 = Shadow plane YZ, D_2 = Max. bond order for atom C, D_3 = Min. (#HA, #HD) (Zefirov PC), D_4 = Min. n-n repulsion for bond H-C, D_5 = Square root of surface area for atom N.

Table S4. Descriptor of the BMLR-QSAR model for the subset group (A+B) against MCF7 (beast) carcinoma cell line.

$N = 17, n = 3, R^2 = 0.711, R^2_{cvOO} = 0.534, R^2_{cvMO} = 0.560, F = 10.637, s^2 = 0.048$				
ID	Coefficient	s	t	Descriptor
0	-10.452	3.874	2.698	Intercept
D_1	0.31127	0.060	5.189	Tot. dipole of the molecule
D_2	12.0309	4.304	2.795	Max. PI-PI bond order
D_3	-0.191204	0.042	-4.544	RNCS Relative negative charged SA (SAMNEG*RNCG) (MOPAC PC)
$\log(\text{IC}_{50}) = -10.452 + (0.31127 \times D_1) + (12.0309 \times D_2) - (0.191204 \times D_3)$				

Table S5. Observed and estimated/predicted activity values for the subset group (A+B) antitumor active agents according to the (A+B)-QSAR model due to MCF7 (breast) carcinoma cell line.

Entry	Compd.	Observed IC ₅₀ , μM	Estimated IC ₅₀ , μM	Error ^a
1	12a	3.4	3.9	-0.5
2	12c	4.4	4.6	-0.2
3	12d	8.3	7.2	1.1
4	12e	9.0	7.9	1.1
5	12f	14.9	13.7	1.2
6	14a	15	14.3	0.7
7	14b	11.3	9.6	1.7
8	14c	6.1	6.1	0.0
9	14d	9.9	10.6	-0.7
10	14e	3.9	5.9	-2.0
11	14g	47.6	31.8	15.8
12	14k	5.4	6.2	-0.8
13	14l	40.4	47.4	-7.0
14	14o	5	4.2	0.8
15	14s	6.4	7.0	-0.6
16	16a	5.5	4.9	0.6
17	16b	44.2	55.7	-11.5

^a Error is the difference between the observed and estimated bio-activity values.

Table S6. Observed and estimated/predicted activity values for the subset group (C, as an external test set) according to the (A+B)-QSAR model due to MCF7 (breast) carcinoma cell line.

Entry	Compd.	Observed IC ₅₀ , μM	Estimated IC ₅₀ , μM	Error ^a
1	12b	4.0	0.5	3.5
2	14f	9.3	7.6	1.7
3	14h	5.9	7.9	-2.0
4	14i	44.4	32.0	12.4
5	14m	6.8	85.5	-78.7
6	14n	21.8	8.4	13.4
7	14q	5.1	18.2	-13.1
8	14r	12.1	20.2	-8.1

^a Error is the difference between the observed and estimated bio-activity values.

Table S7. Descriptor of the BMLR-QSAR model for the subset group (A+C) against MCF7 (beast) carcinoma cell line.

$N = 17, n = 3, R^2 = 0.768, R^2_{cvOO} = 0.606, R^2_{cvMO} = 0.663, F = 14.370, s^2 = 0.039$				
ID	Coefficient	s	t	Descriptor
0	-99.318	31.049	-3.199	Intercept
D_1	3.94371	0.716	5.508	Max. resonance energy for bond C-C
D_2	6.21007	2.093	2.967	Min. resonance energy for bond H-C
D_3	-6.2108	1.291	-4.811	Min. atomic state energy for atom H
$\log(\text{IC}_{50}) = -99.318 + (3.94371 \times D_1) + (6.21007 \times D_2) - (6.2108 \times D_3)$				

Table S8. Observed and estimated/predicted activity values for the subset group (A+C) antitumor active agents according to the (A+C)-QSAR model due to MCF7 (breast) carcinoma cell line.

Entry	Compd.	Observed IC ₅₀ , μM	Estimated IC ₅₀ , μM	Error ^a
1	12a	3.4	3.7	-0.3
2	12b	4.0	3.6	0.4
3	12c	4.4	4.7	-0.3
4	12d	8.3	7.7	0.6
5	12f	14.9	15.4	-0.5
6	14c	6.1	4.6	1.5
7	14d	9.9	11.8	-1.9
8	14f	9.3	8.7	0.6
9	14g	47.6	47.7	-0.1
10	14h	5.9	6.9	-1.0
11	14i	44.4	52.2	-7.8
12	14k	5.4	6.4	-1.0
13	14l	40.4	26.9	13.5
14	14m	6.8	6.6	0.2
15	14n	21.8	23.6	-1.8
16	14q	5.1	5.8	-0.7
17	14r	12.1	10.9	1.2

^a Error is the difference between the observed and estimated bio-activity values.

Table S9. Observed and estimated/predicted activity values for the subset group (B, as an external test set) according to the (A+C)-QSAR model due to MCF7 (breast) carcinoma cell line.

Entry	Compd.	Observed IC ₅₀ , μM	Estimated IC ₅₀ , μM	Error ^a
1	12e	9.0	6.2	2.8
2	14a	15.0	8.1	6.9
3	14b	11.3	22.8	-11.5
4	14e	3.9	9.0	-5.1
5	14o	5.0	4.7	0.3
6	14s	6.4	28.9	-22.5
7	16a	5.5	0.0	5.5
8	16b	44.2	0.3	43.9

^a Error is the difference between the observed and estimated bio-activity values.

Table S10. Descriptor of the BMLR-QSAR model for the subset group (B+C) against MCF7 (beast) carcinoma cell line.

$N = 16, n = 3, R^2 = 0.790, R^2_{cvOO} = 0.654, R^2_{cvMO} = 0.664, F = 15.068, s^2 = 0.029$				
ID	Coefficient	s	t	Descriptor
0	-109.922	21.329	-5.154	Intercept
D_1	9.2227	1.918	4.808	Min. resonance energy for bond H-C
D_2	119.521	27.531	4.341	Max. partial charge (Zefirov) for atoms for atom H
D_3	11.7365	3.601	3.260	Max. PI-PI bond order
$\log(\text{IC}_{50}) = -109.922 + (9.2227 \times D_1) + (119.521 \times D_2) - (11.7365 \times D_3)$				

Table S11. Observed and estimated/predicted activity values for the subset group (B+C) antitumor active agents according to the (B+C)-QSAR model due to MCF7 (breast) carcinoma cell line.

Entry	Compd.	Observed IC ₅₀ , μM	Estimated IC ₅₀ , μM	Error ^a
1	12b	4.0	4.4	-0.4
2	12e	9.0	8.5	0.5
3	14a	15.0	12.7	2.3
4	14b	11.3	11.8	-0.5
5	14e	3.9	6.4	-2.5
6	14f	9.3	6.6	2.7
7	14h	5.9	5.0	0.9
8	14i	44.4	44.5	-0.1
9	14m	6.8	7.4	-0.6
10	14n	21.8	19.4	2.4
11	14o	5.0	4.7	0.3
12	14q	5.1	4.9	0.2
13	14r	12.1	15.4	-3.3
14	14s	6.4	6.0	0.4
15	16a	5.5	5.9	-0.4
16	16b	44.2	43.9	0.3

^a Error is the difference between the observed and estimated bio-activity values.

Table S12. Observed and estimated/predicted activity values for the subset group (A, as an external test set) according to the (B+C)-QSAR model due to MCF7 (breast) carcinoma cell line.

Entry	Compd.	Observed IC ₅₀ , μM	Estimated IC ₅₀ , μM	Error ^a
1	12a	3.4	11.2	-7.8
2	12c	4.4	14.5	-10.1
3	12d	8.3	9.8	-1.5
4	12f	14.9	5.6	9.3
5	14c	6.1	2.0	4.1
6	14d	9.9	11.1	-1.2
7	14g	47.6	15.7	31.9
8	14k	5.4	4.3	1.1
9	14l	40.4	3.9	36.5

^a Error is the difference between the observed and estimated bio-activity values.

Table S13. Crystal data and structure refinement parameters of compound **14a**.

Crystal data	Compound 14a
Chemical formula	C ₂₈ H ₂₇ N ₃
<i>M</i> _r	405.54
Crystal system, space group	Orthorhombic, <i>Pc21n</i>
Temperature (K)	298
<i>a</i> , <i>b</i> , <i>c</i> (Å)	6.0216 (1), 18.9648 (4), 19.6590 (5)
<i>V</i> (Å ³)	2245.03 (6)
<i>Z</i>	4
Radiation type	Mo <i>K</i> α
μ (mm ⁻¹)	0.07
Crystal size (mm)	0.30 × 0.25 × 0.21
<i>T</i> _{min} , <i>T</i> _{max}	0.72, 0.99
No. of measured, independent and observed [<i>I</i> > 2.0σ(<i>I</i>)] reflections	4030, 4030, 1254
(sin θ/λ) _{max} (Å ⁻¹)	0.780
<i>R</i> [<i>F</i> ² > 2σ(<i>F</i> ²)], <i>wR</i> (<i>F</i> ²), <i>S</i>	0.038, 0.078, 1.07
No. of reflections	1254
No. of parameters	282
Δρ _{max} , Δρ _{min} (e Å ⁻³)	0.16, -0.17
CCDC Number	1499063

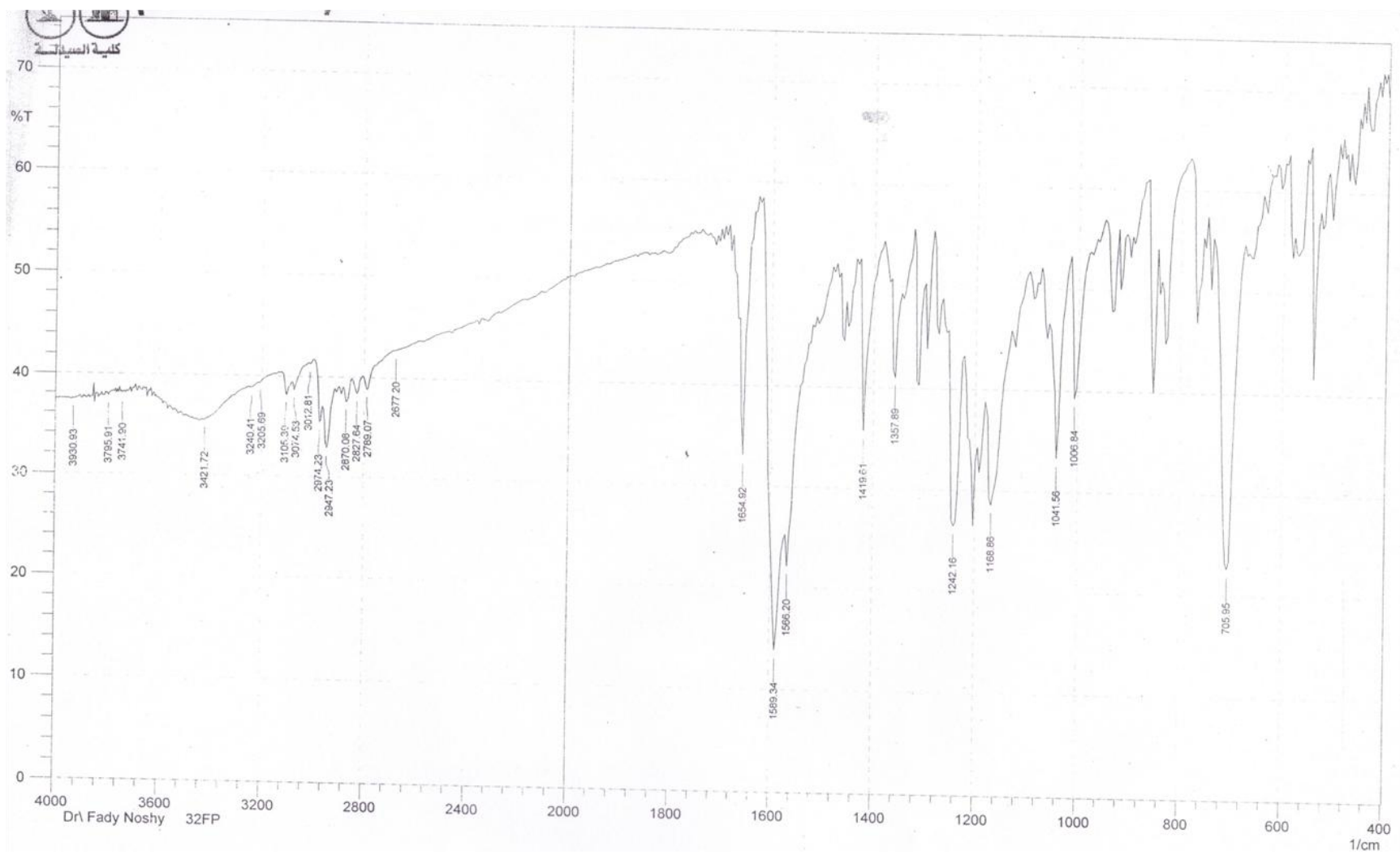


Fig. S1. IR spectrum of compound **12f** (KBr pellet).

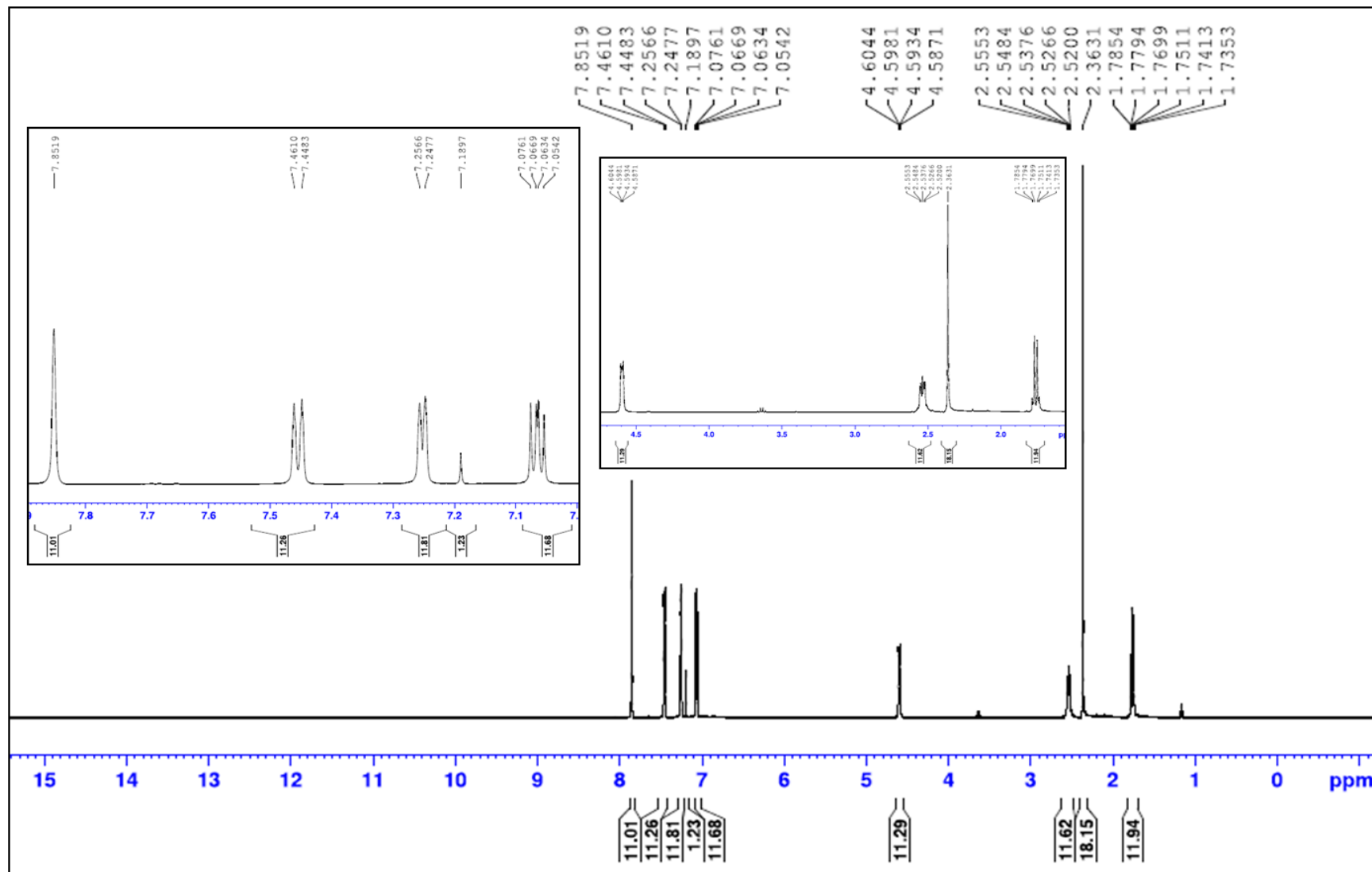


Fig. S2. ^1H -NMR spectrum of compound **12f** in CDCl_3 .

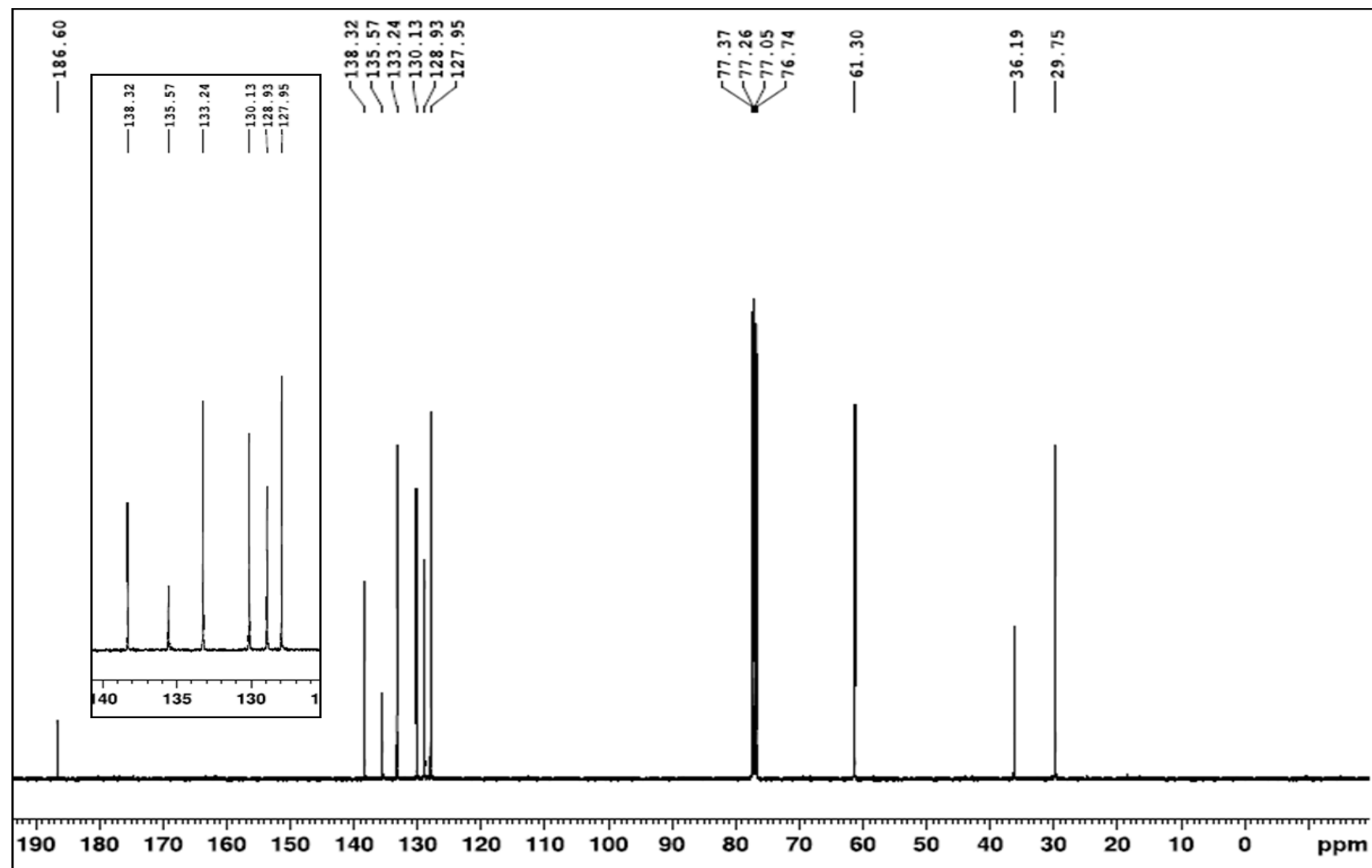


Fig. S3. ^{13}C -NMR spectrum of compound **12f** in CDCl_3 .

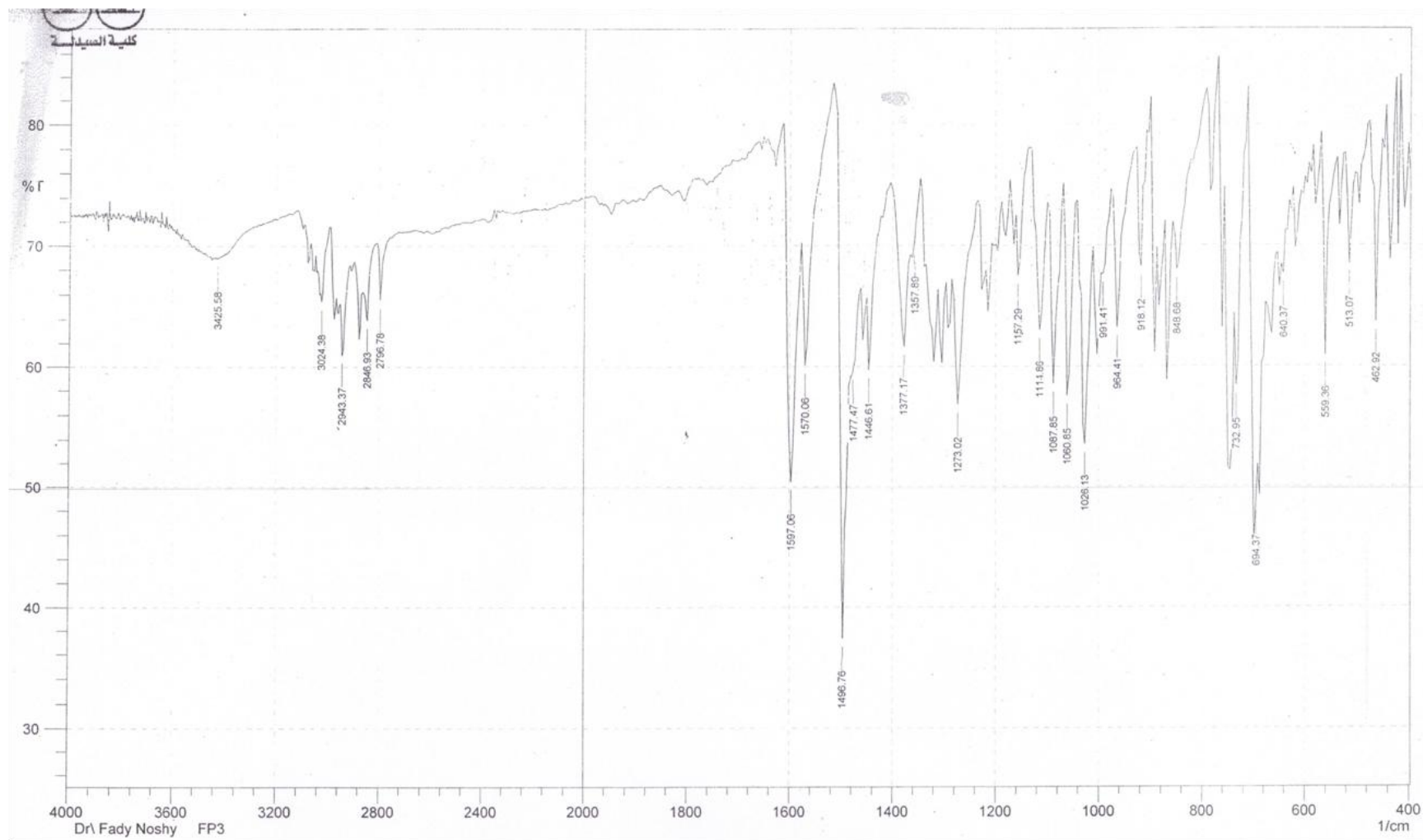
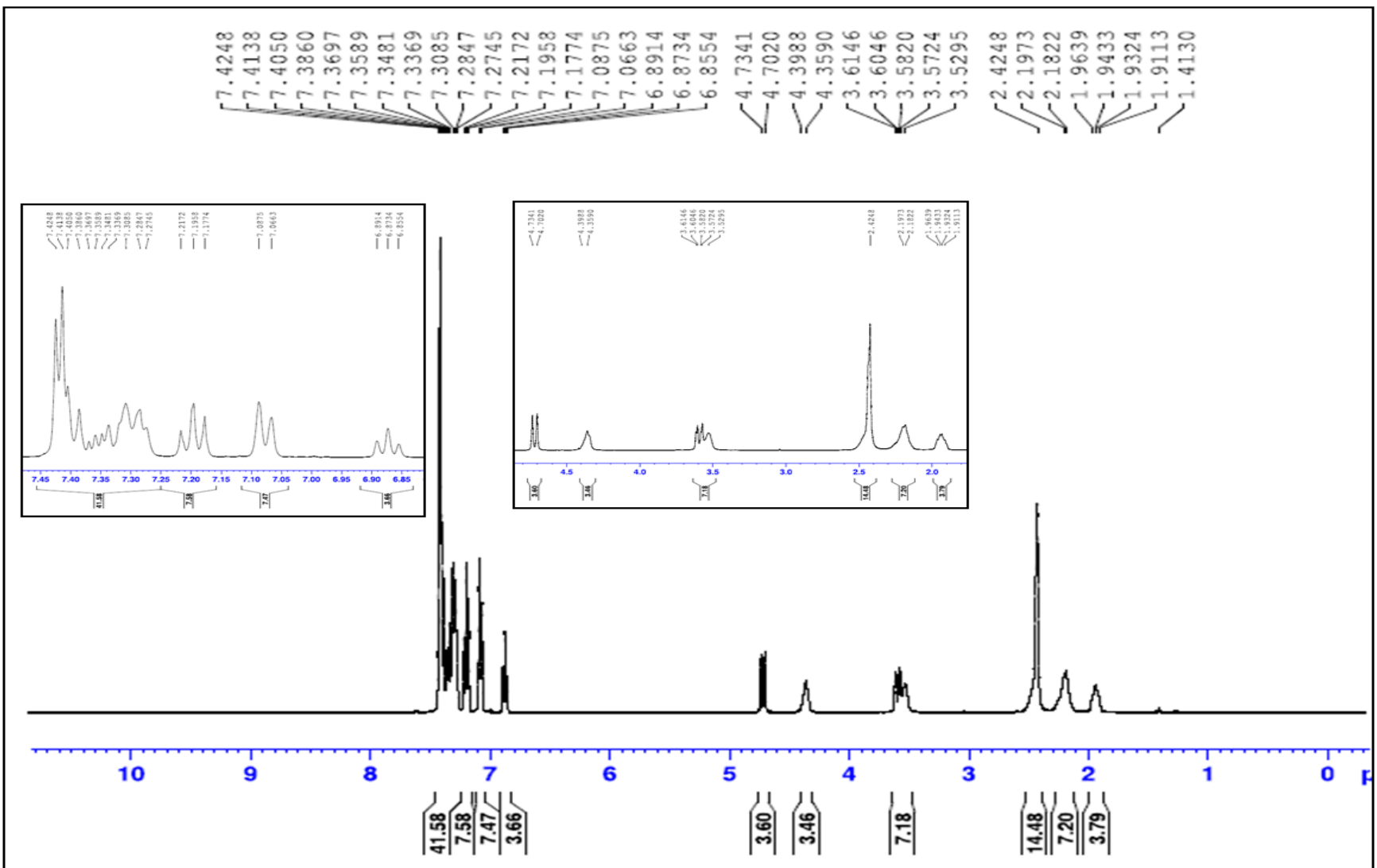


Fig. S4. IR spectrum of compound **14a** (KBr pellet).



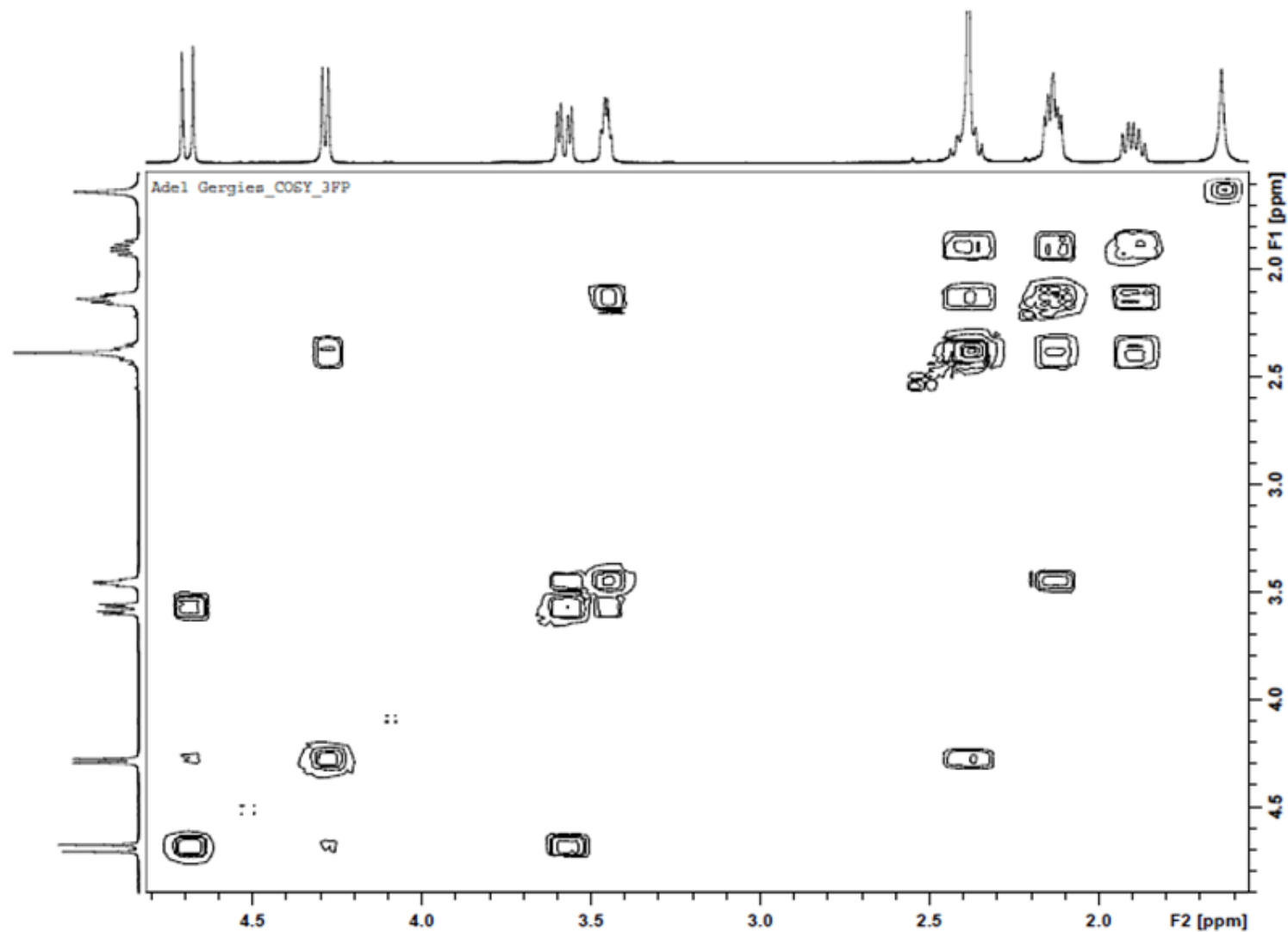


Fig. S6. ^1H , ^1H -COSY spectrum of compound **14a** in CDCl_3 .

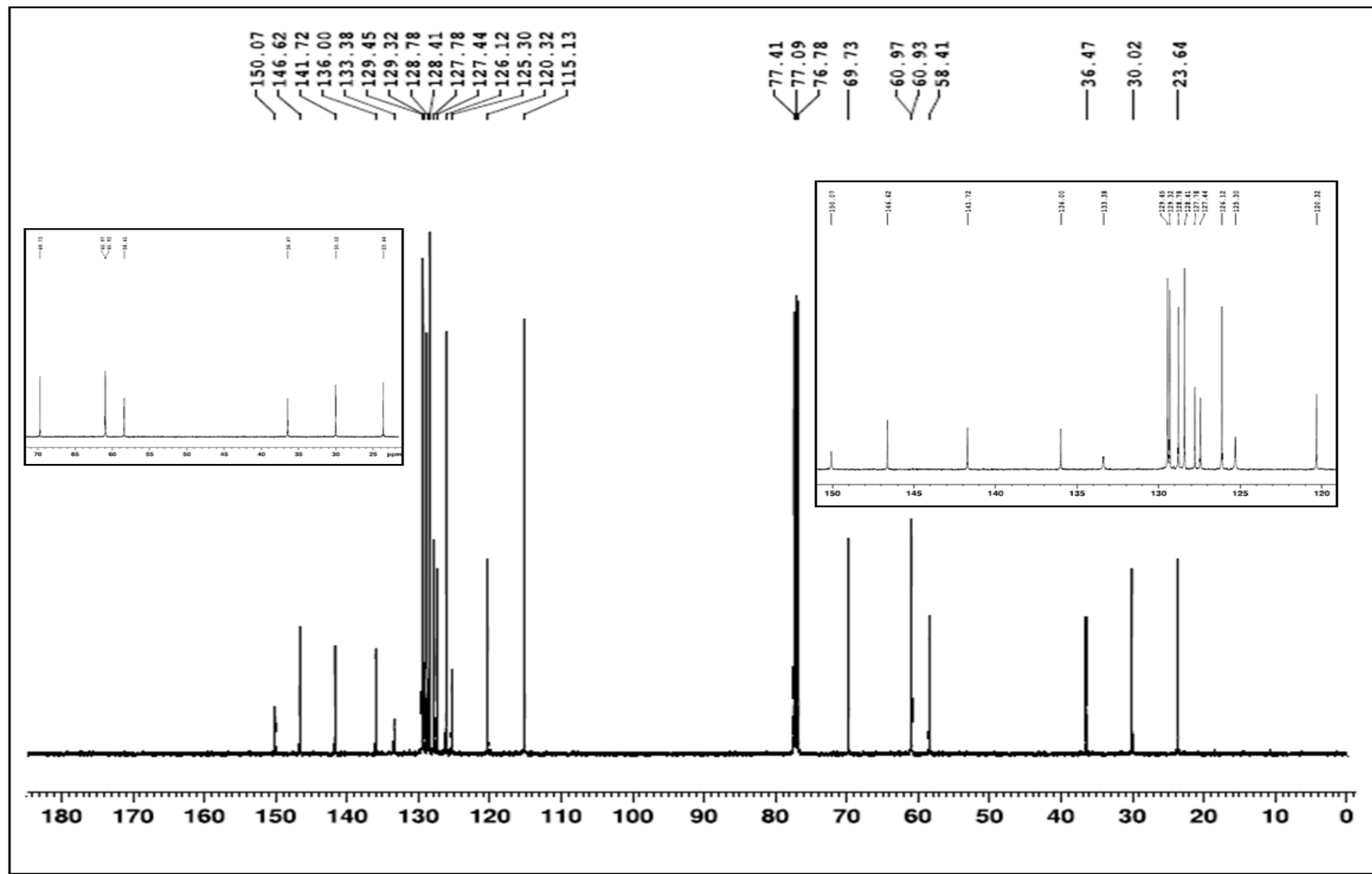


Fig. S7. ^{13}C -NMR spectrum of compound 14a in CDCl_3 .

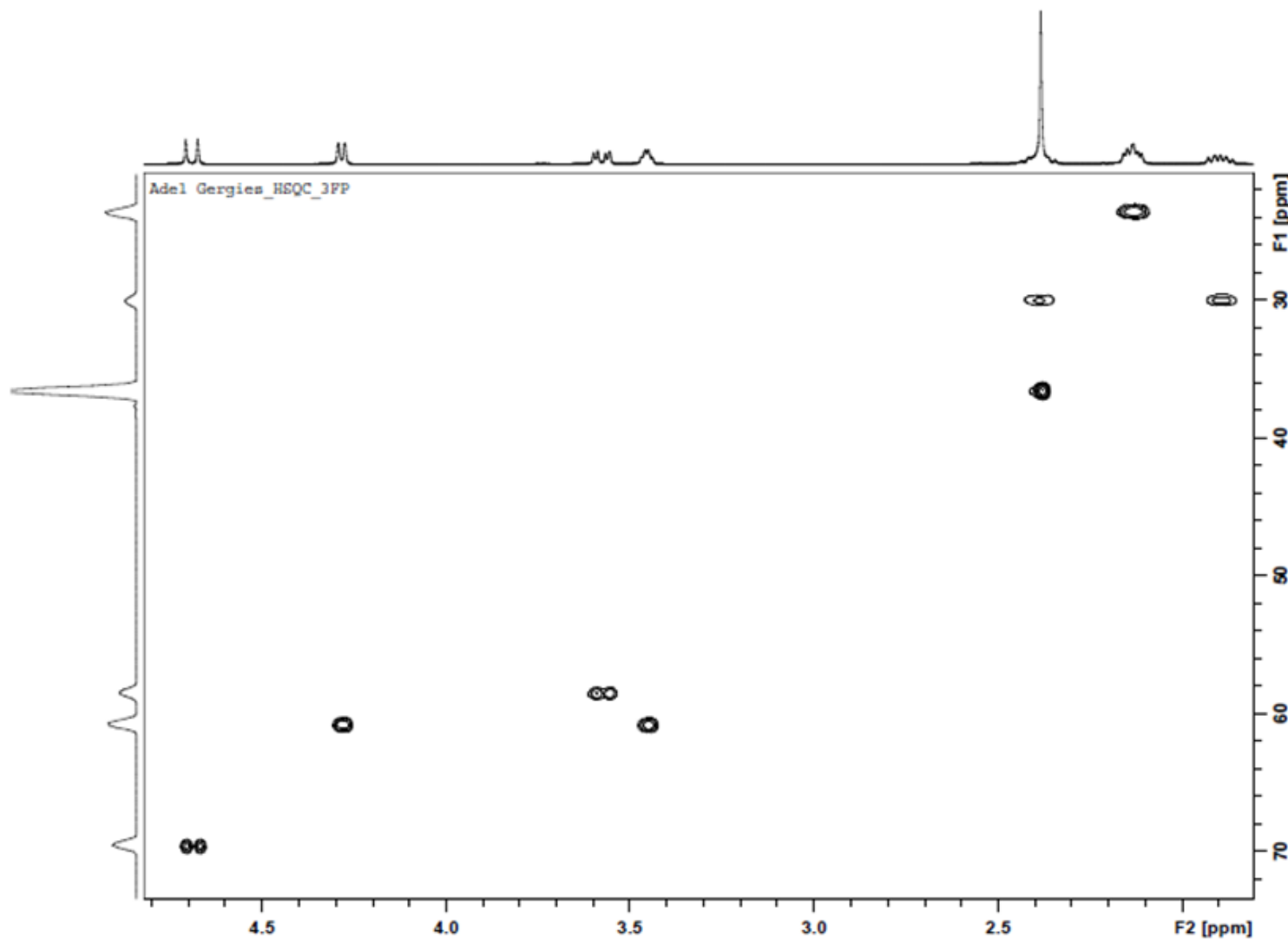


Fig. S8. ¹H,¹³C-Heteronuclear Single Quantum Coherence (HSQC) spectrum of compound **14a** in CDCl₃.

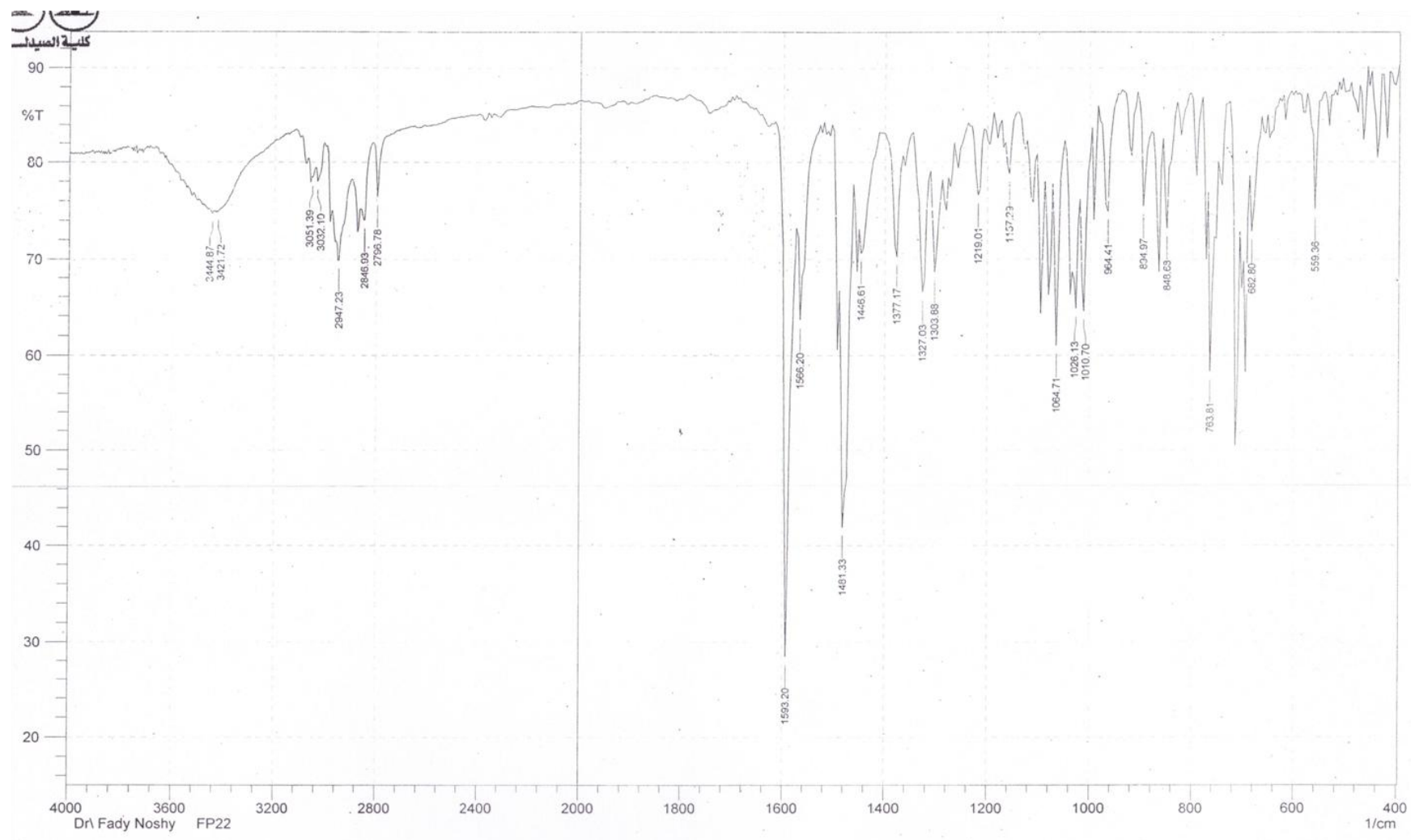


Fig. S9. IR spectrum of compound **14b** (KBr pellet).

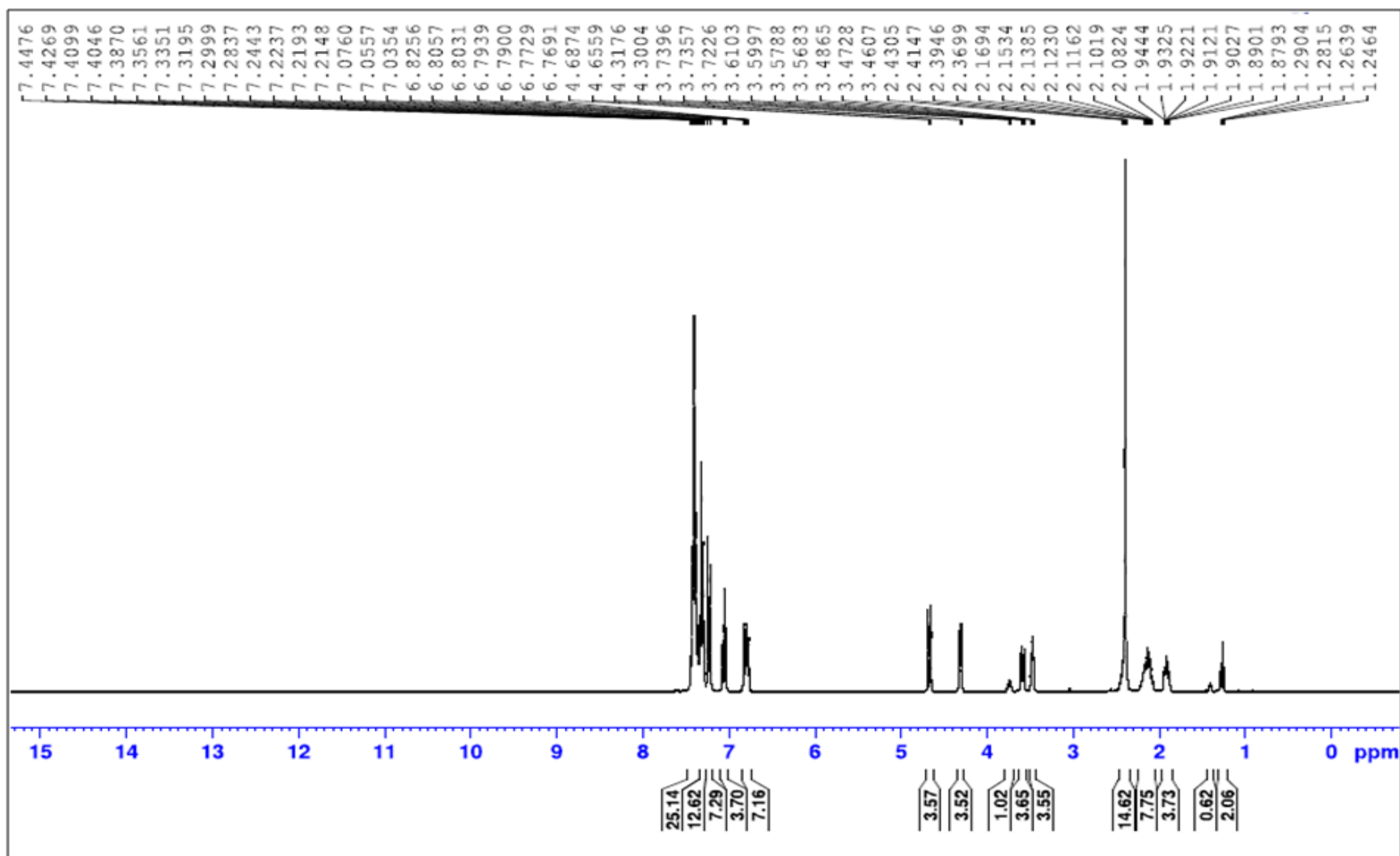


Fig. S10. ^1H -NMR spectrum of compound **14b** in CDCl_3 .

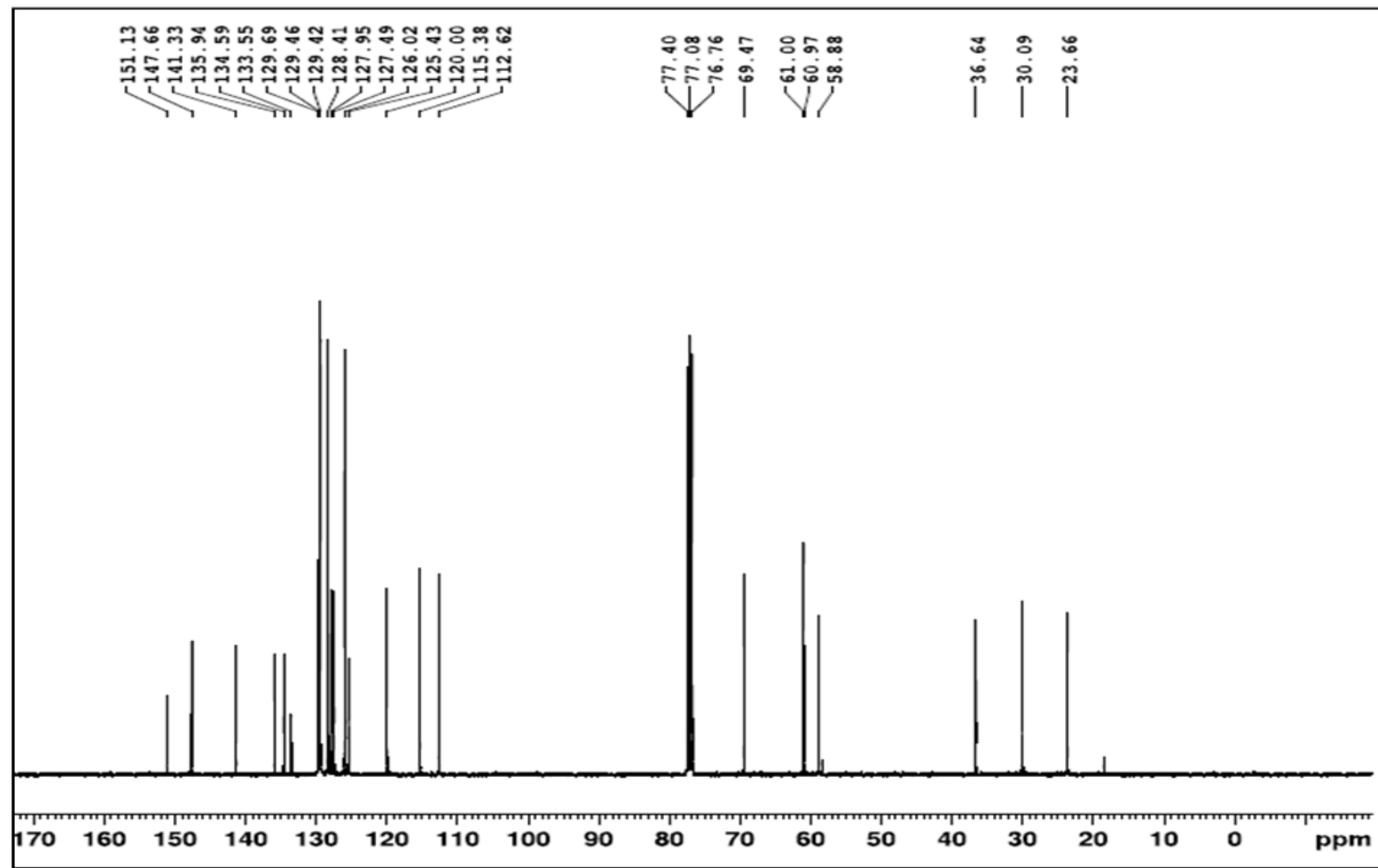


Fig. S11. ^{13}C -NMR spectrum of compound **14b** in CDCl_3 .

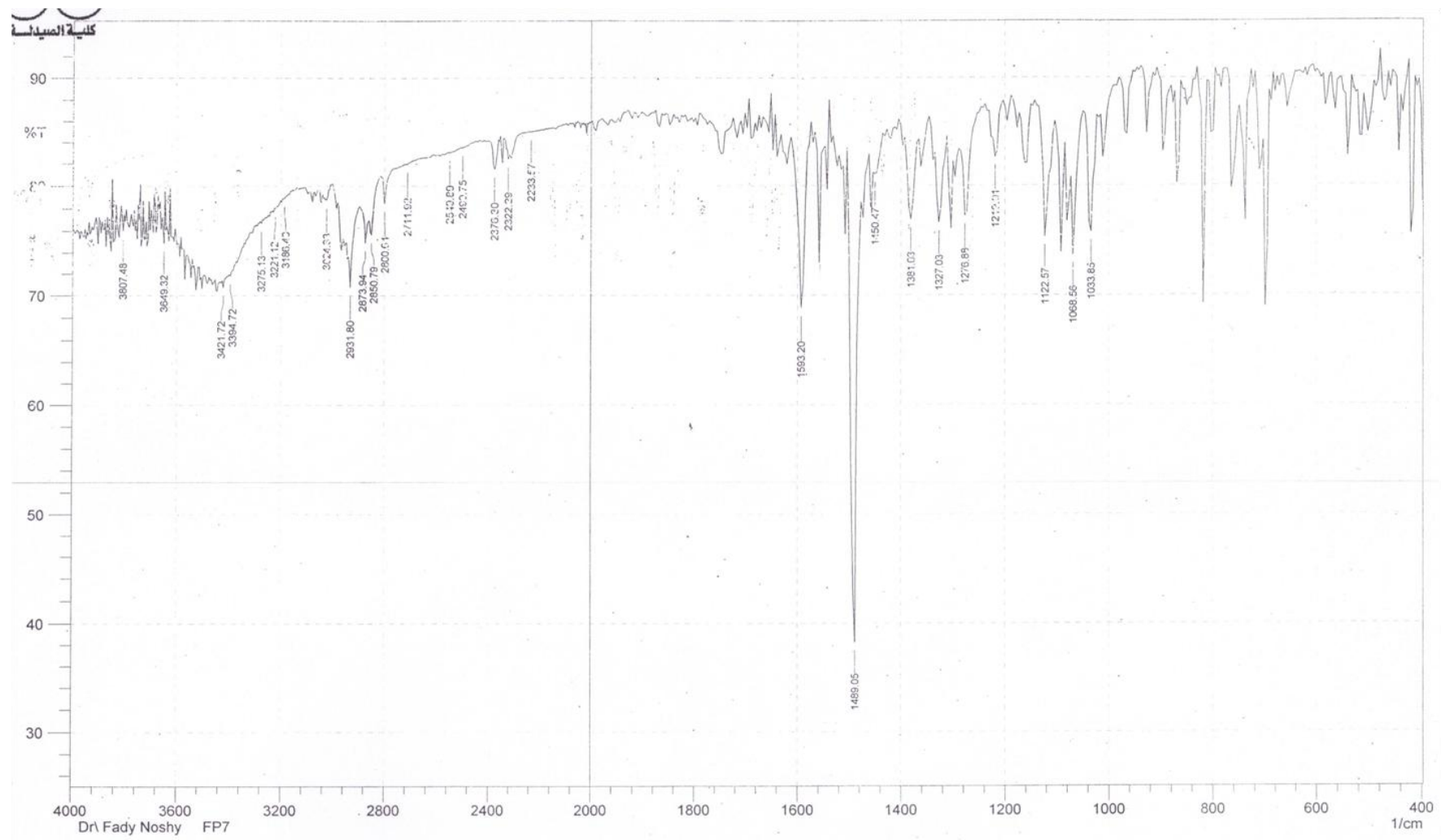


Fig. S12. IR spectrum of compound **14c** (KBr pellet).

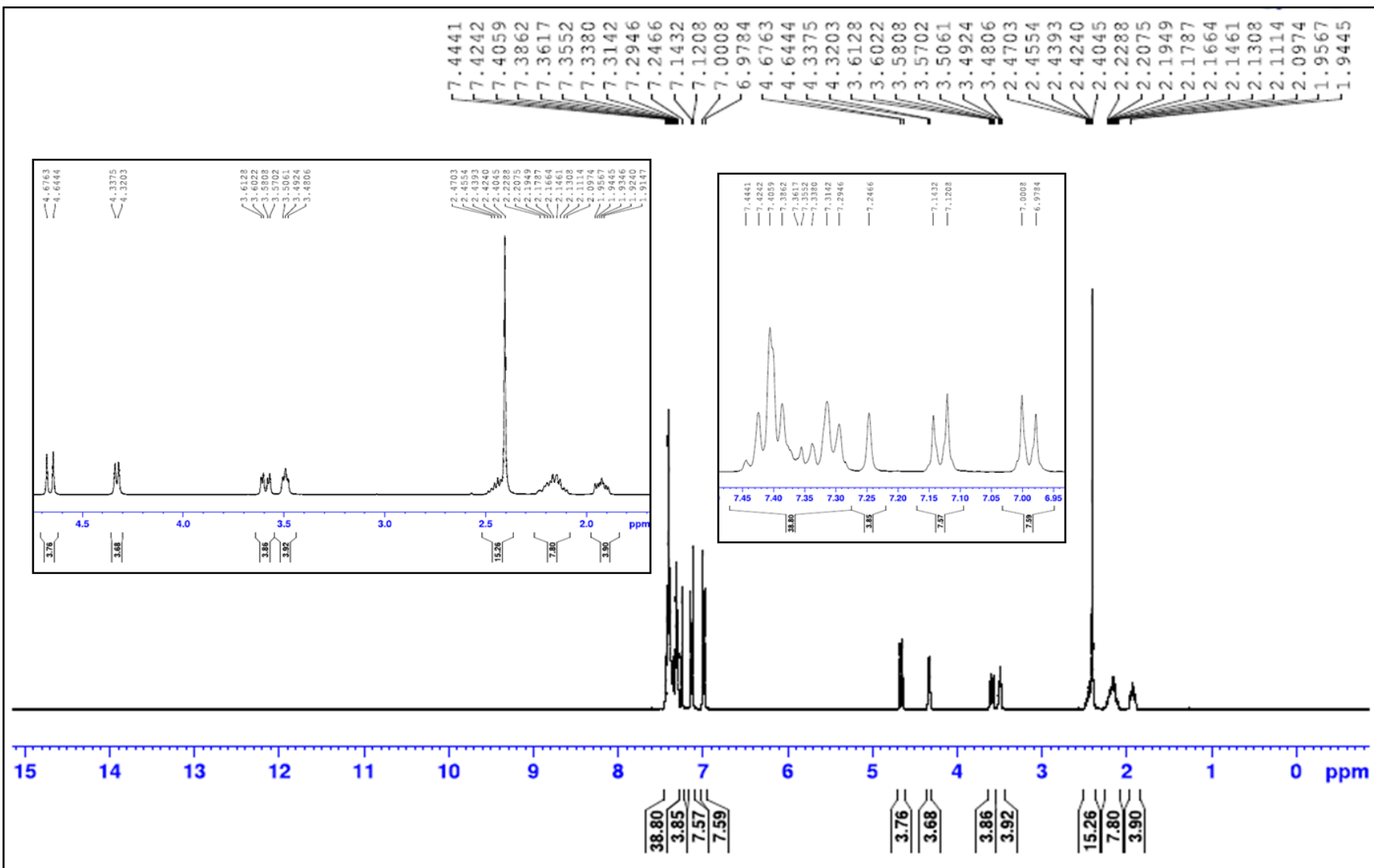


Fig. S13. ^1H -NMR spectrum of compound **14c** in CDCl_3 .

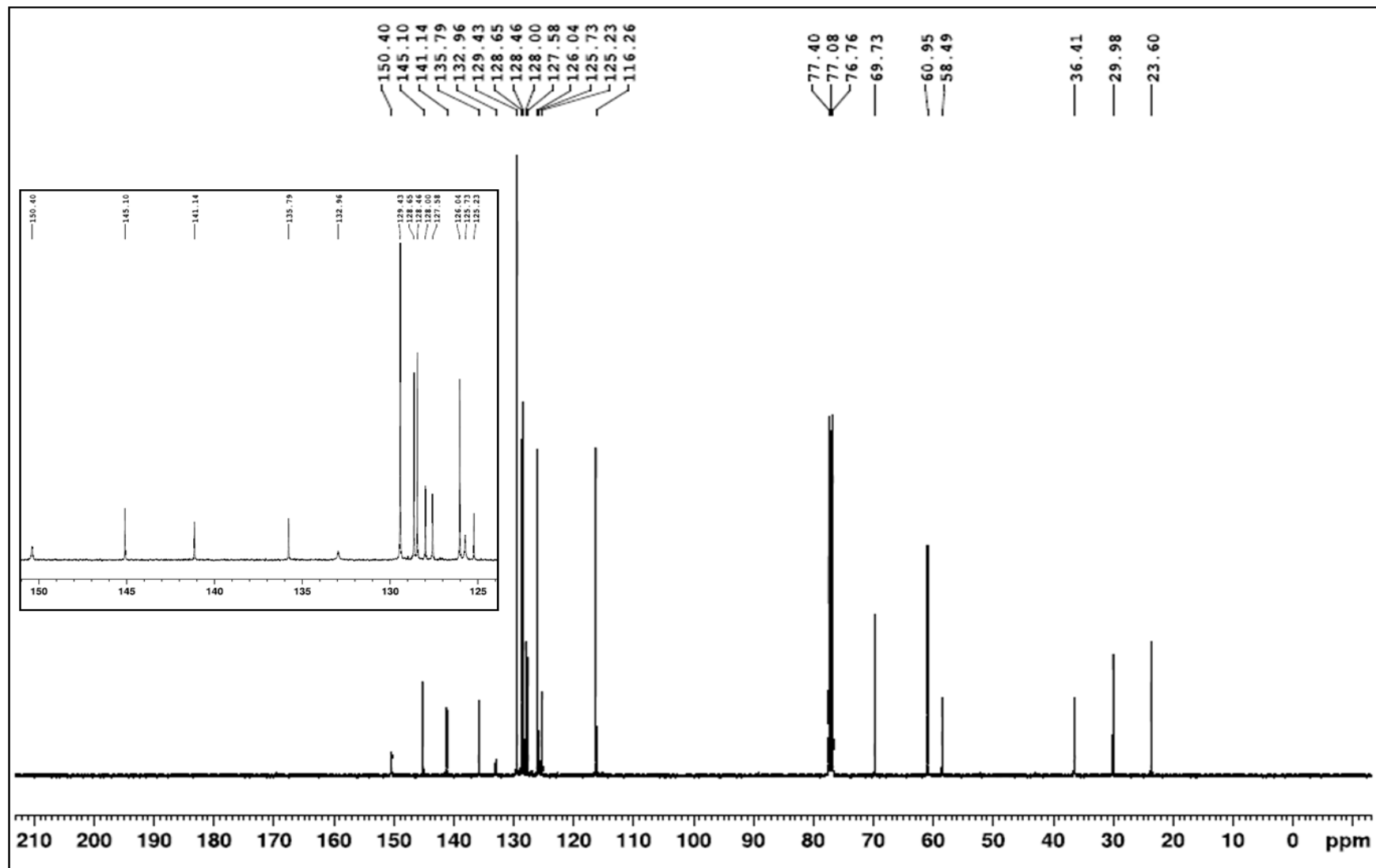


Fig. S14. ^{13}C -NMR spectrum of compound **14c** in CDCl_3 .

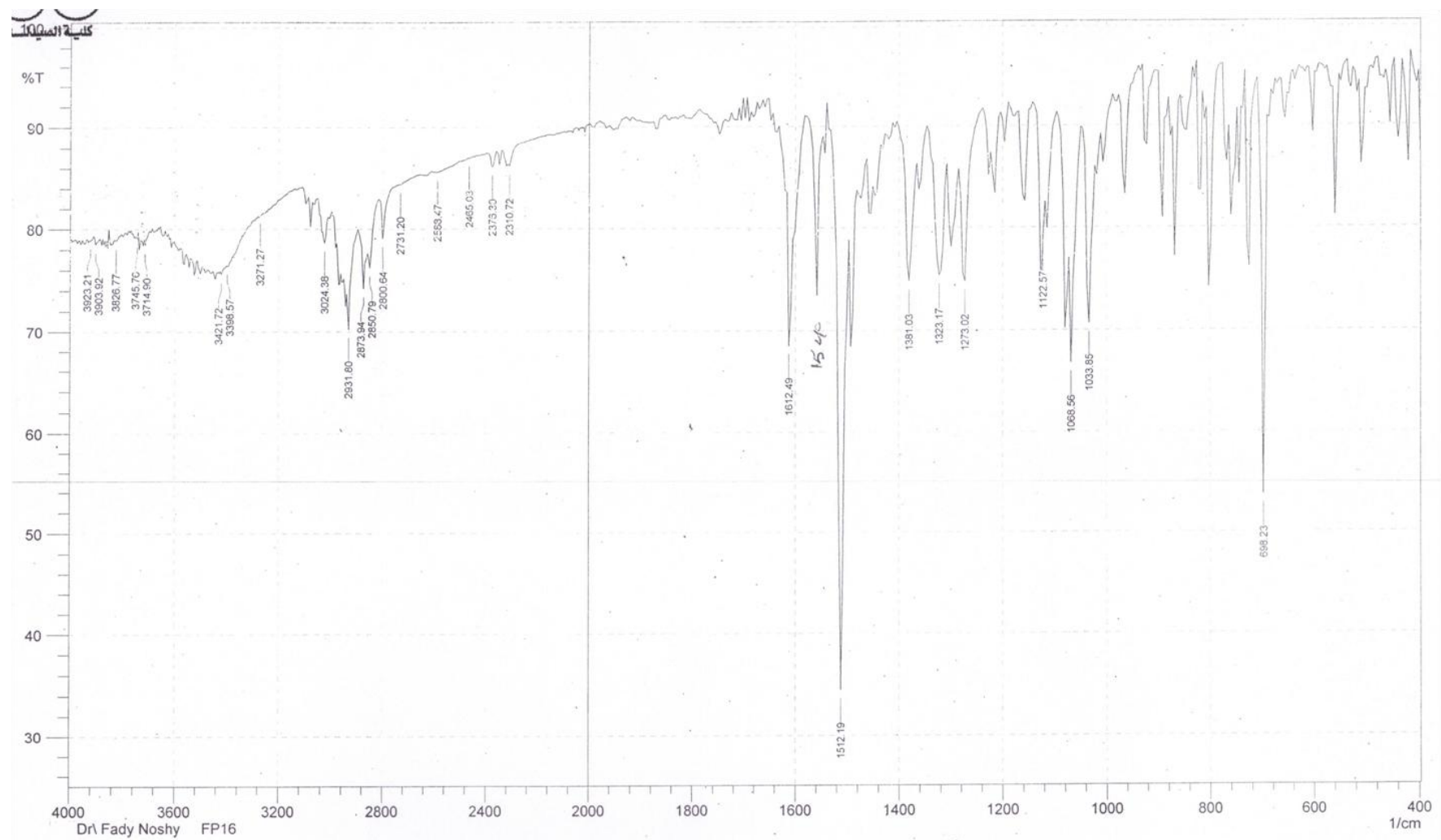


Fig. S15. IR spectrum of compound **14d** (KBr pellet).

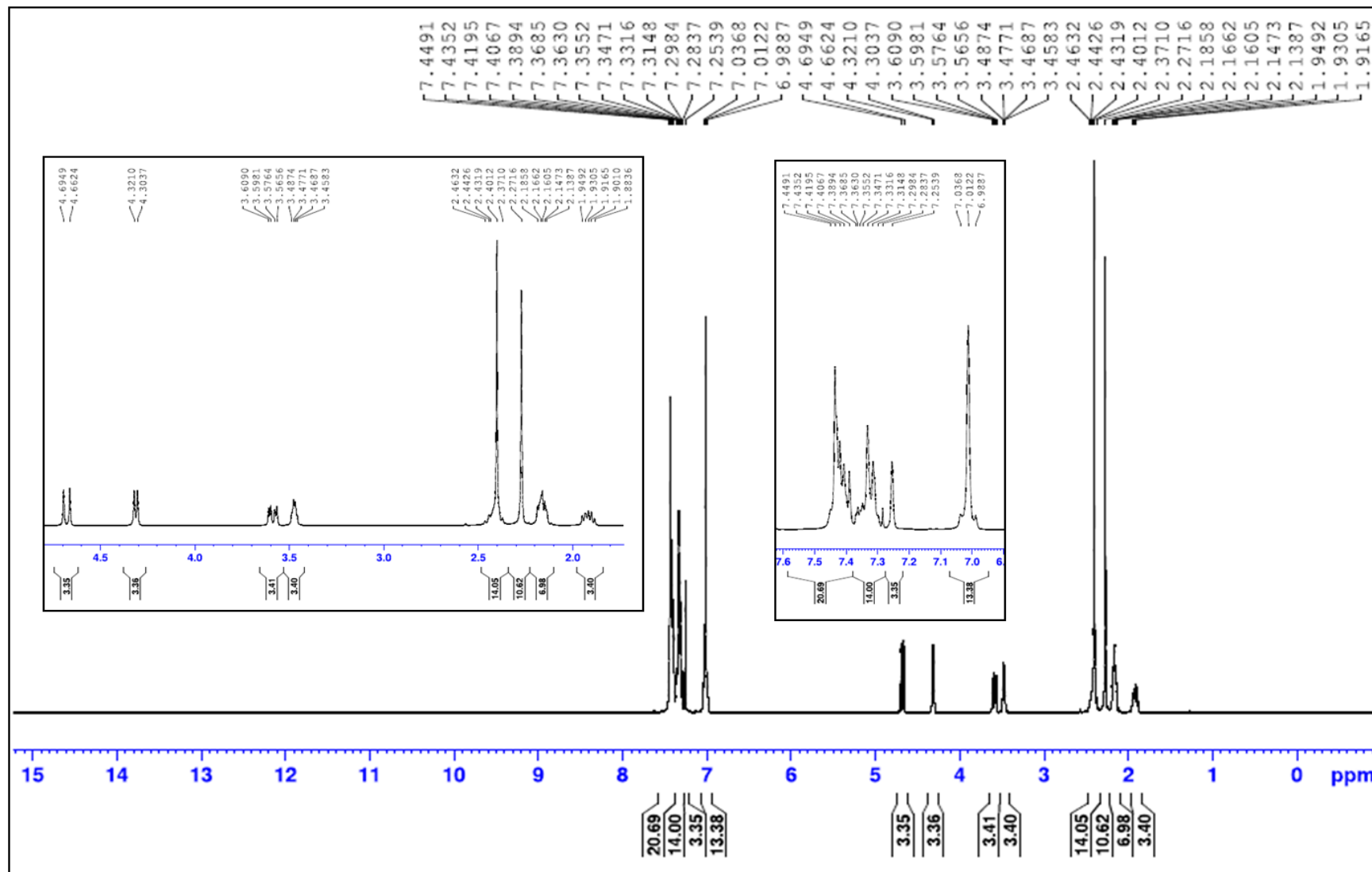


Fig. S16. ^1H -NMR spectrum of compound **14d** in CDCl_3 .

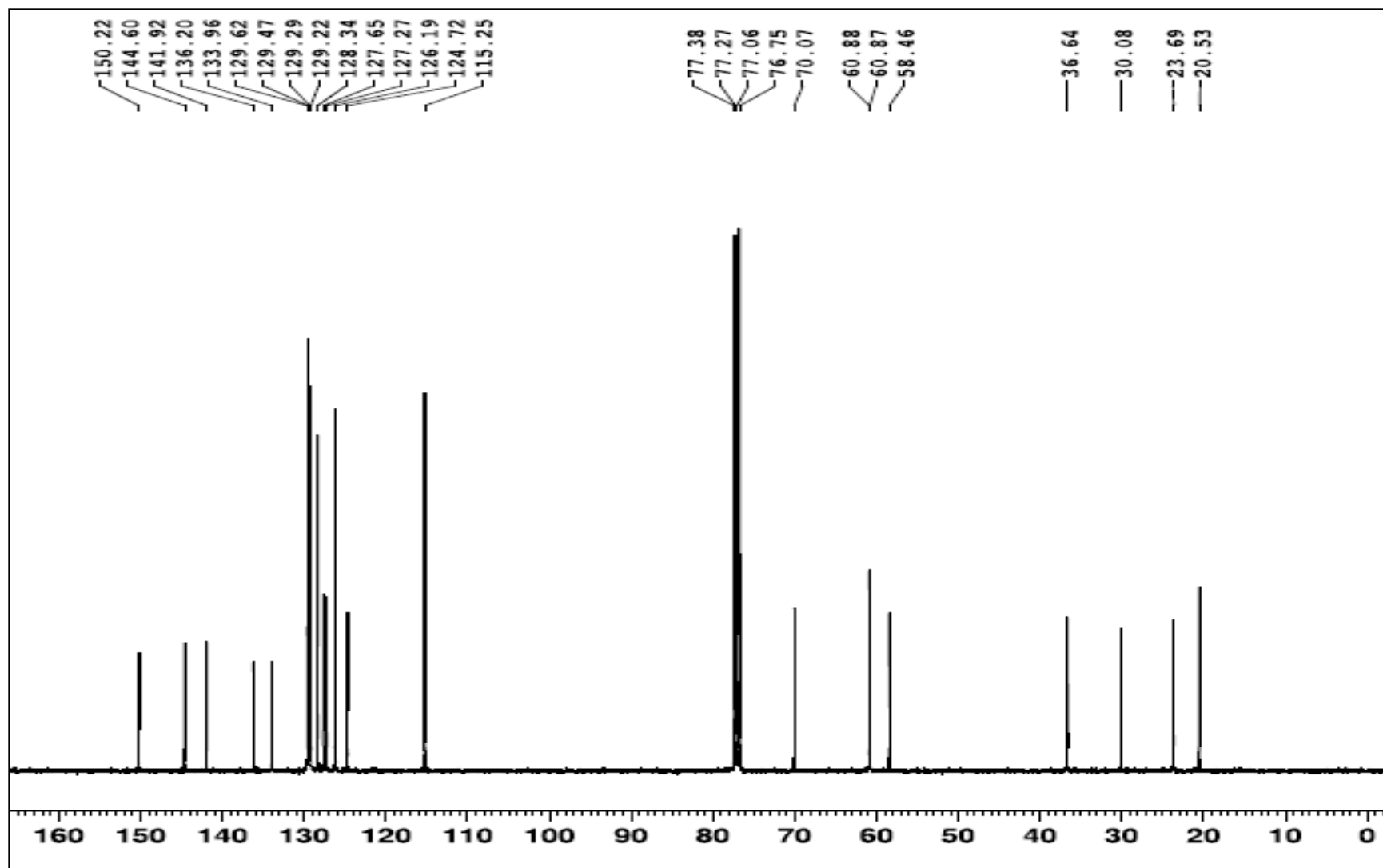


Fig. S17. ^{13}C -NMR spectrum of compound 14d in CDCl_3 .

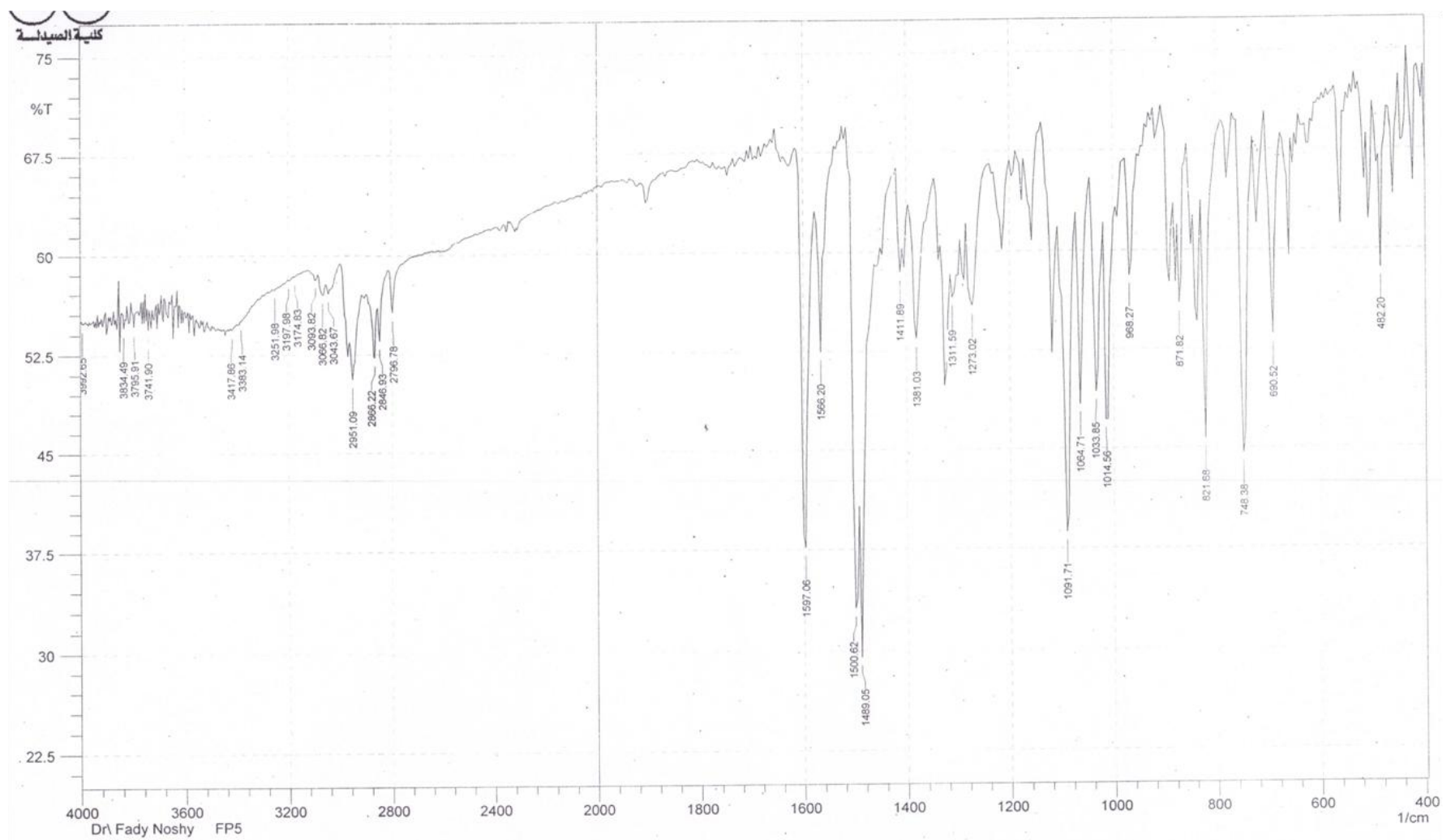


Fig. S18. IR spectrum of compound **14e** (KBr pellet).

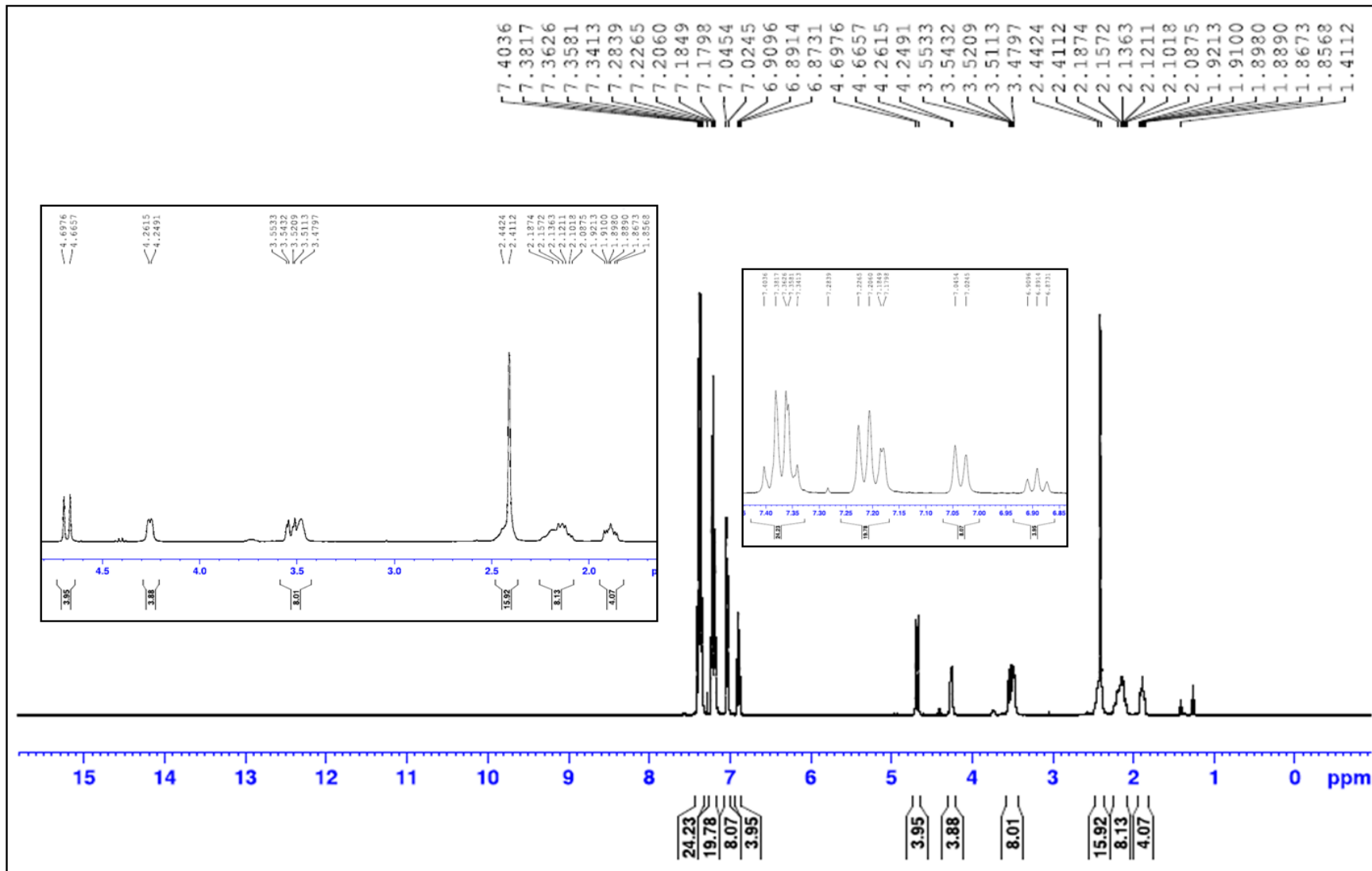


Fig. S19. ¹H-NMR spectrum of compound 14e in CDCl₃.

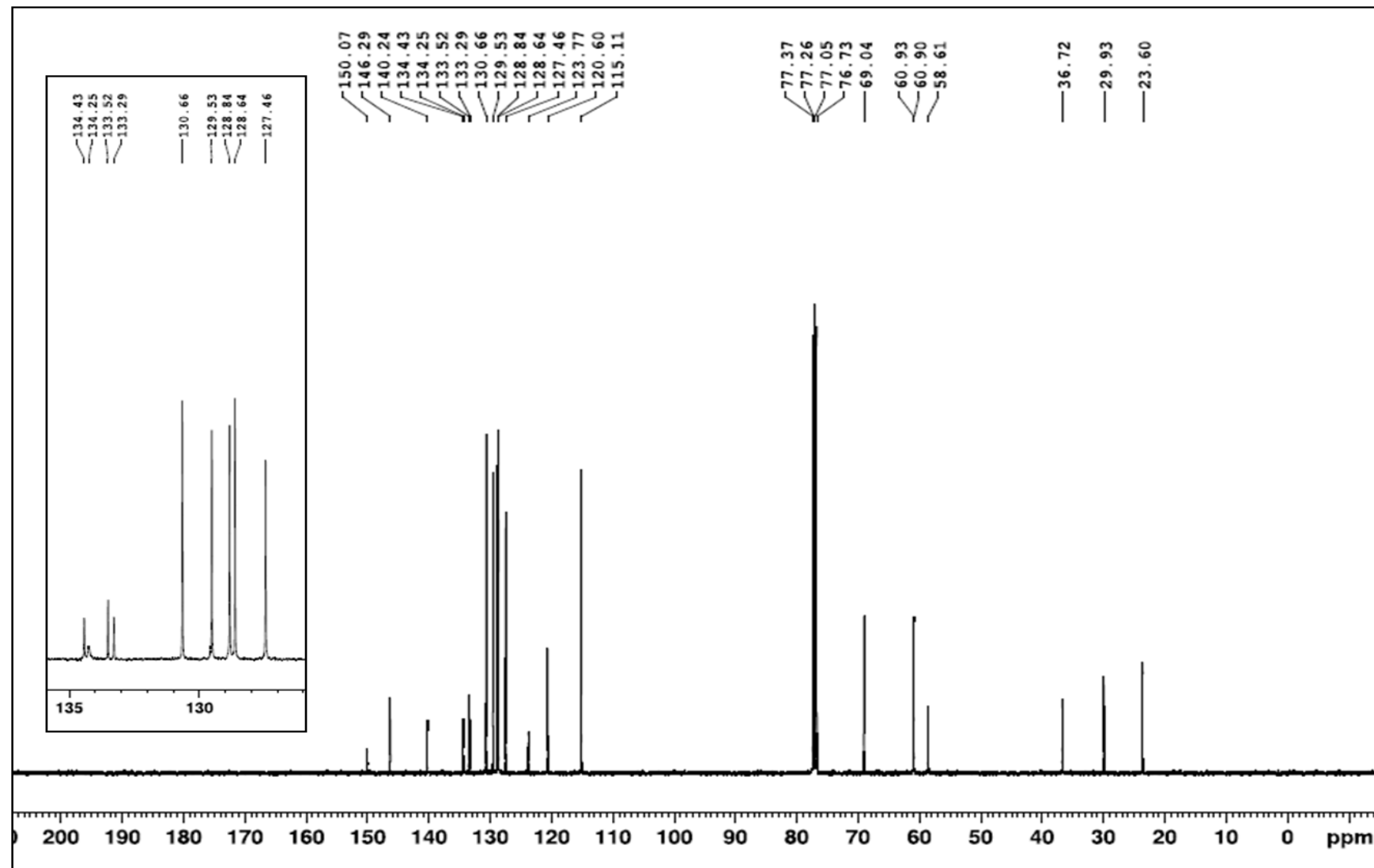


Fig. S20. ^{13}C -NMR spectrum of compound **14e** in CDCl_3 .

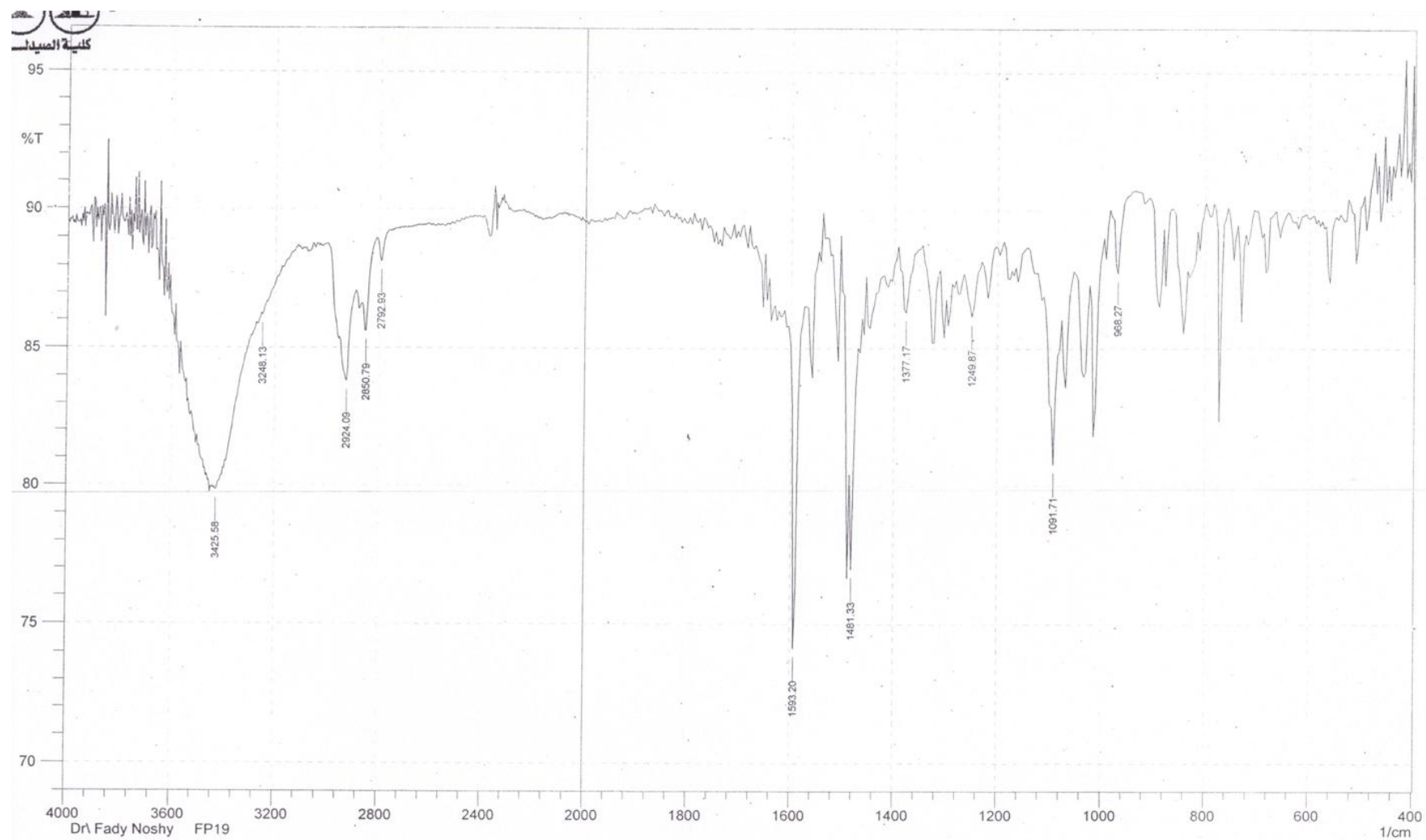


Fig. S21. IR spectrum of compound **14f** (KBr pellet).

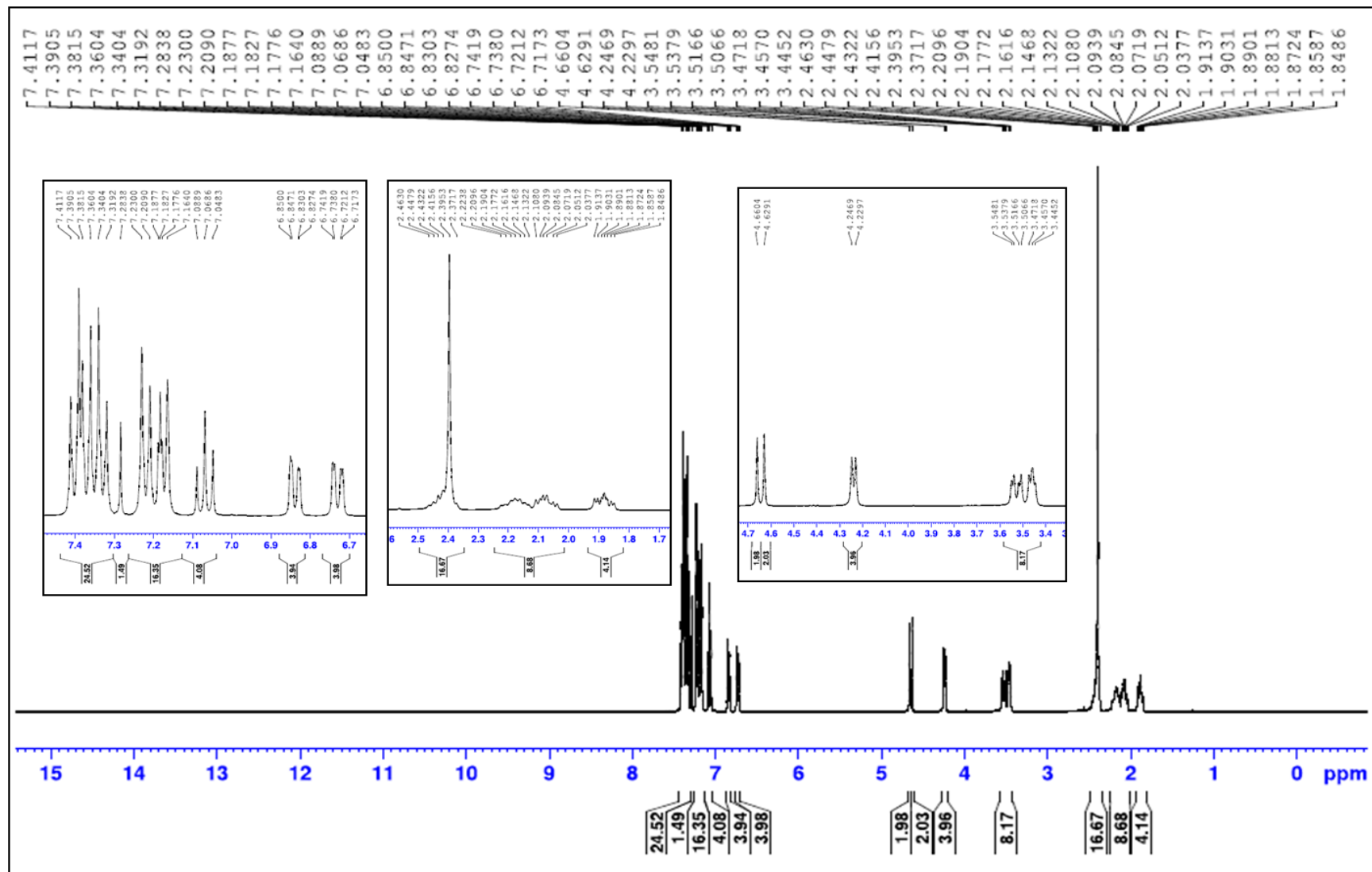


Fig. S22. ^1H -NMR spectrum of compound **14f** in CDCl_3 .

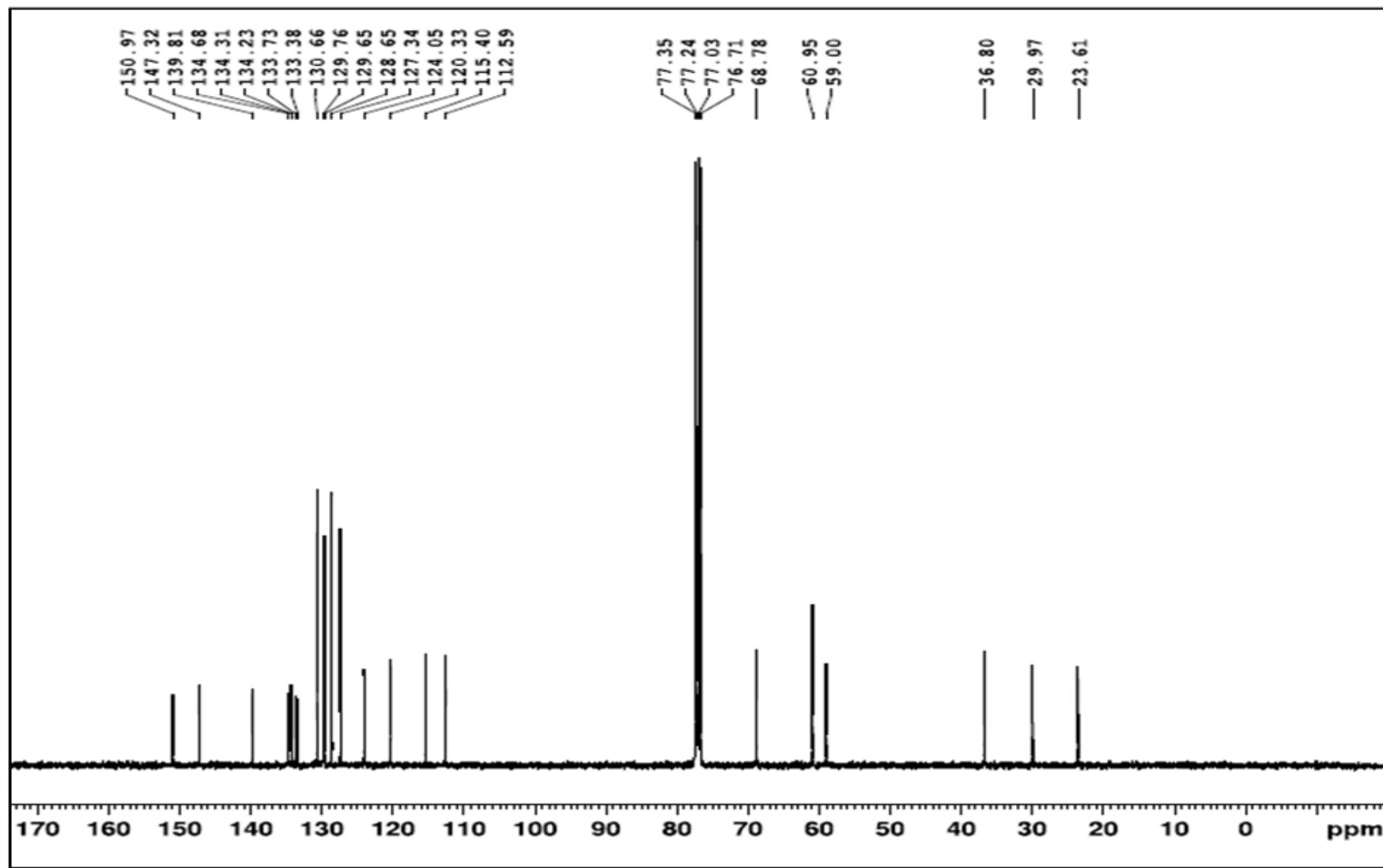


Fig. S23. ^{13}C -NMR spectrum of compound **14f** in CDCl_3 .

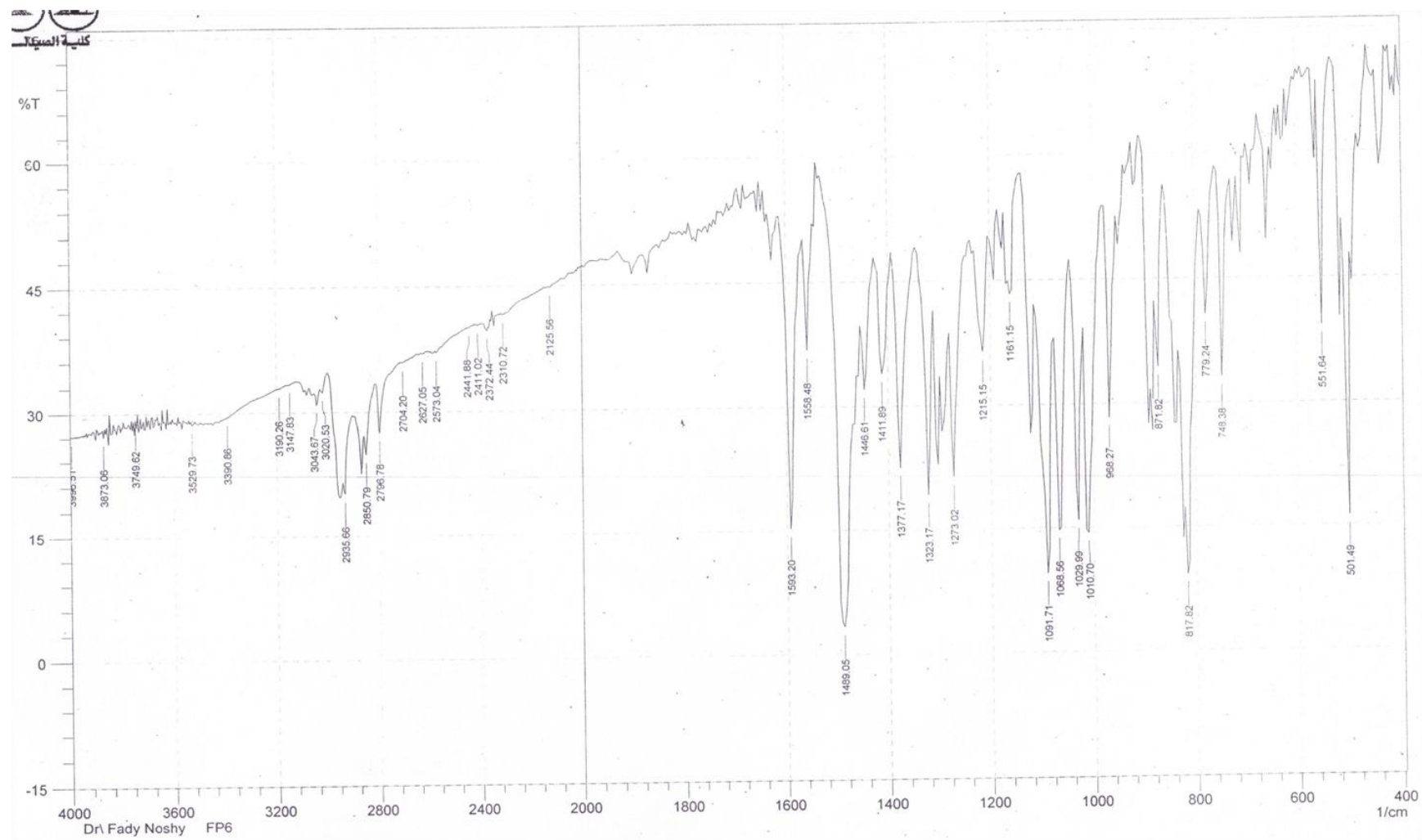


Fig. S24. IR spectrum of compound **14g** (KBr pellet).

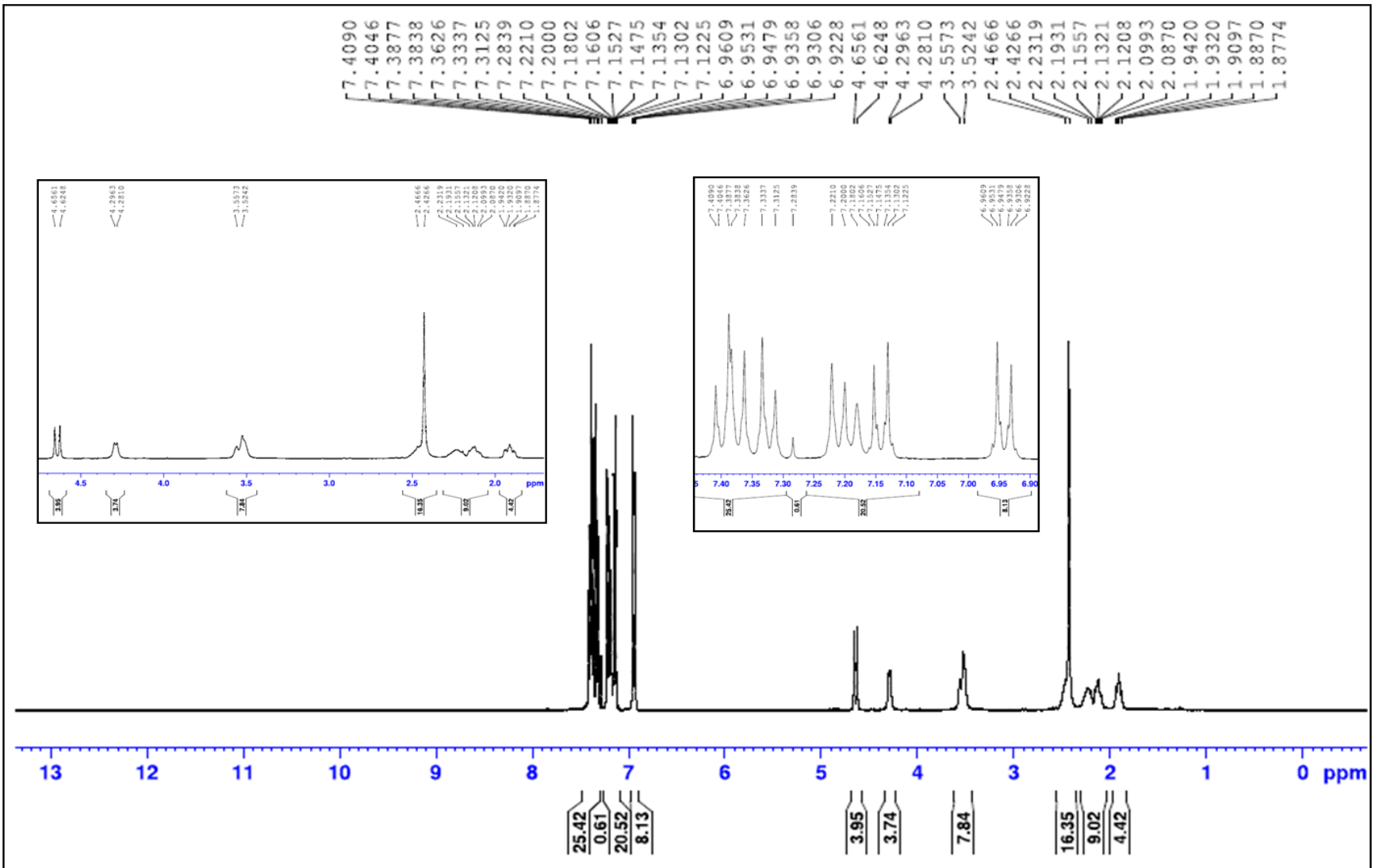


Fig. S25. ^1H -NMR spectrum of compound **14g** in CDCl_3 .

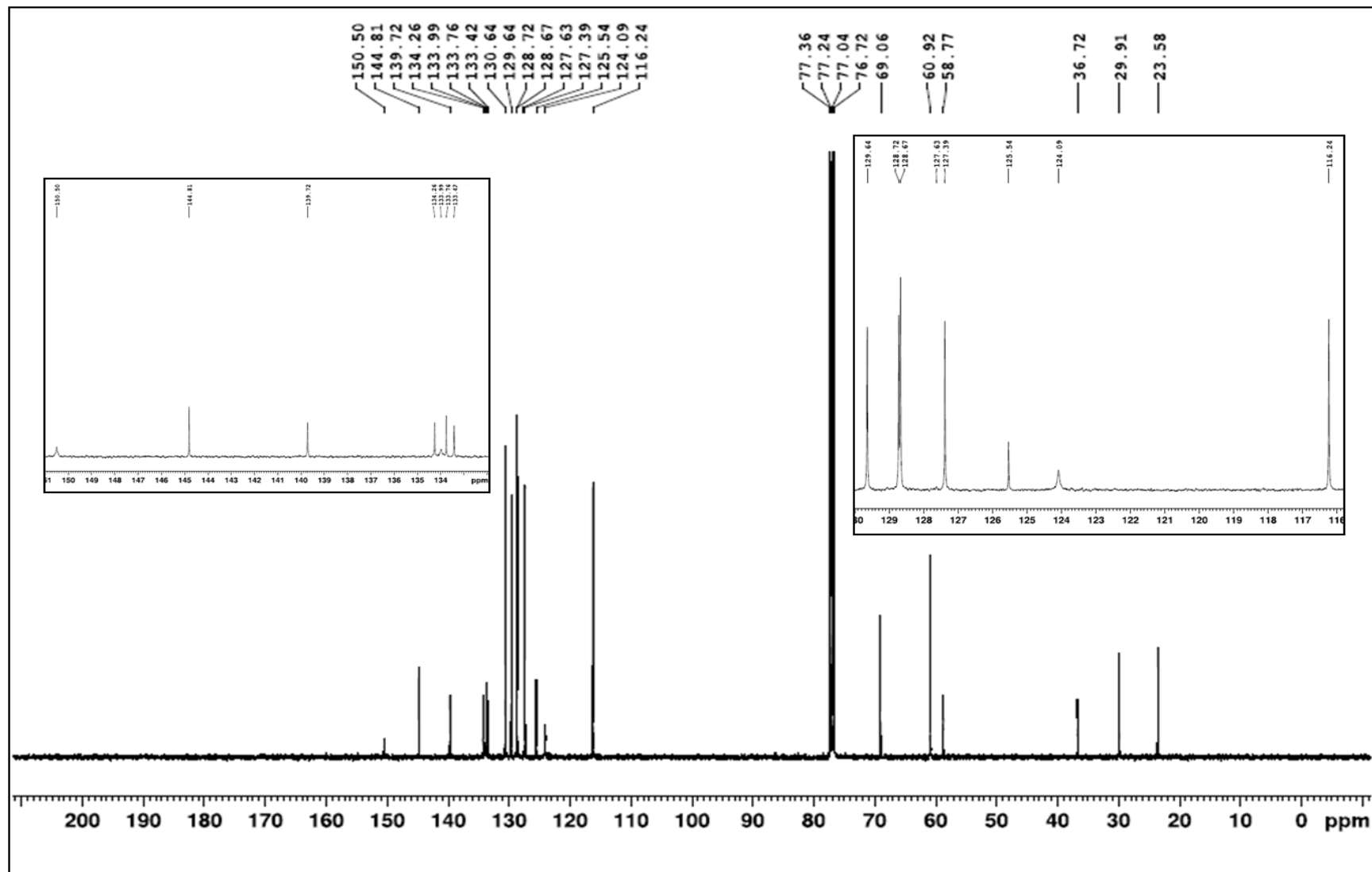


Fig. S26. ^{13}C -NMR spectrum of compound 14g in CDCl_3 .

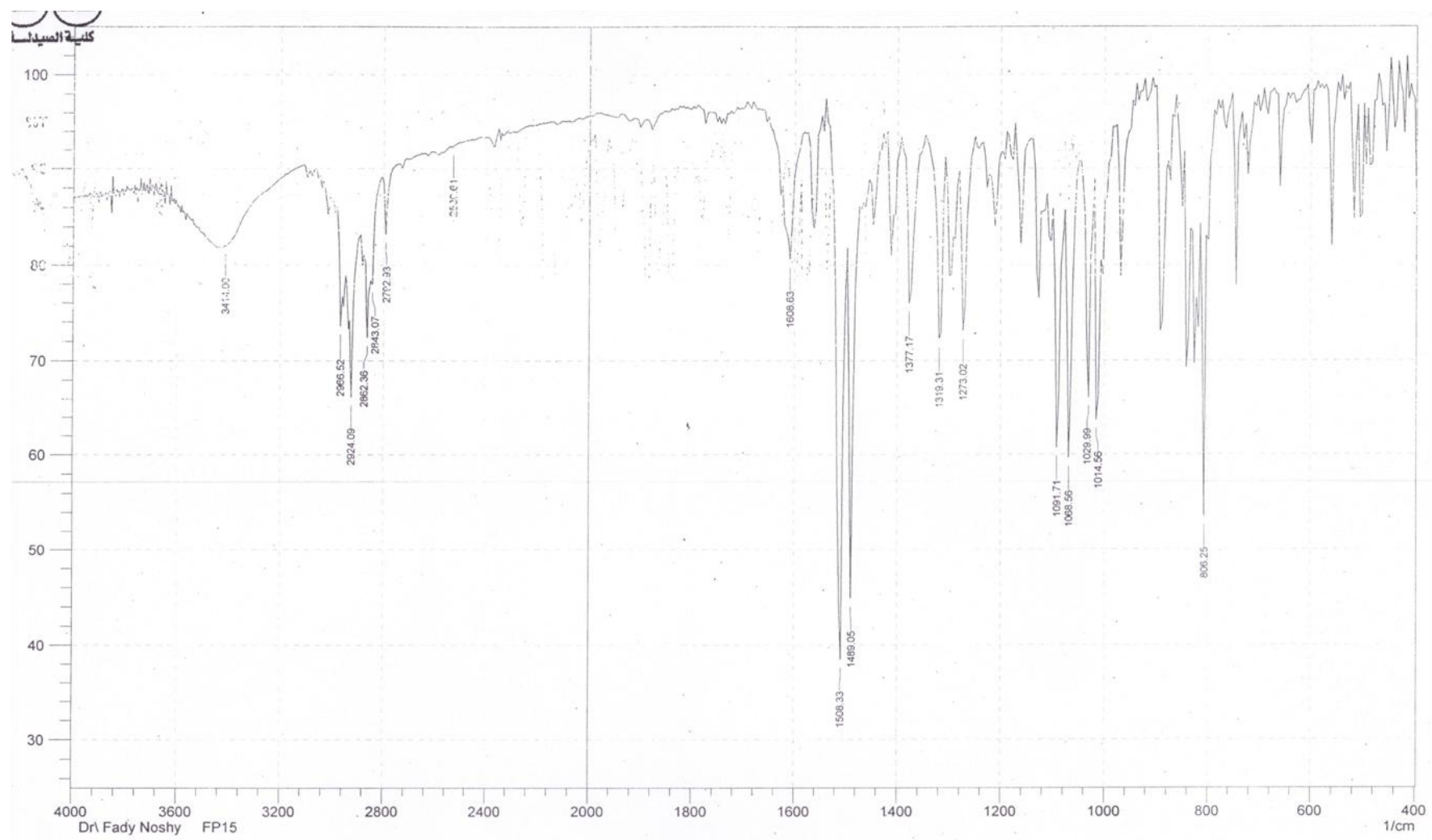


Fig. S27. IR spectrum of compound **14h** (KBr pellet).

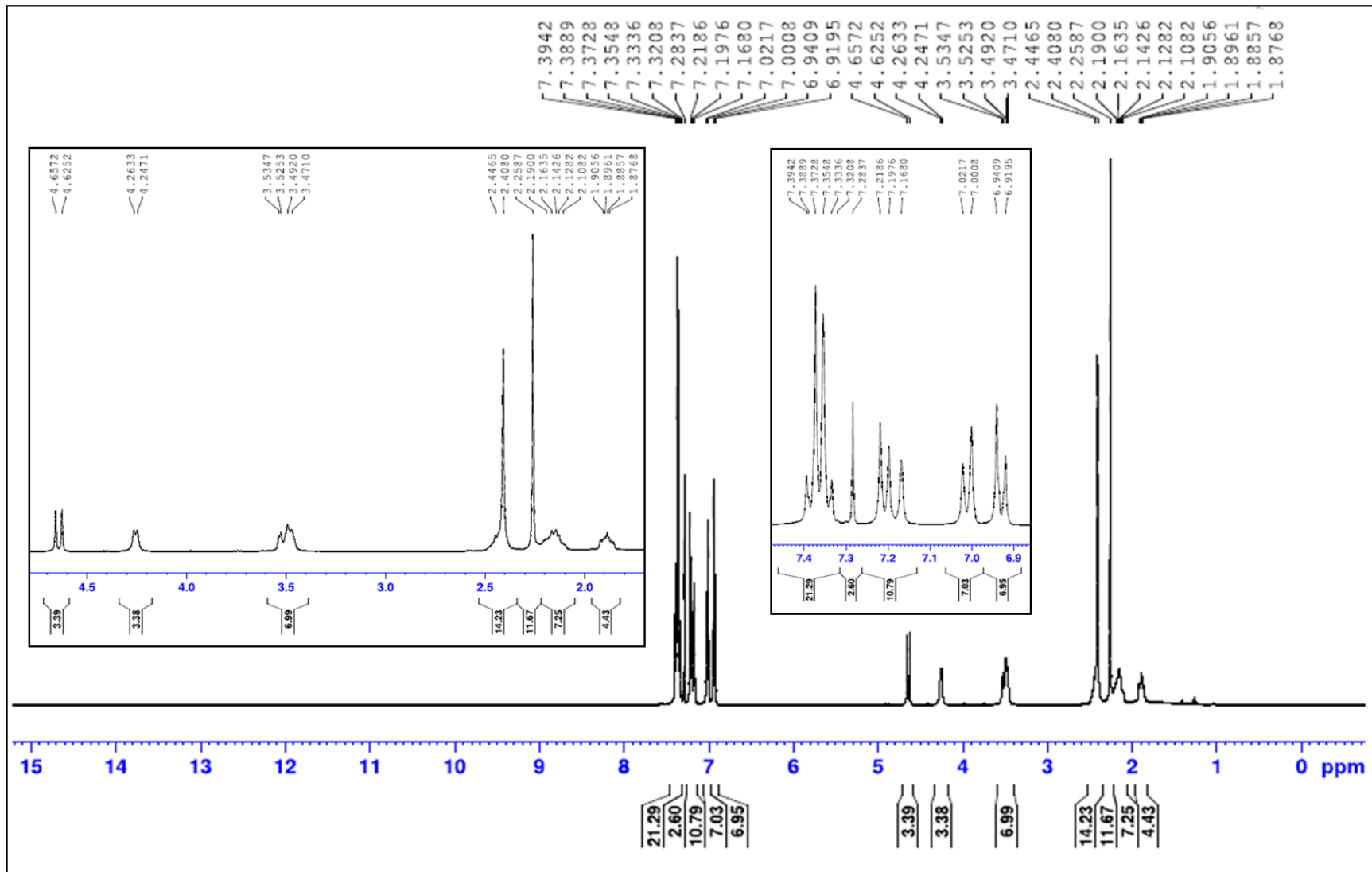


Fig. S28. ^1H -NMR spectrum of compound **14h** in CDCl_3 .

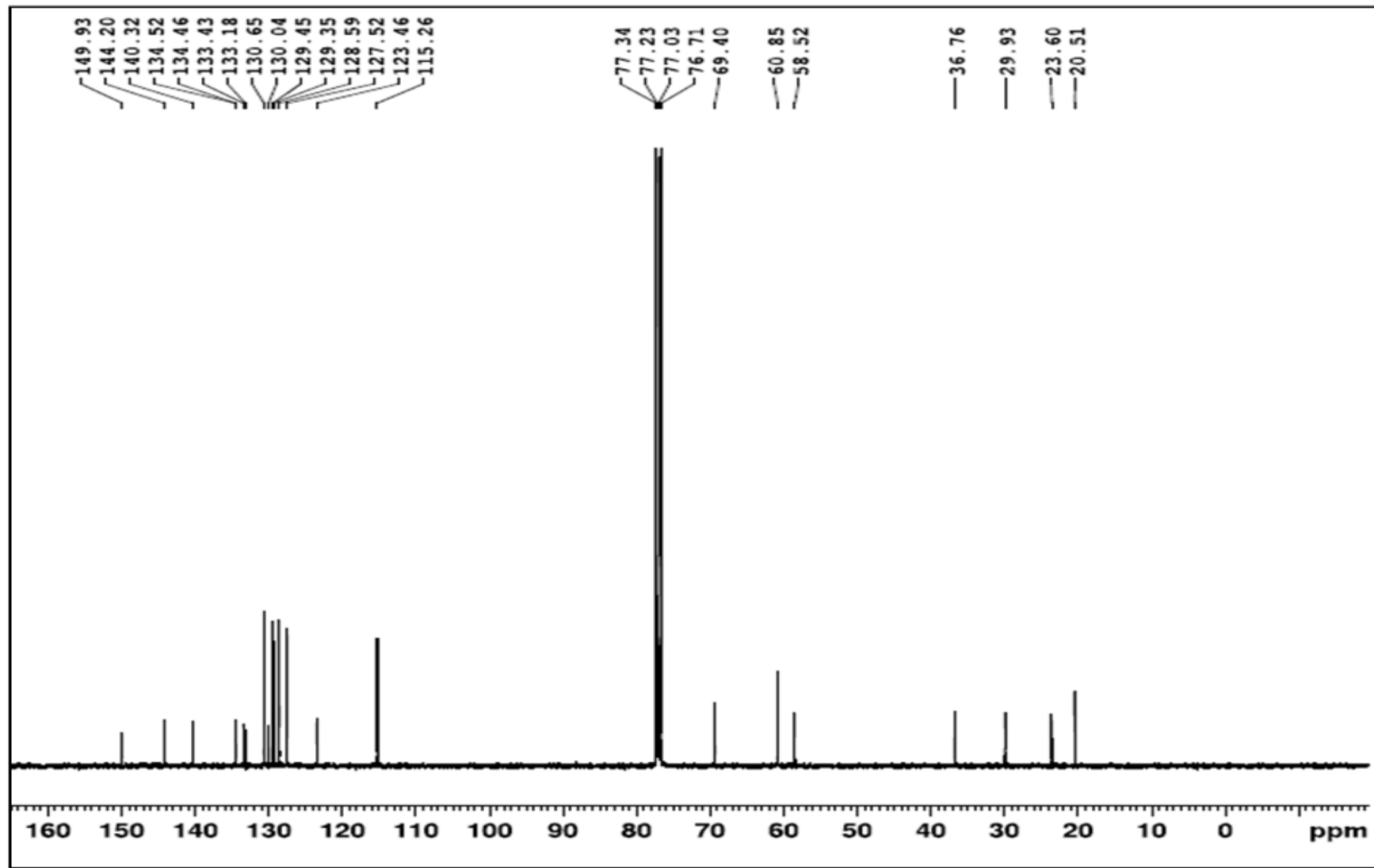


Fig. S29. ^{13}C -NMR spectrum of compound **14h** in CDCl_3 .

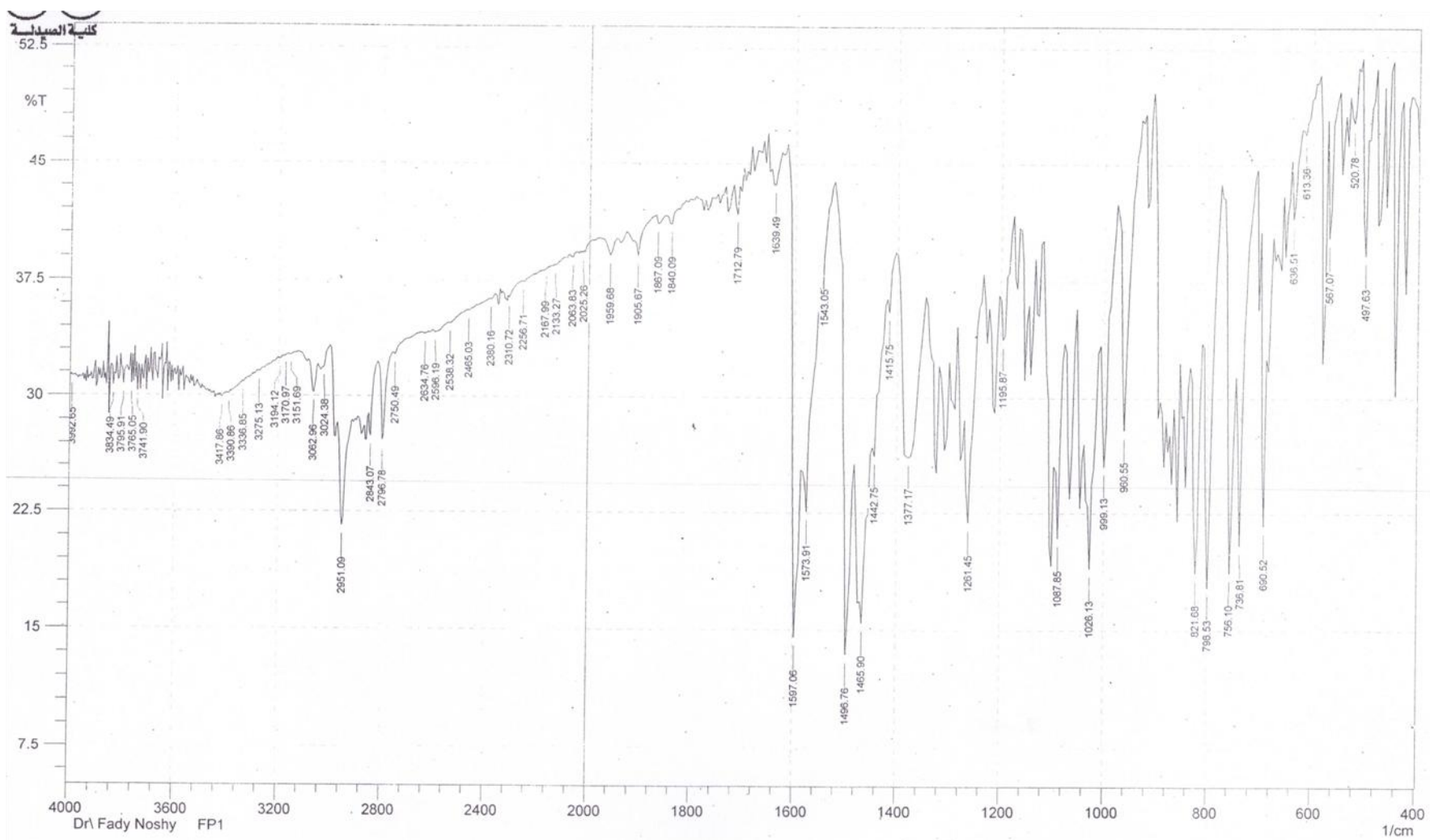


Fig. S30. IR spectrum of compound **14i** (KBr pellet).

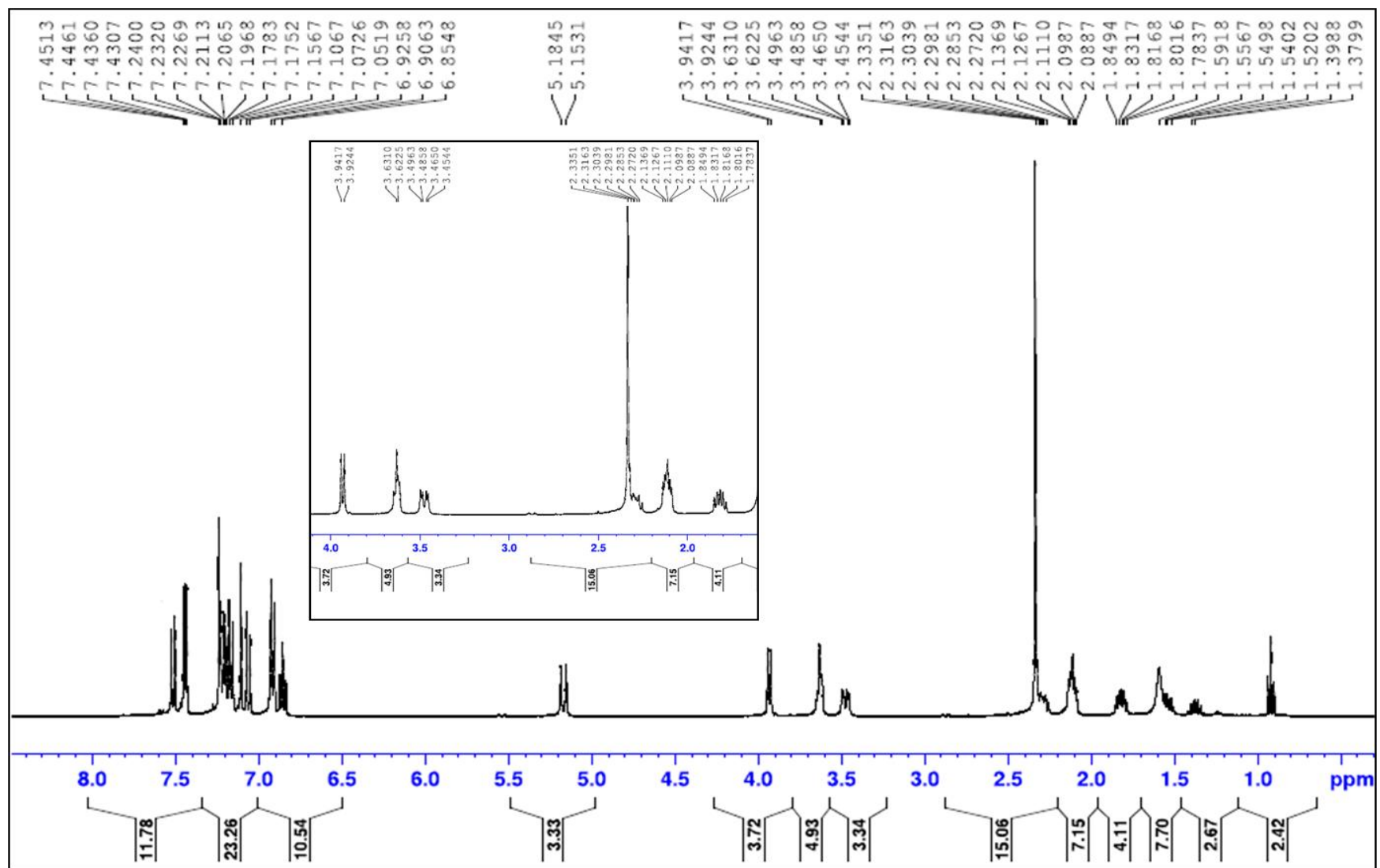


Fig. S31. ^1H -NMR spectrum of compound **14i** in CDCl_3 .

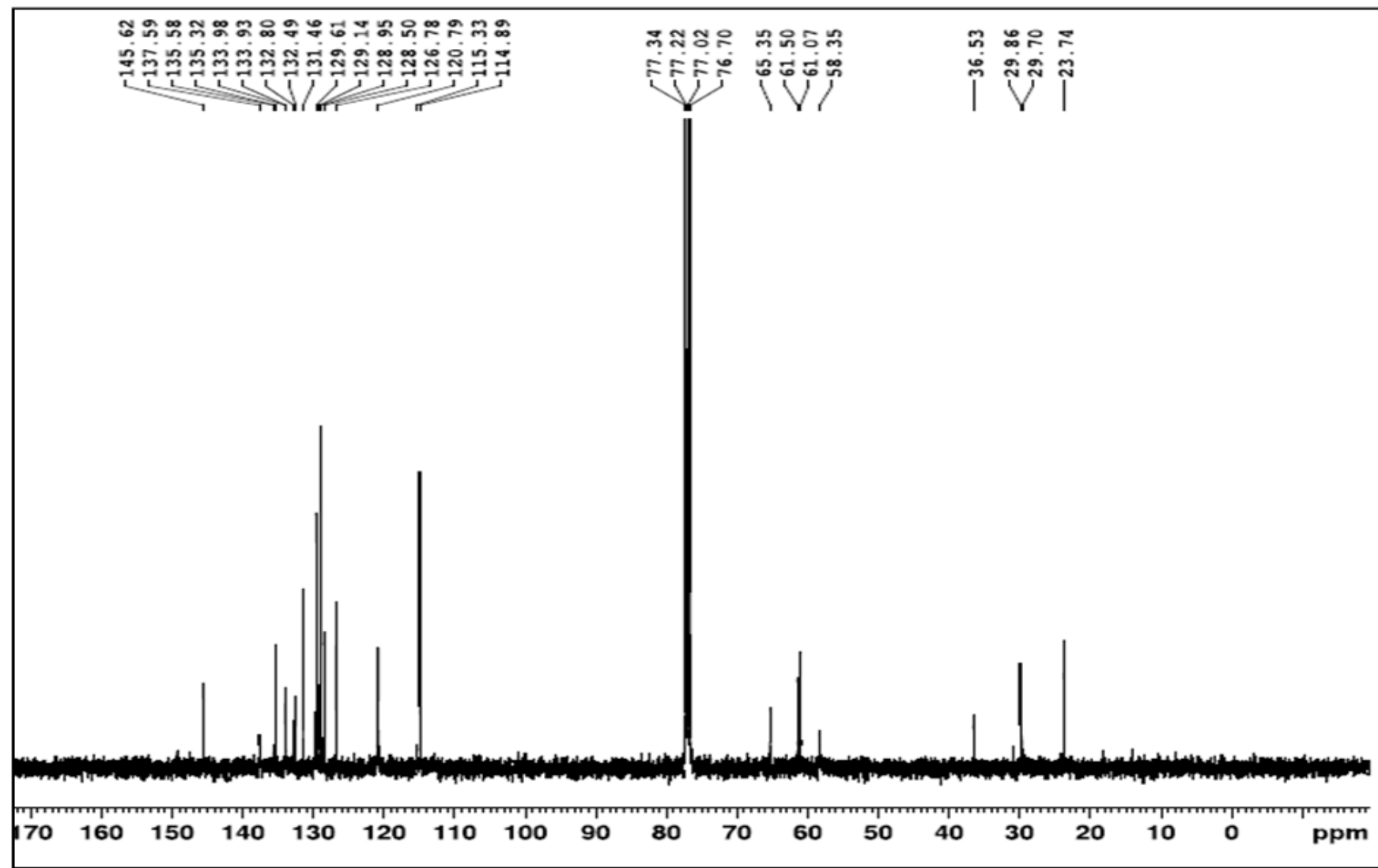


Fig. S32. ^{13}C -NMR spectrum of compound **14i** in CDCl_3 .

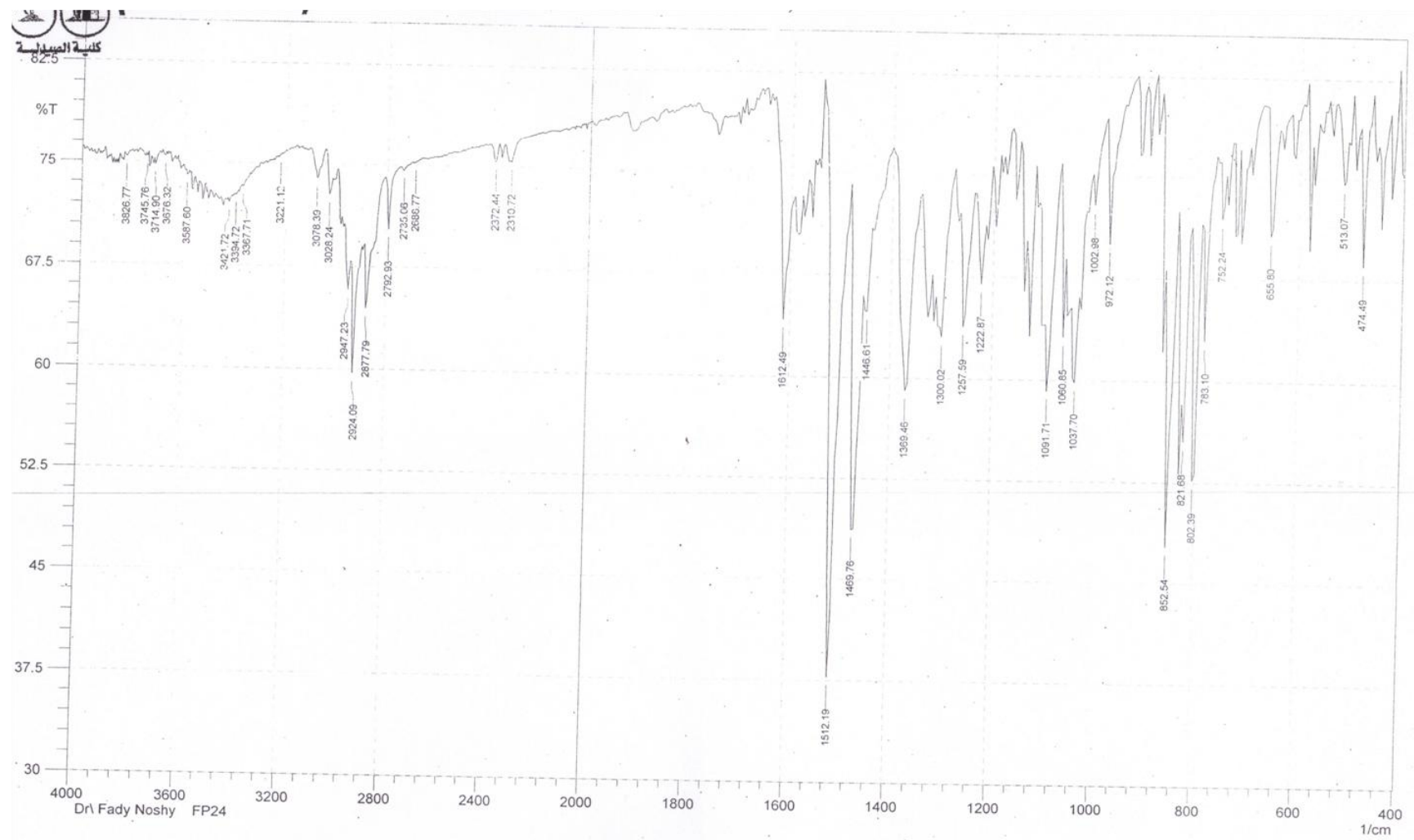


Fig. S33. IR spectrum of compound **14j** (KBr pellet).

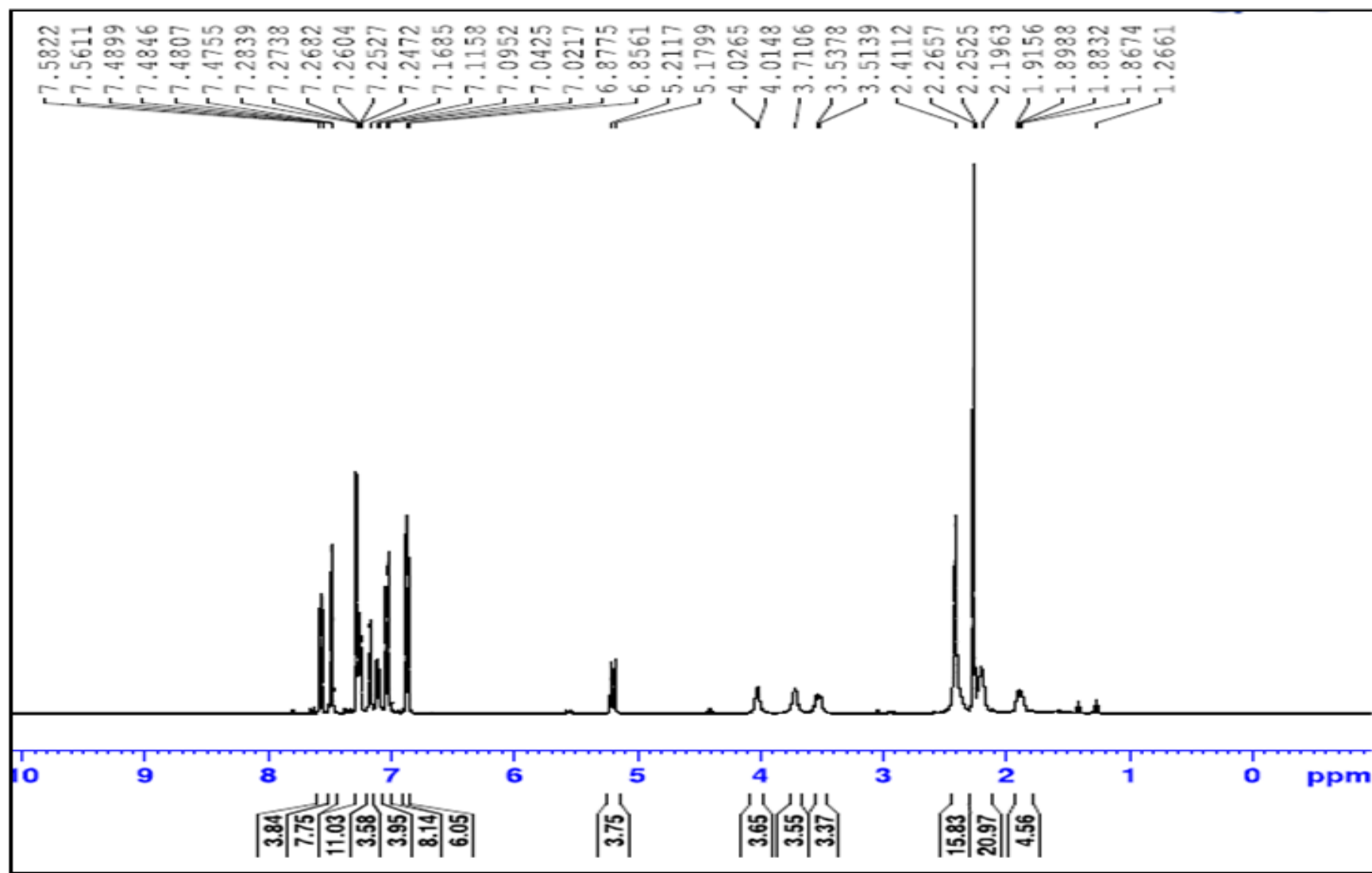


Fig. S34. ¹H-NMR spectrum of compound 14j in CDCl_3 .

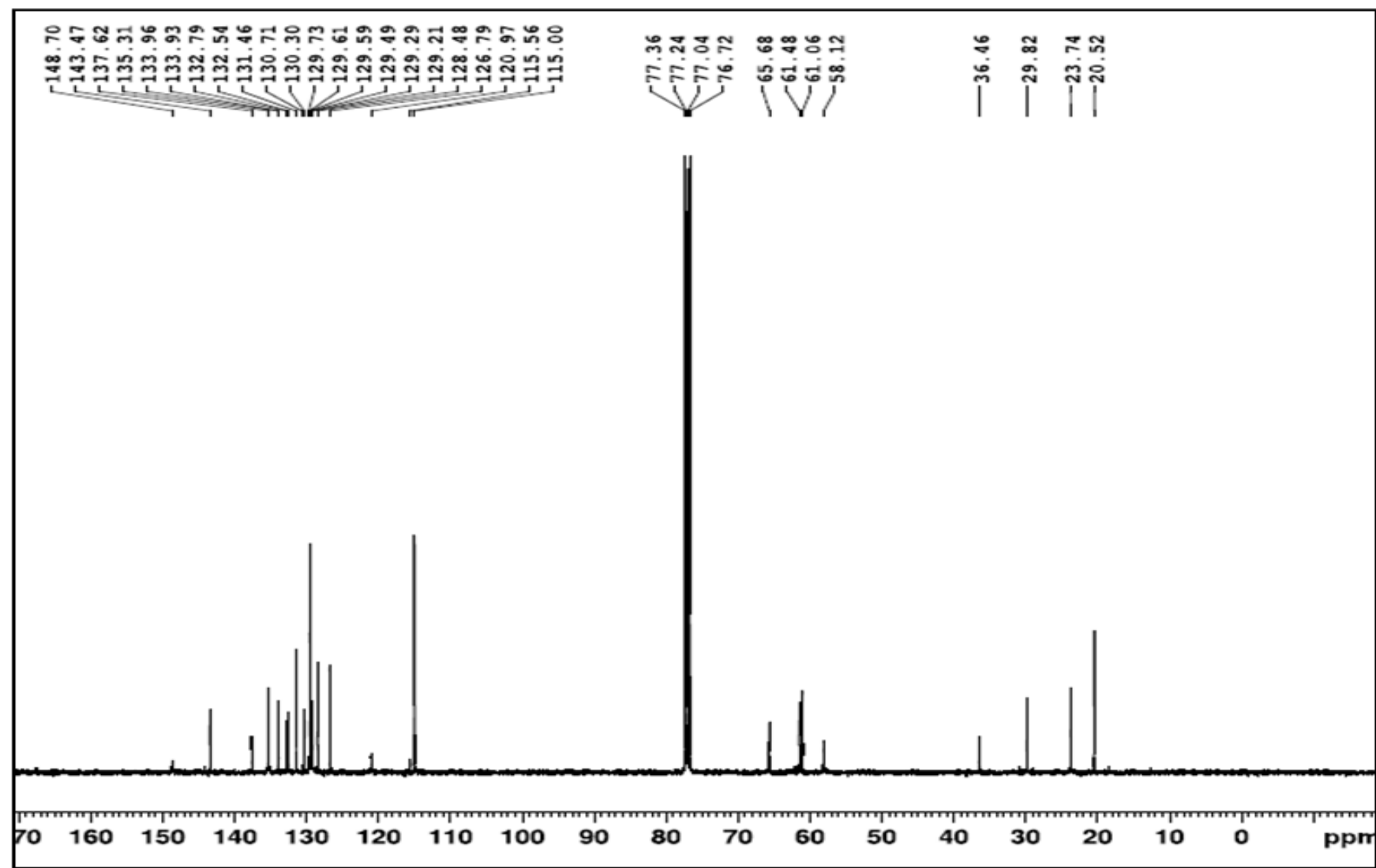


Fig. S35. ^{13}C -NMR spectrum of compound **14j** in CDCl_3 .

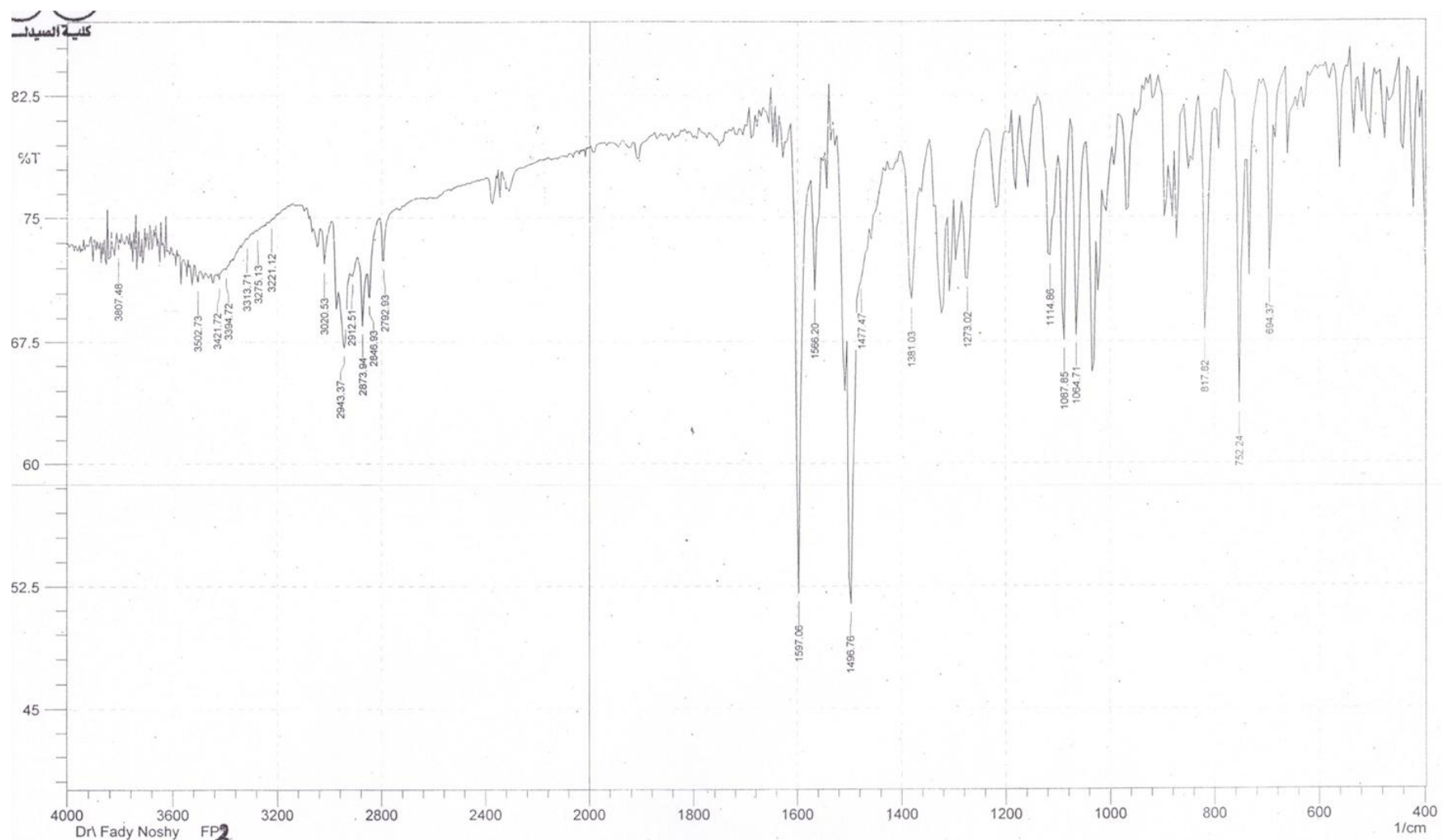


Fig. S36. IR spectrum of compound **14k** (KBr pellet).

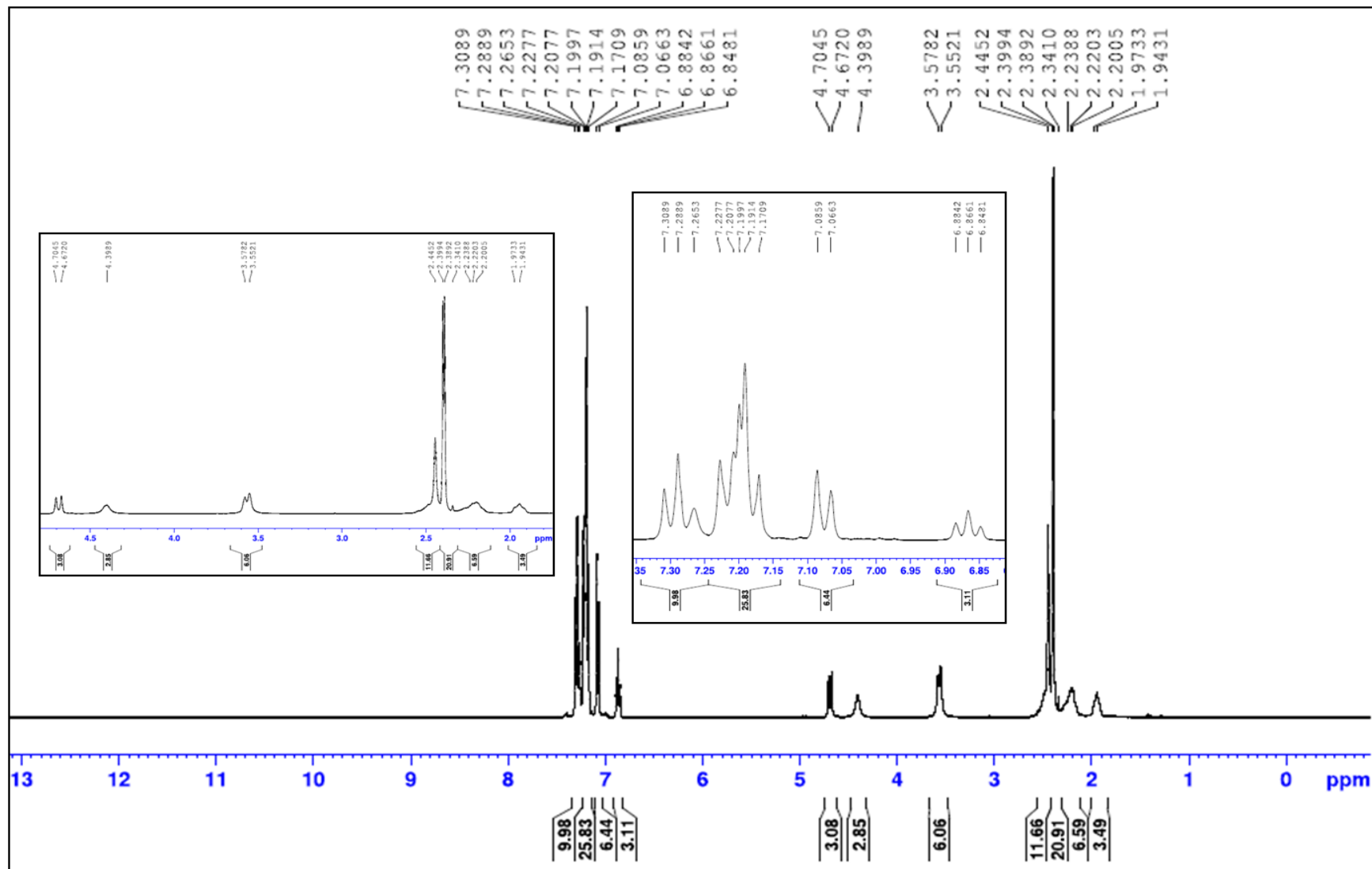


Fig. S37. ^1H -NMR spectrum of compound **14k** in CDCl_3 .

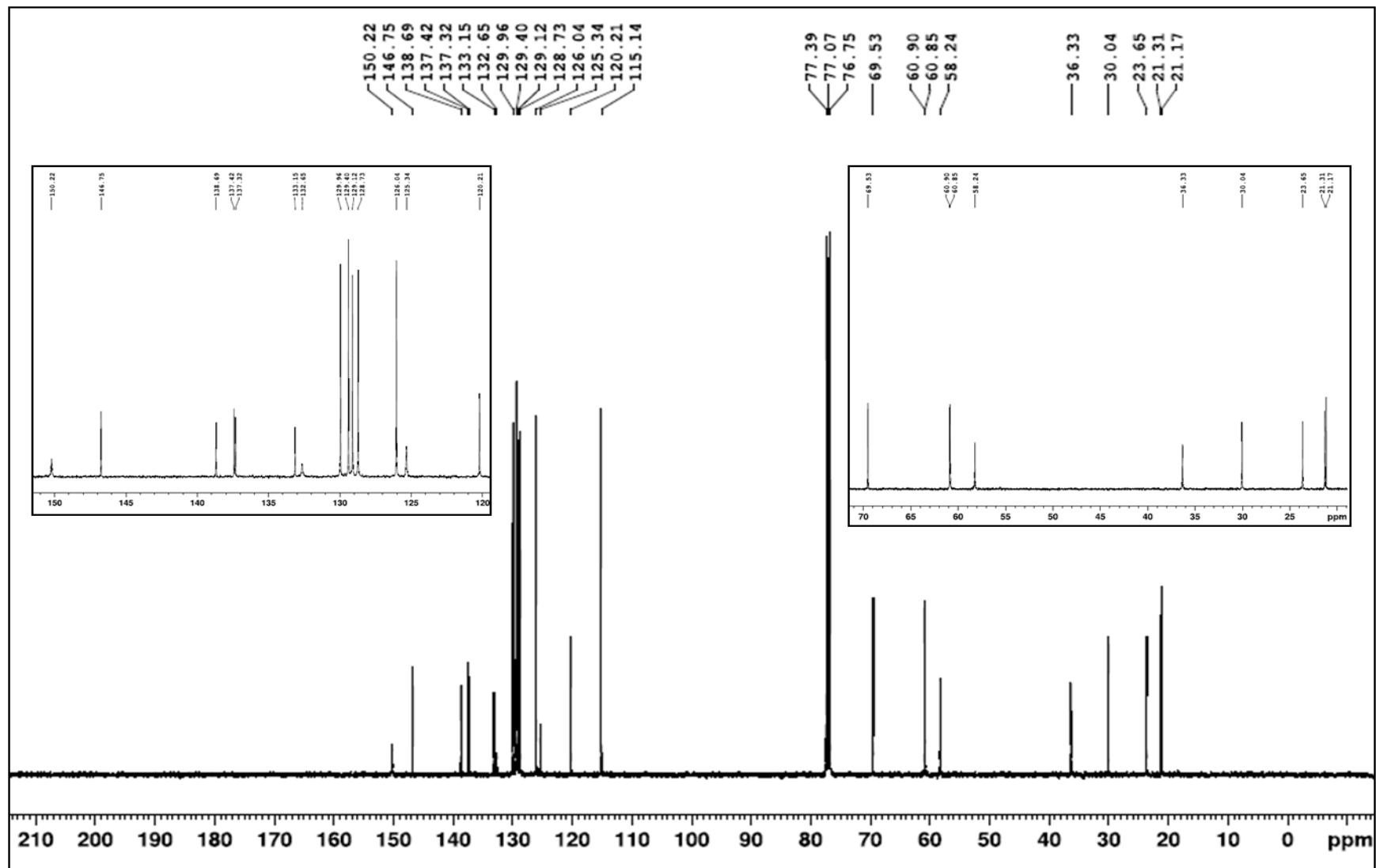


Fig. S38. ^{13}C -NMR spectrum of compound **14k** in CDCl_3 .

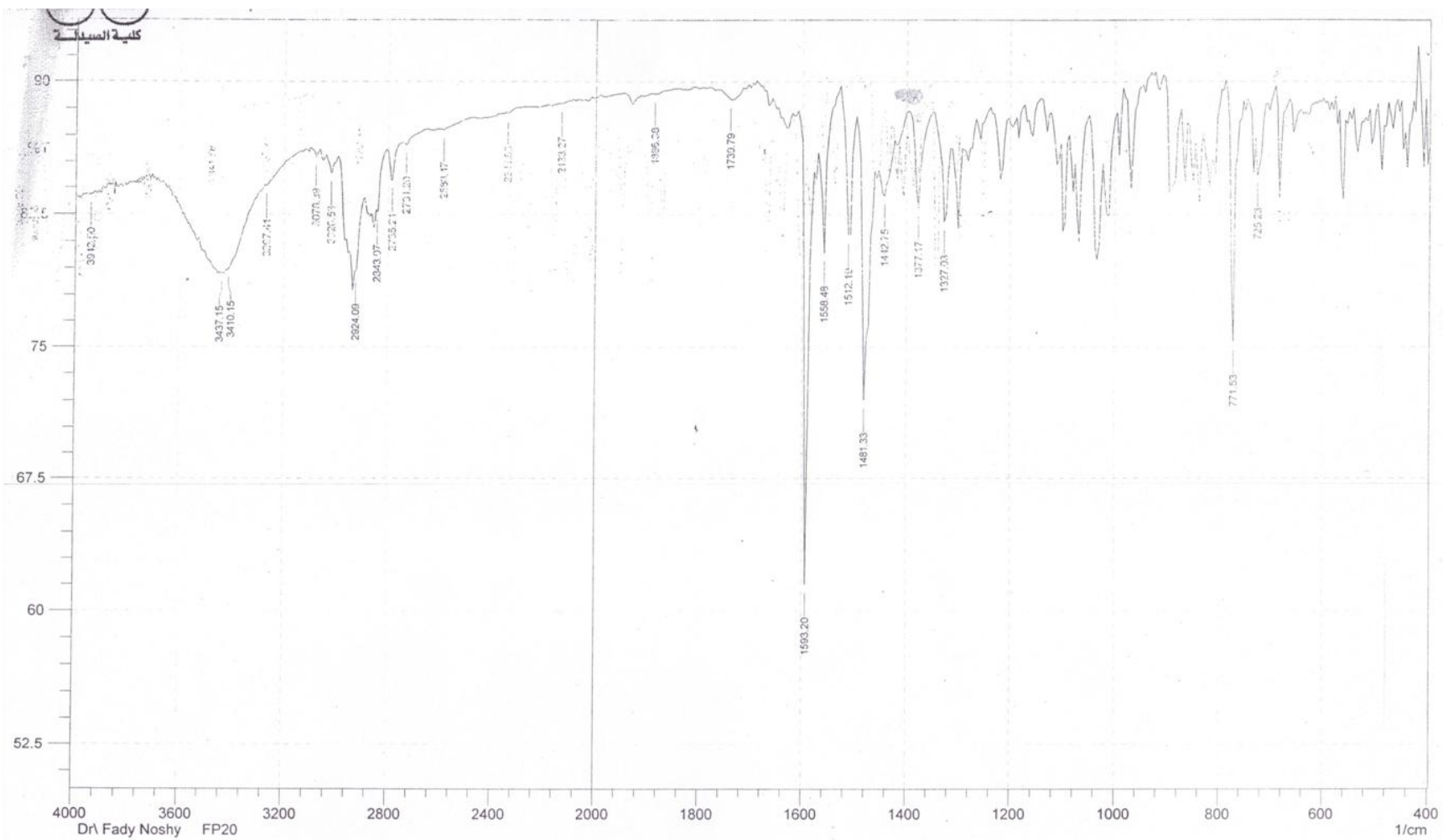


Fig. S39. IR spectrum of compound **14l** (KBr pellet).

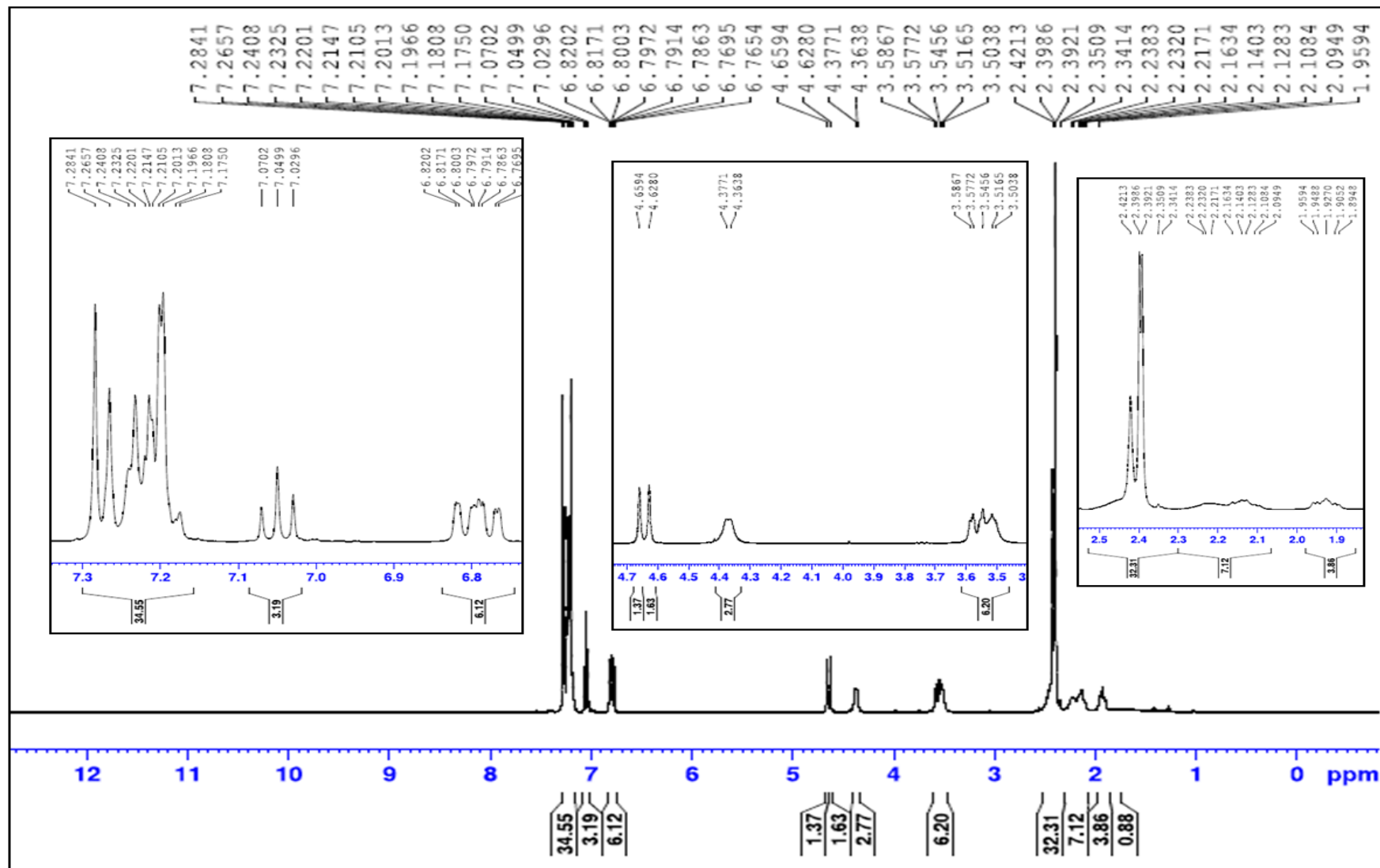


Fig. S40. ^1H -NMR spectrum of compound **14l** in CDCl_3 .

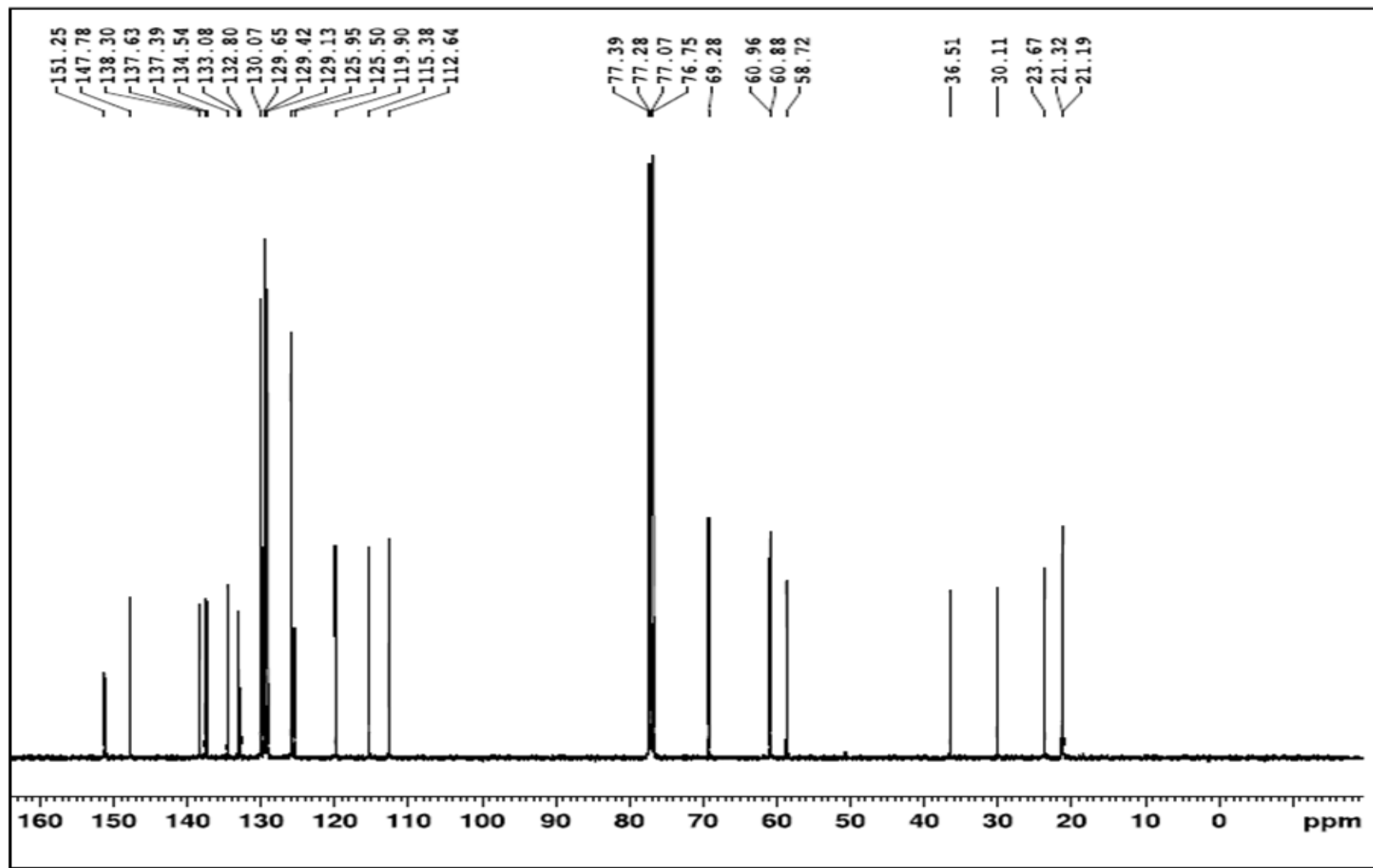


Fig. S41. ^{13}C -NMR spectrum of compound **14l** in CDCl_3 .

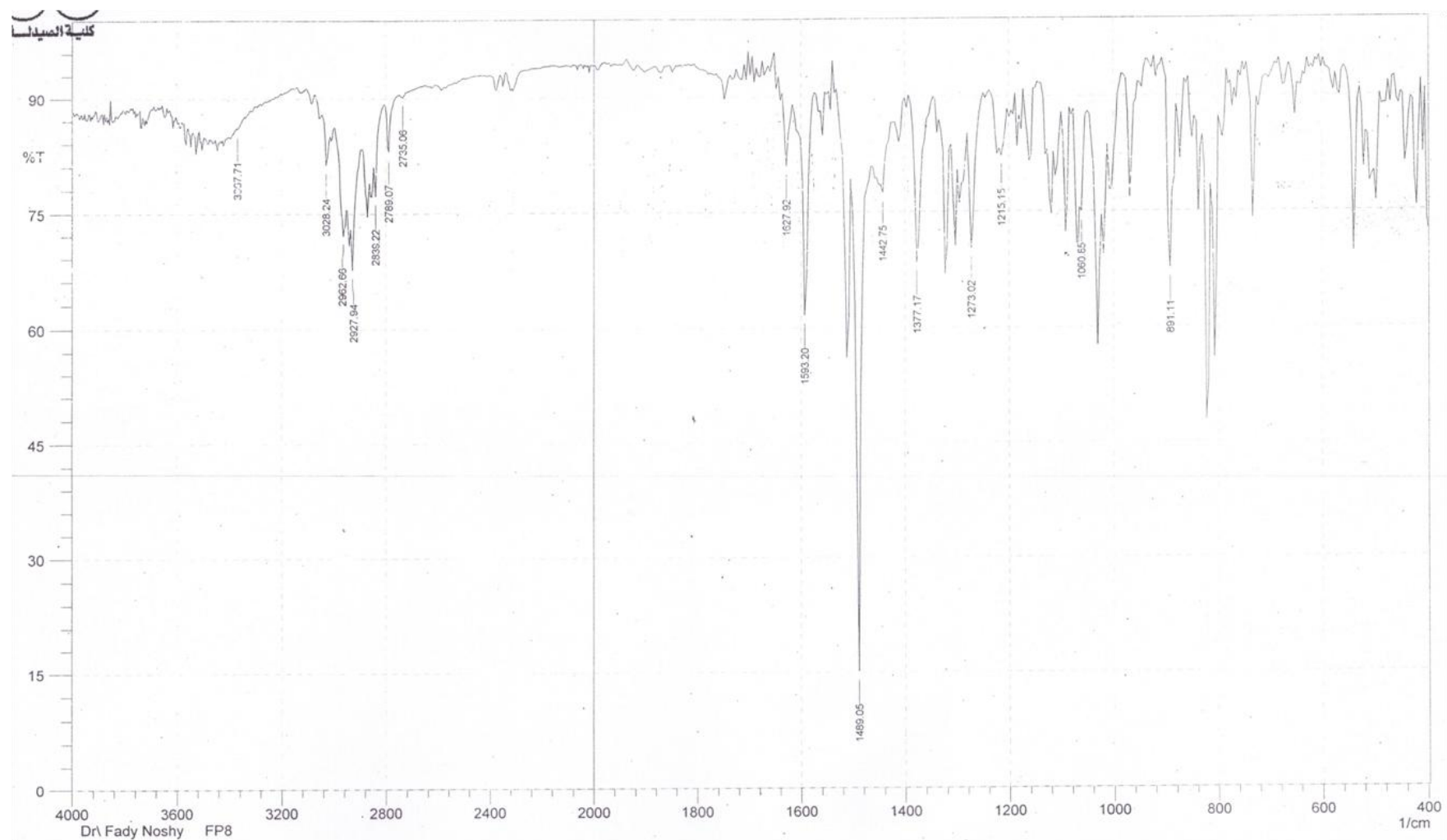


Fig. S42. IR spectrum of compound **14m** (KBr pellet).

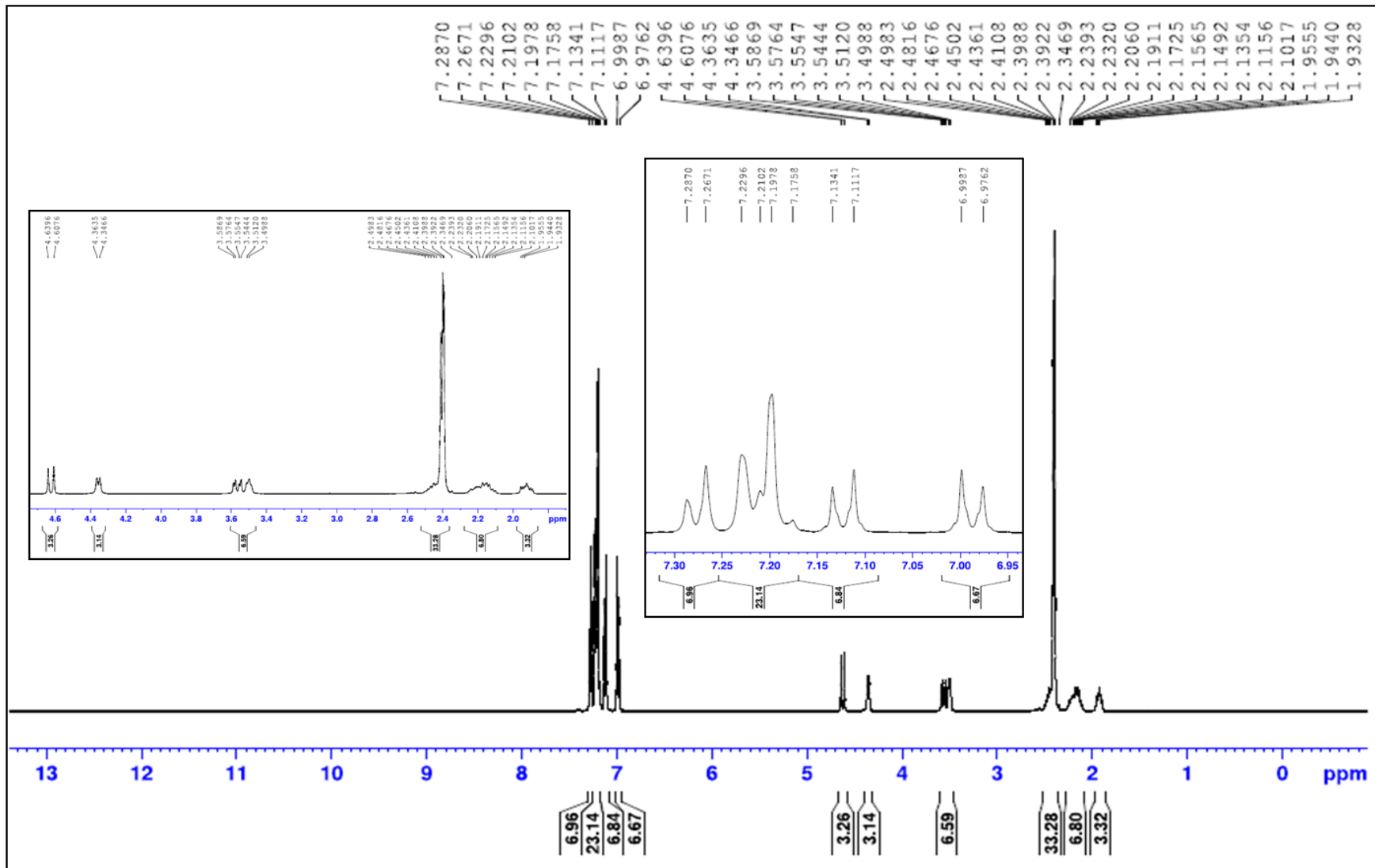


Fig. S43. ^1H -NMR spectrum of compound **14m** in CDCl_3 .

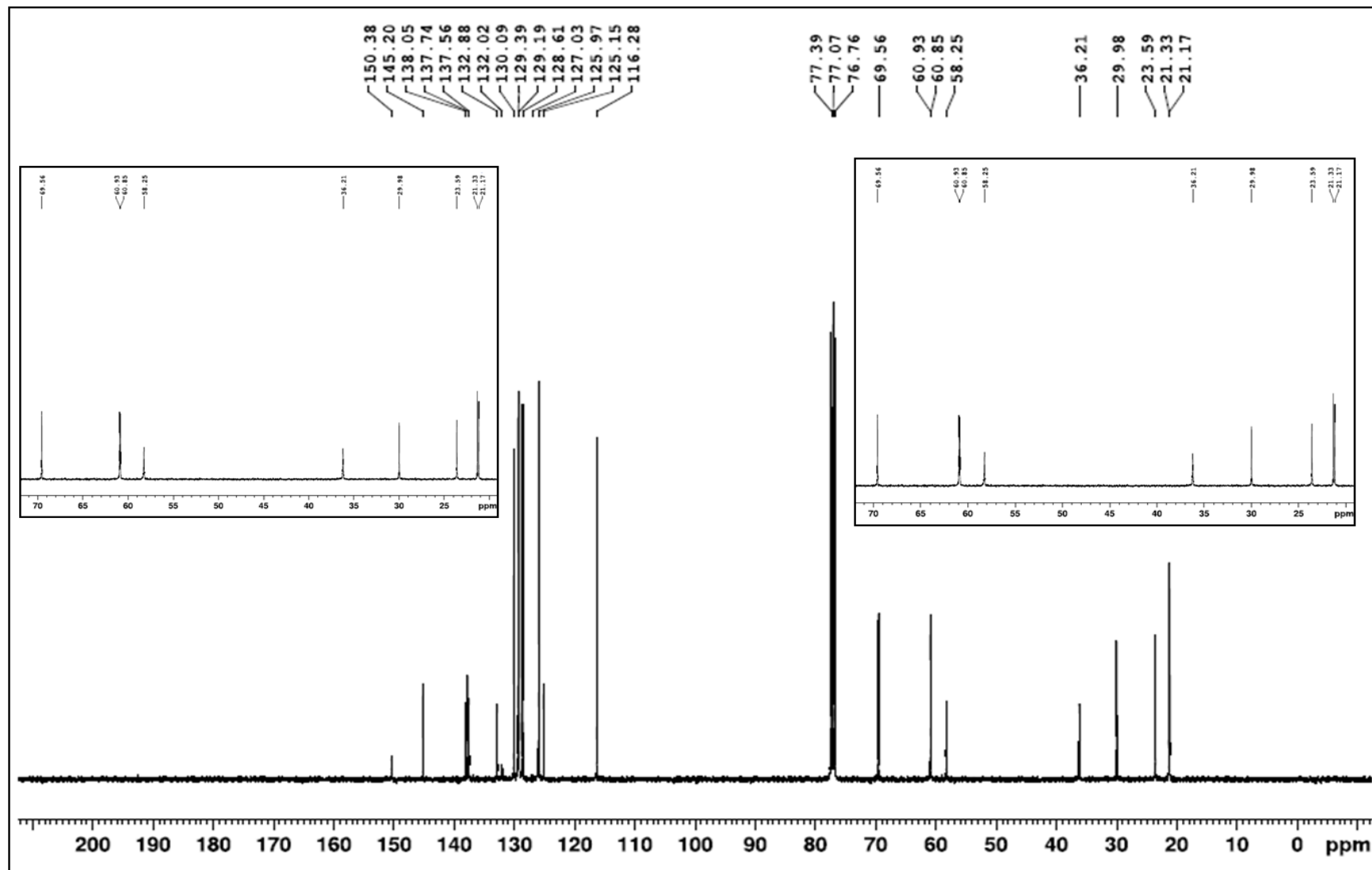


Fig. S44. ^{13}C -NMR spectrum of compound **14m** in CDCl_3 .

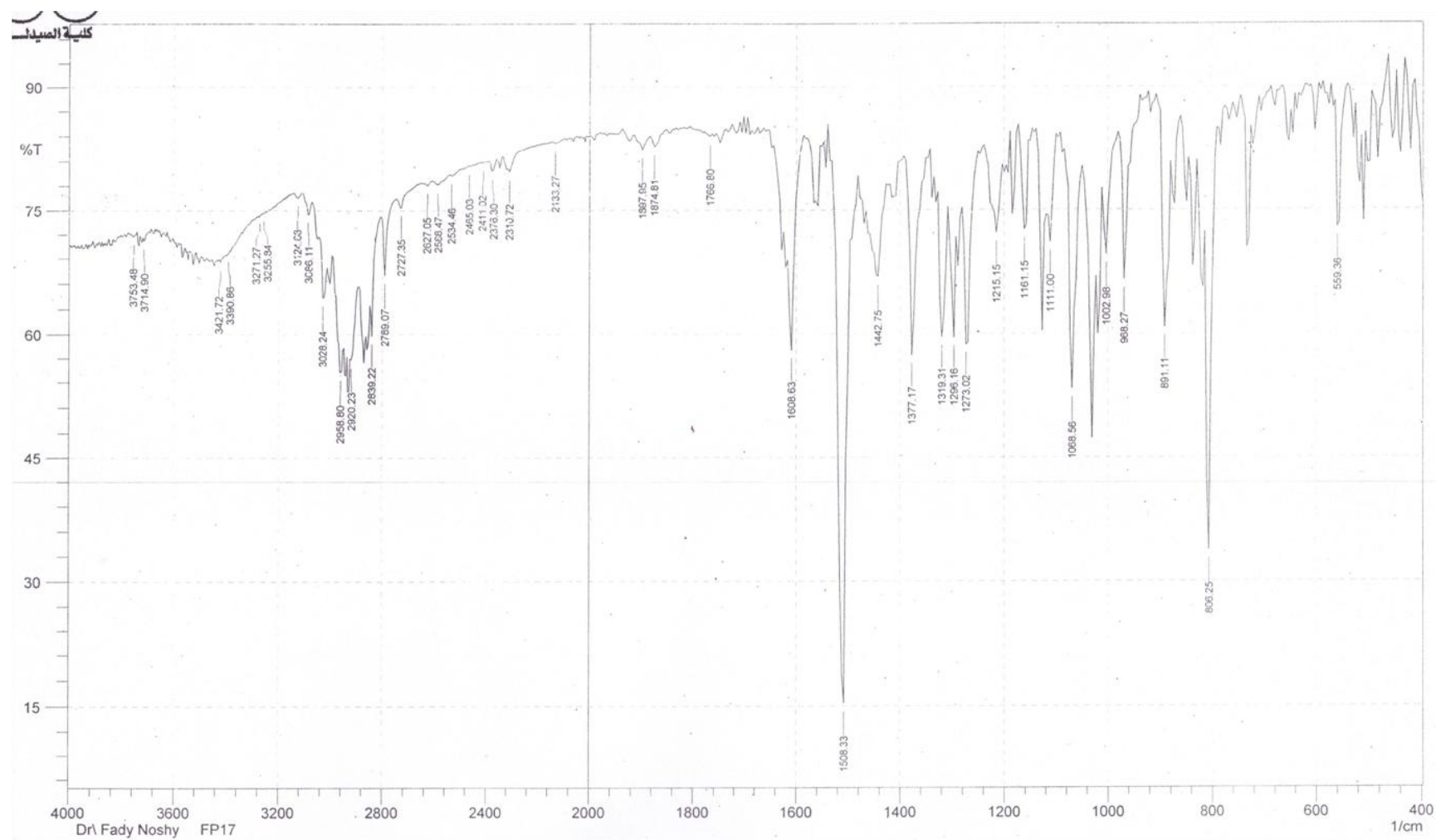


Fig. S45. IR spectrum of compound **14n** (KBr pellet).

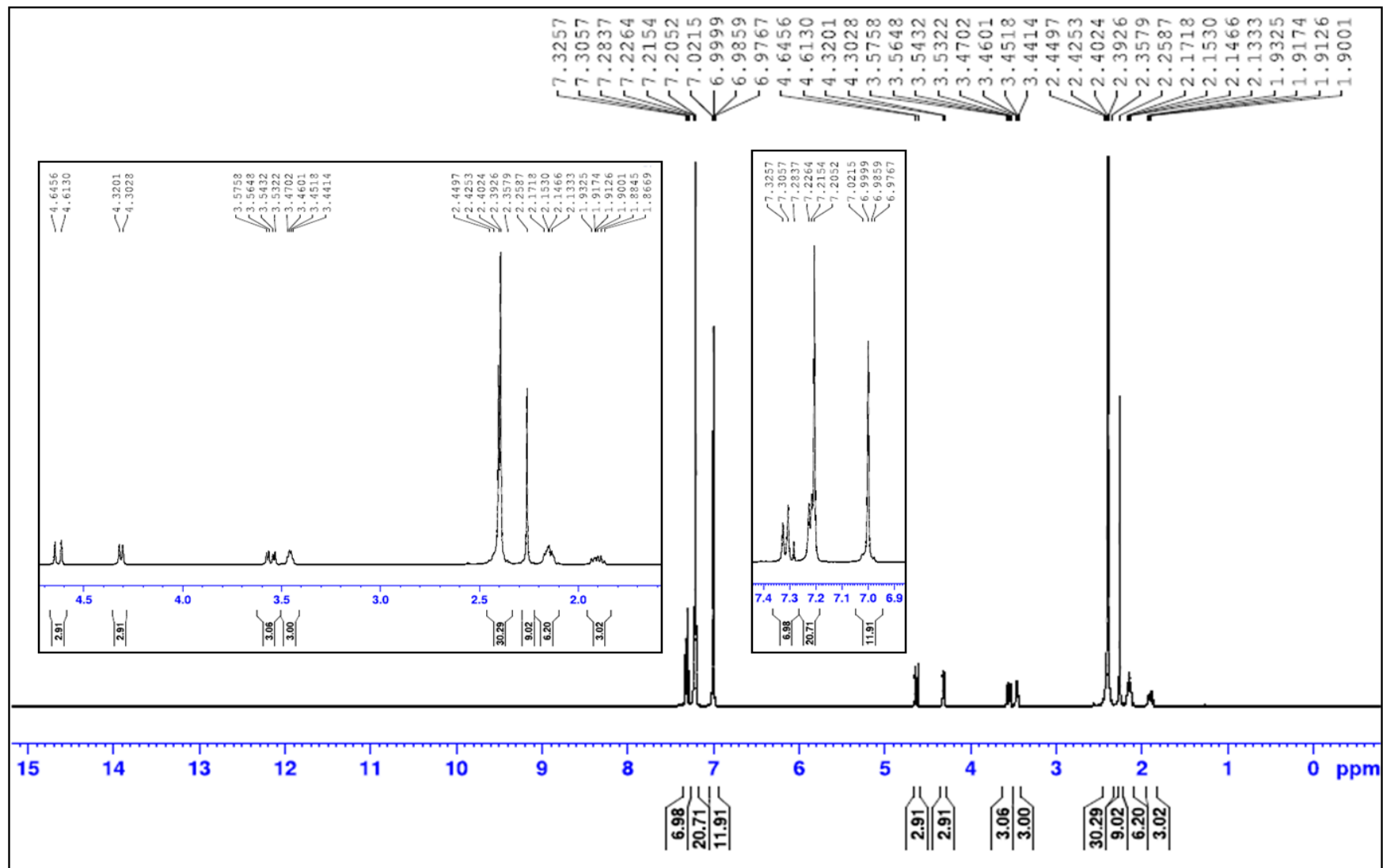


Fig. S46. ^1H -NMR spectrum of compound **14n** in CDCl_3 .

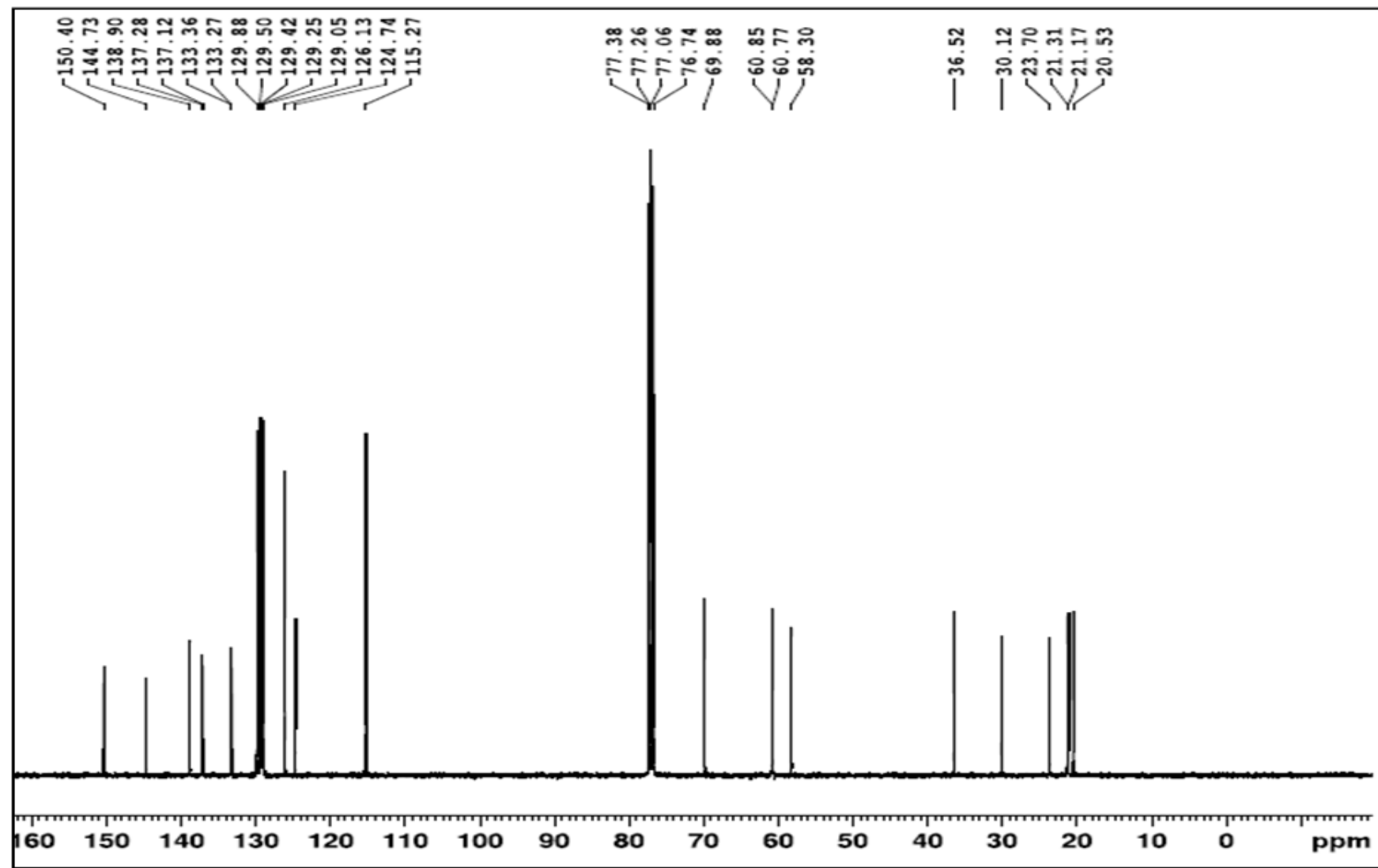


Fig. S47. ^{13}C -NMR spectrum of compound **14n** in CDCl_3 .

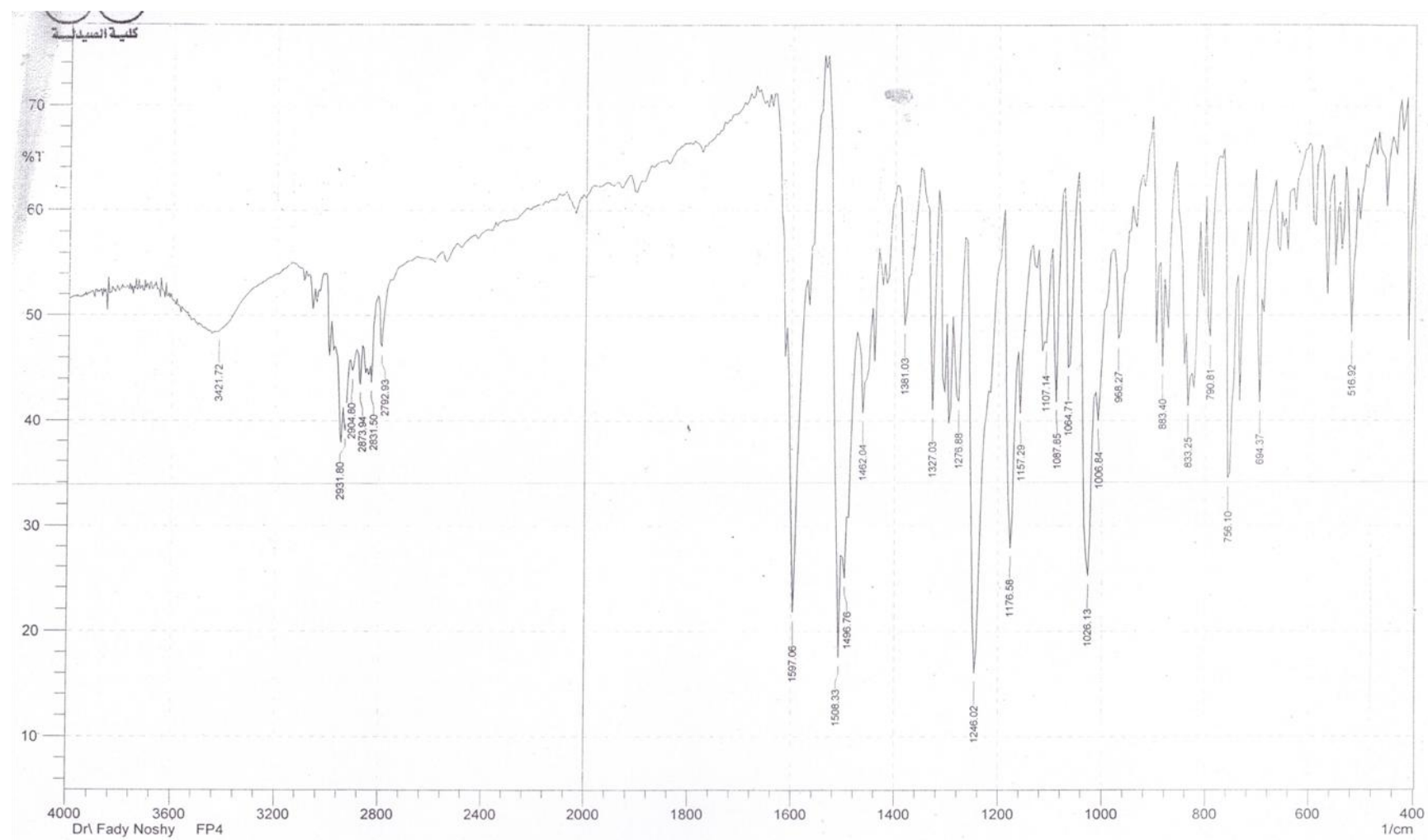


Fig. S48. IR spectrum of compound **14o** (KBr pellet).

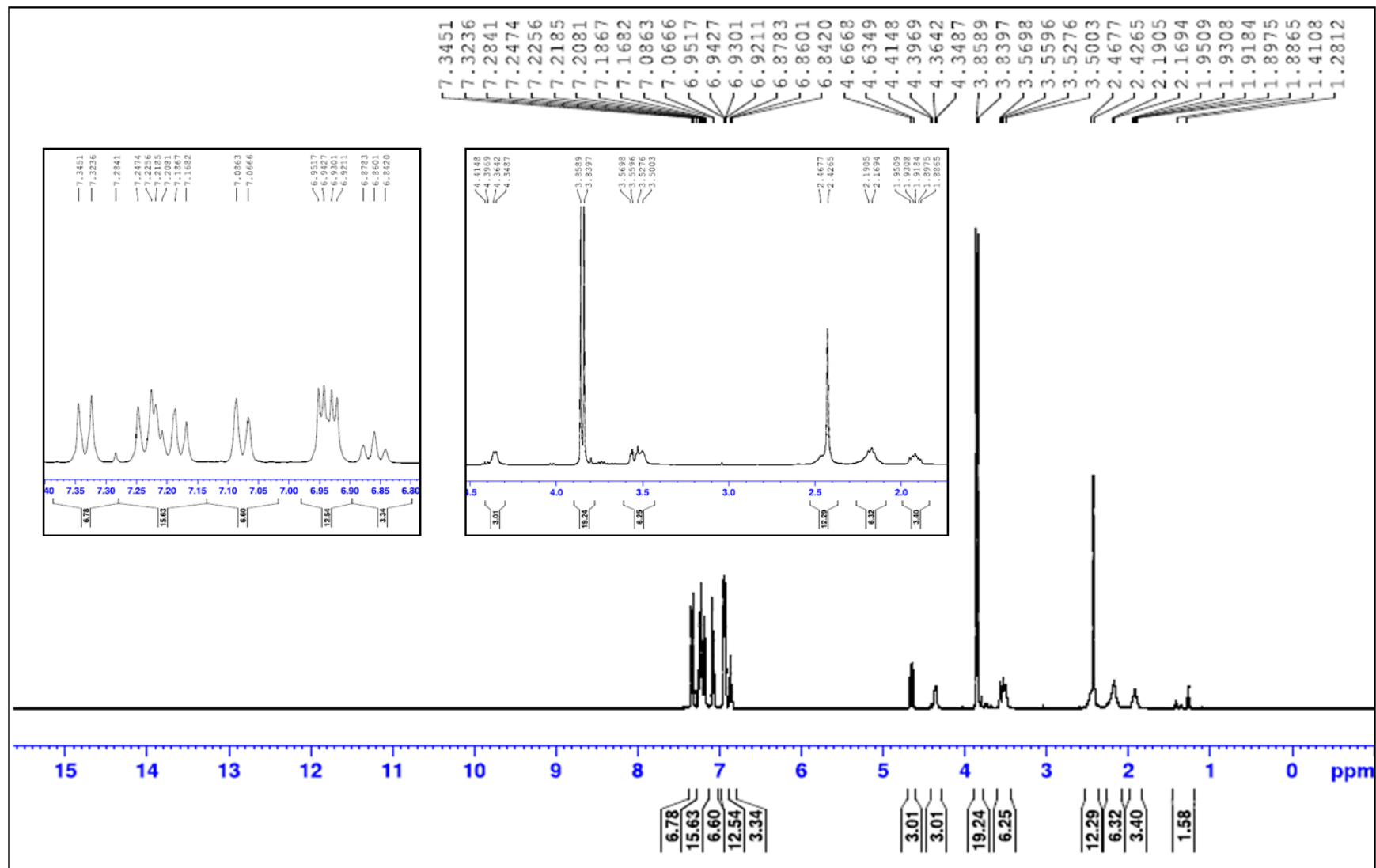


Fig. S49. ^1H -NMR spectrum of compound **14o** in CDCl_3 .

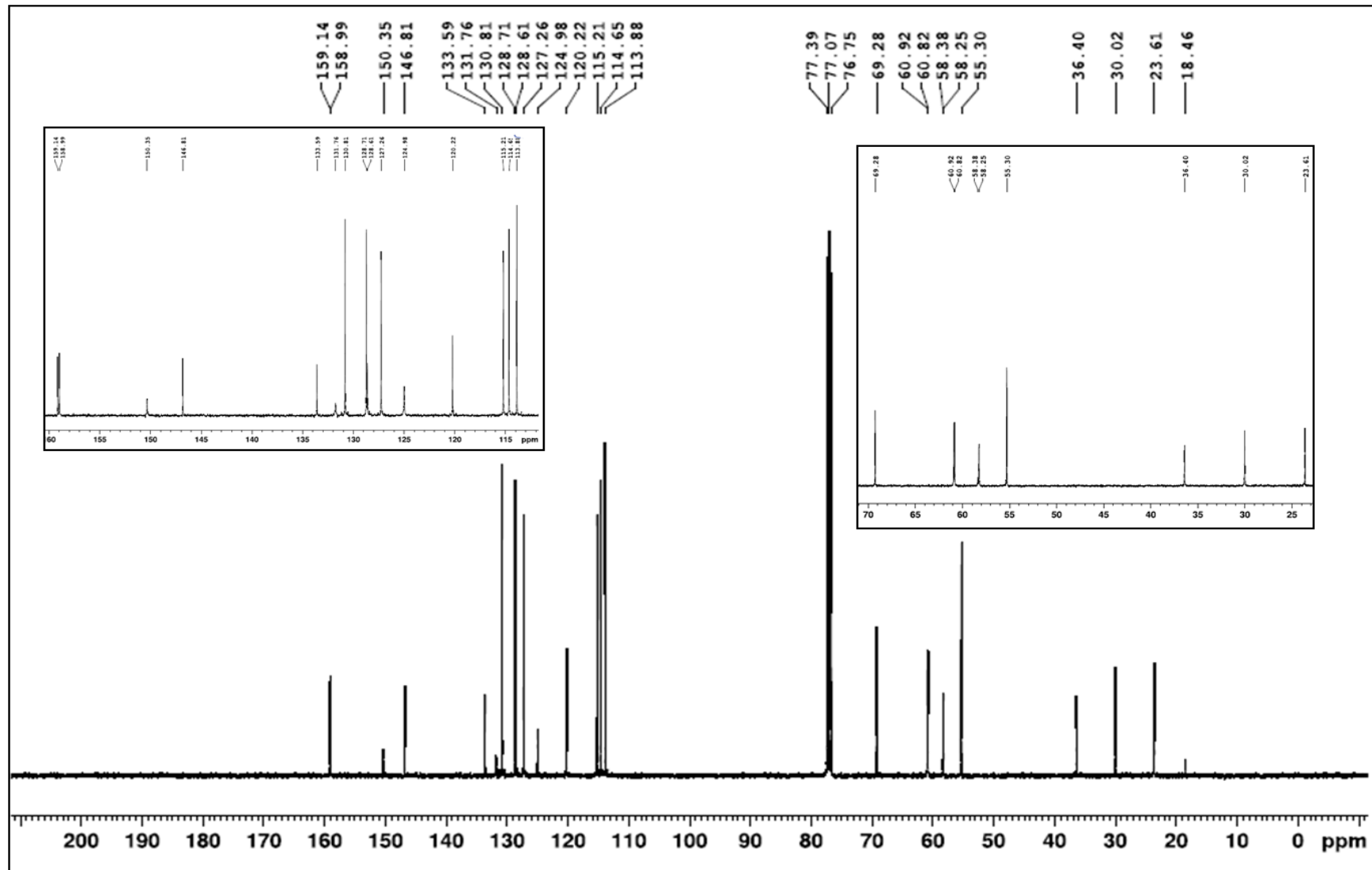


Fig. S50. ^{13}C -NMR spectrum of compound **14o** in CDCl_3 .

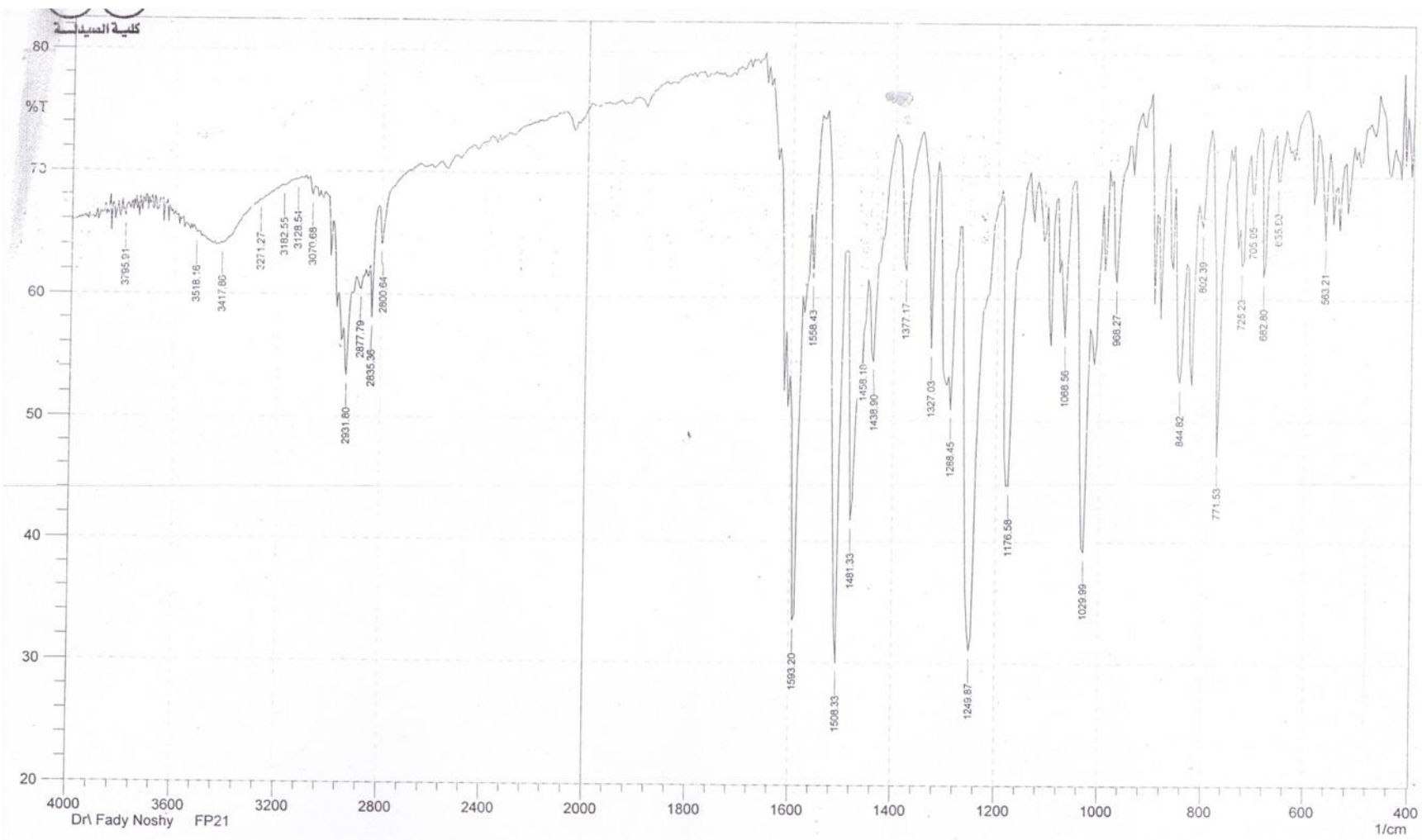


Fig. S51. IR spectrum of compound **14p** (KBr pellet).

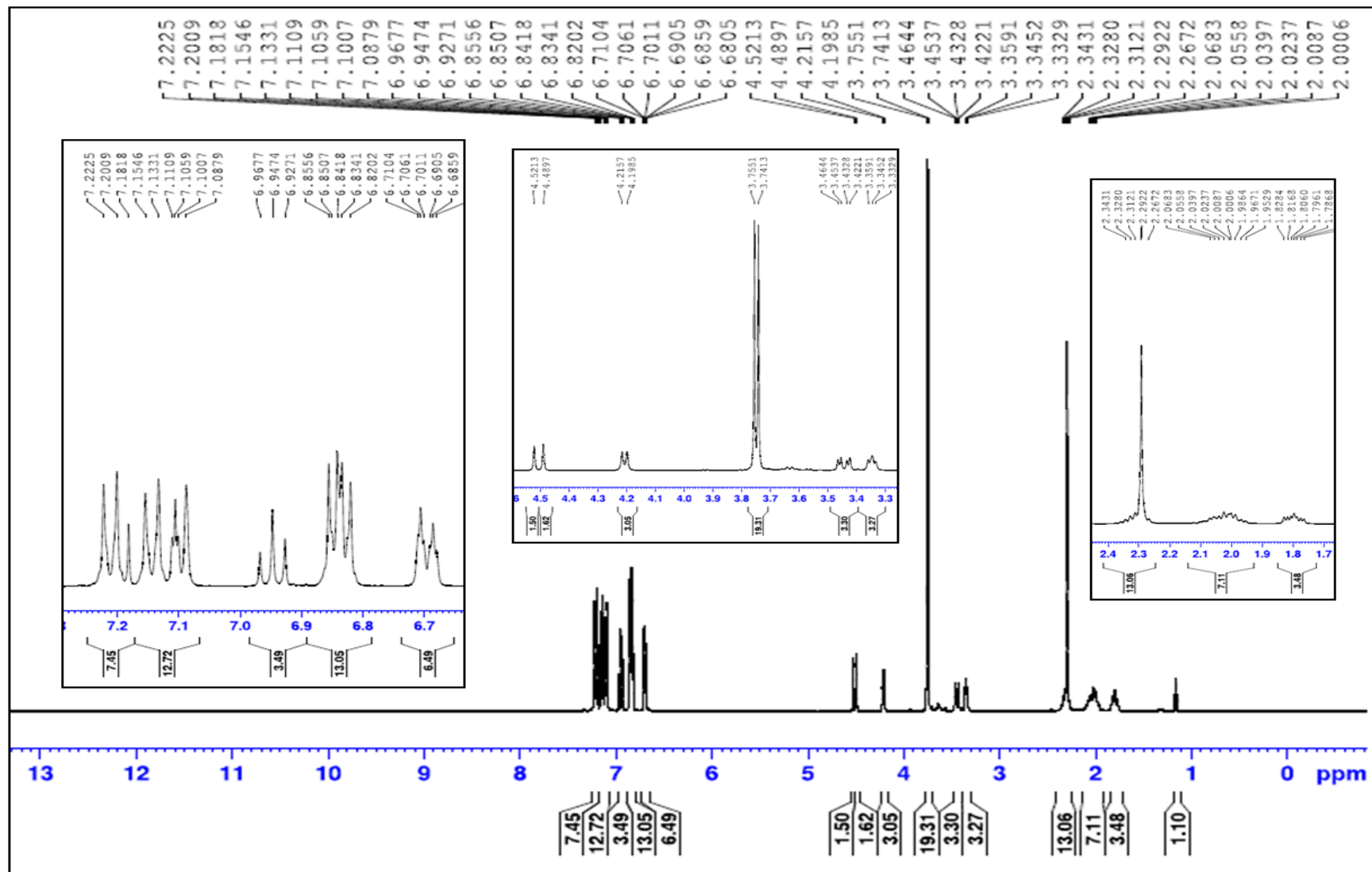


Fig. S52. ^1H -NMR spectrum of compound **14p** in CDCl_3 .

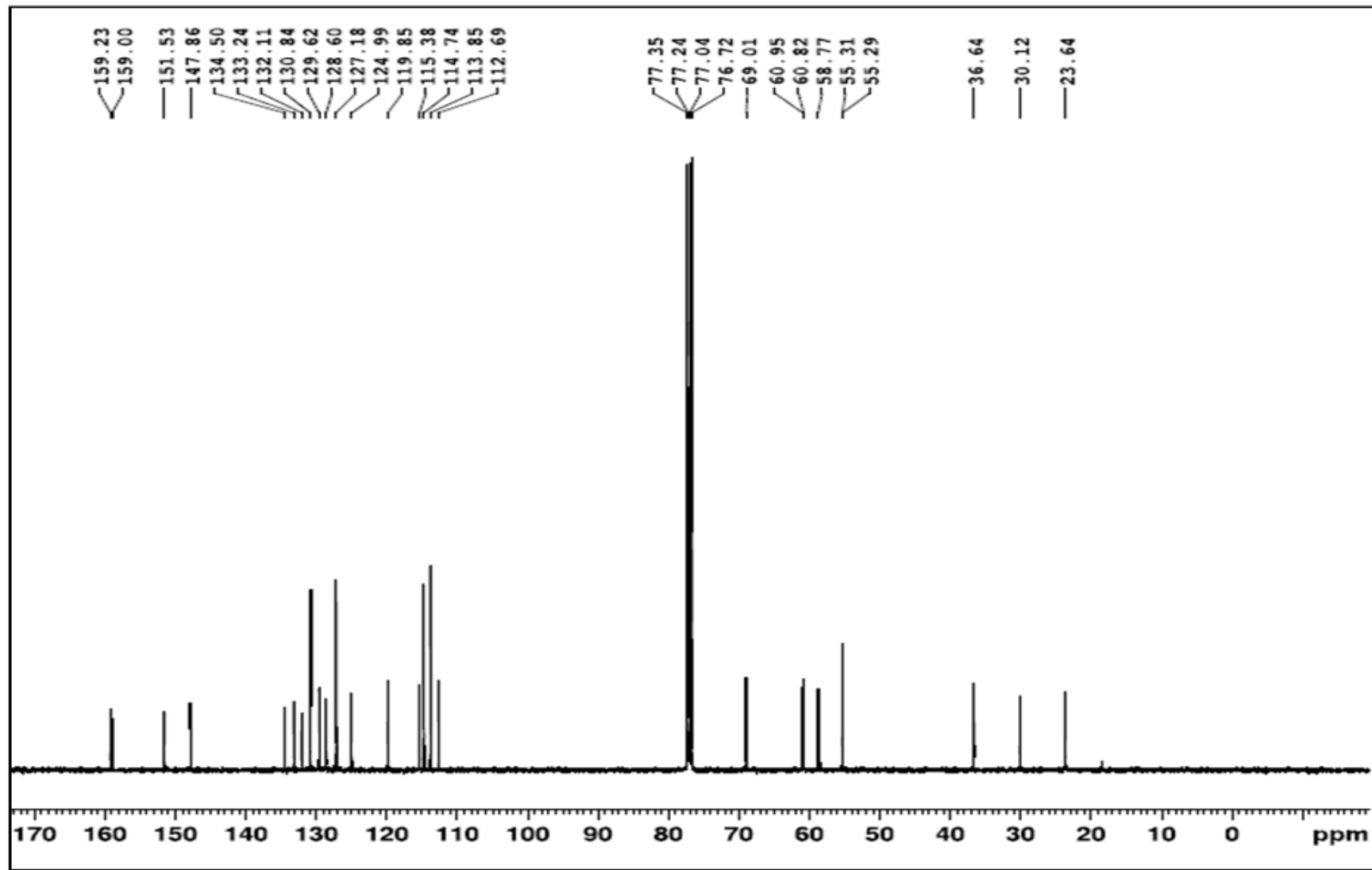


Fig. S53. ^{13}C -NMR spectrum of compound **14p** in CDCl_3 .

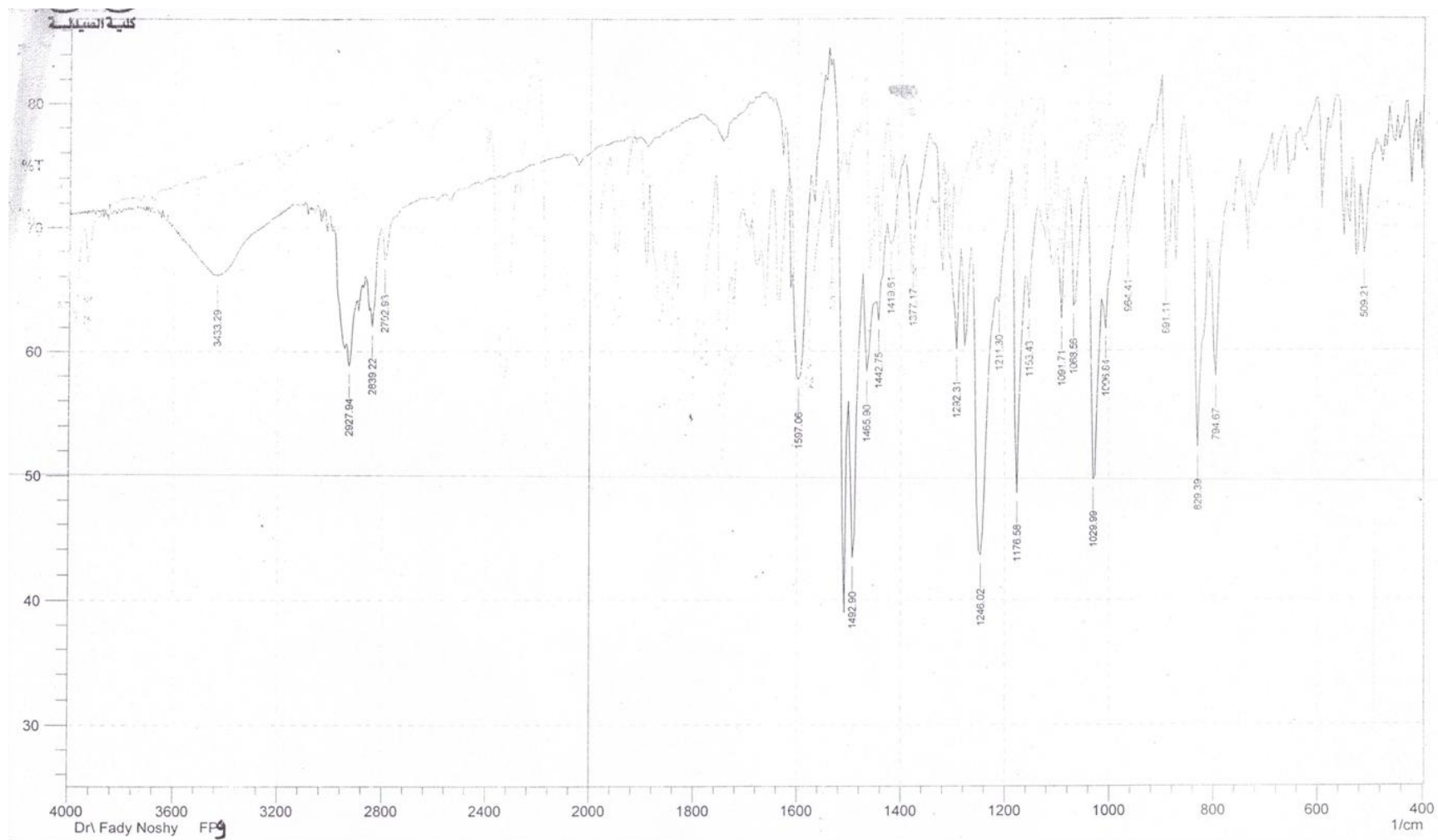


Fig. S54. IR spectrum of compound **14q** (KBr pellet).

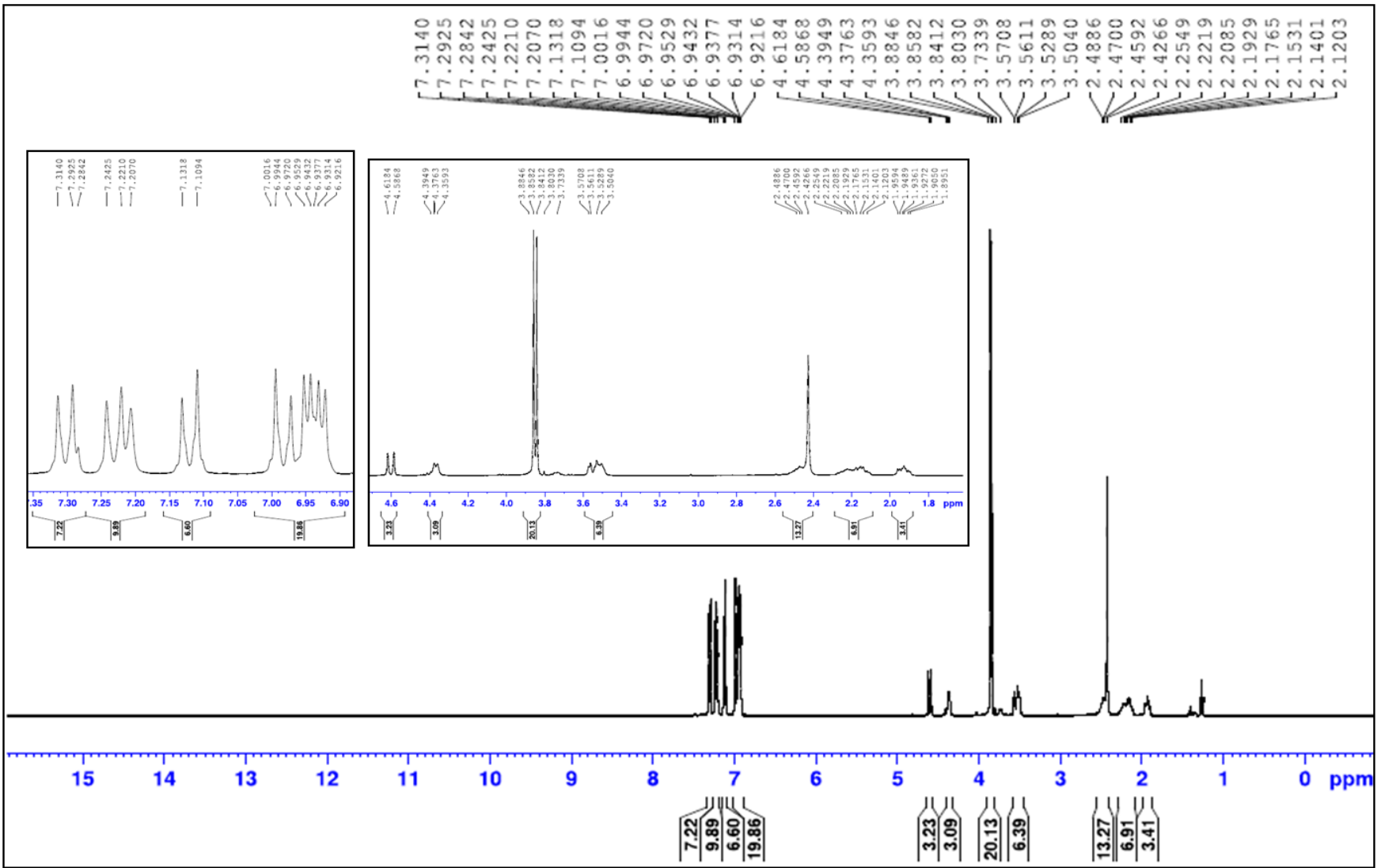


Fig. S55. ^1H -NMR spectrum of compound **14q** in CDCl_3 .

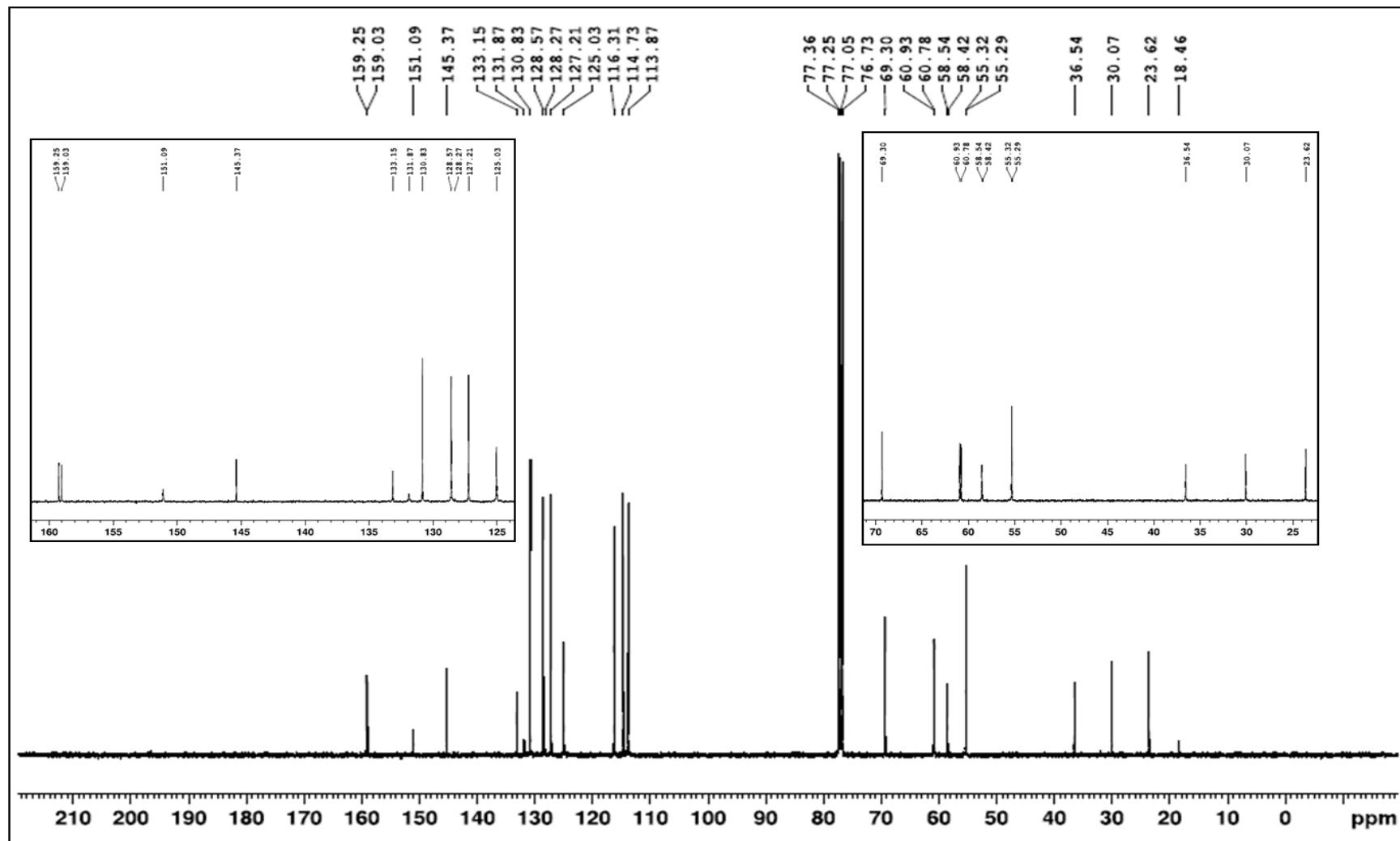


Fig. S56. ^{13}C -NMR spectrum of compound **14q** in CDCl_3 .

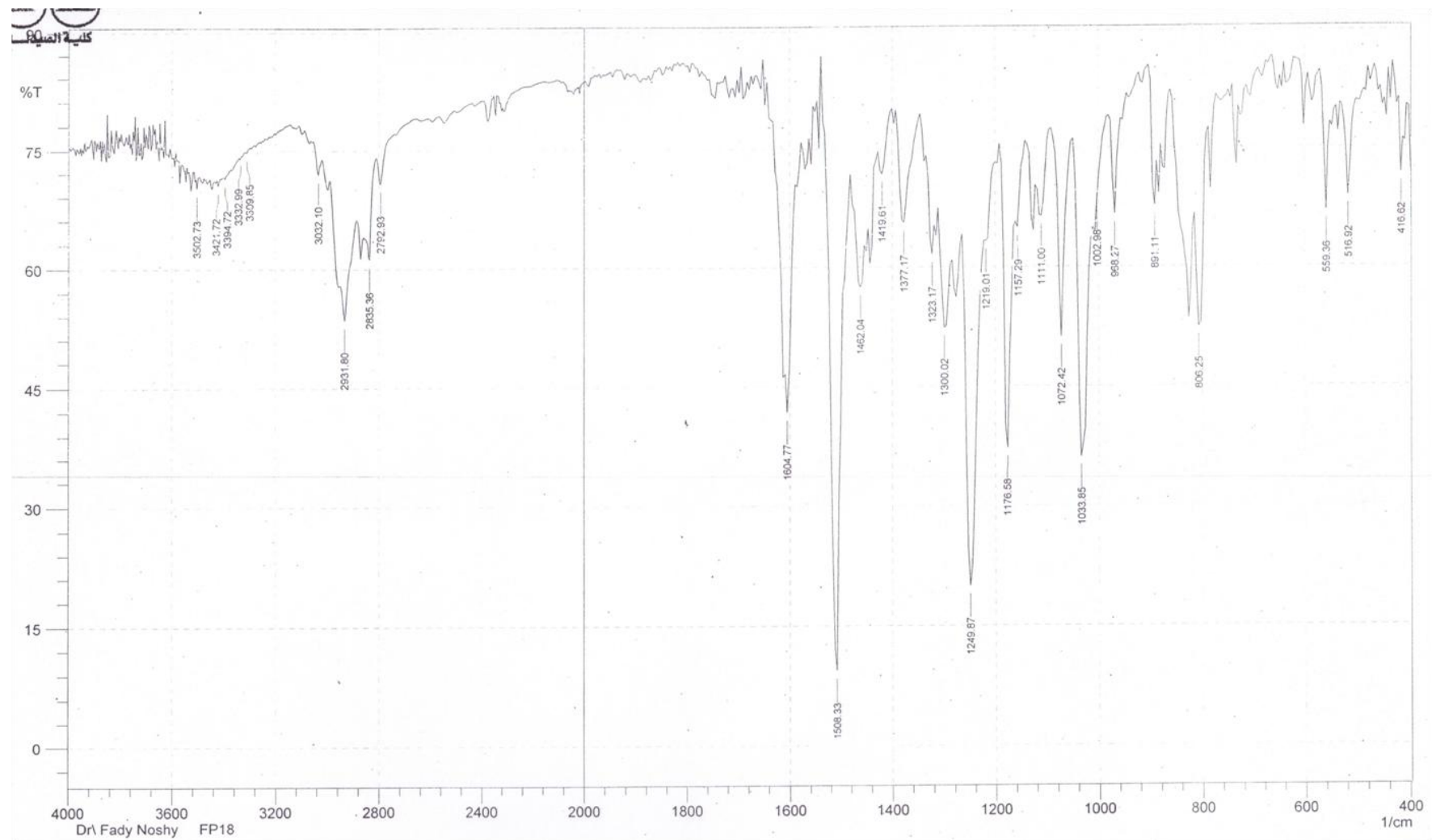


Fig. S57. IR spectrum of compound **14r** (KBr pellet).

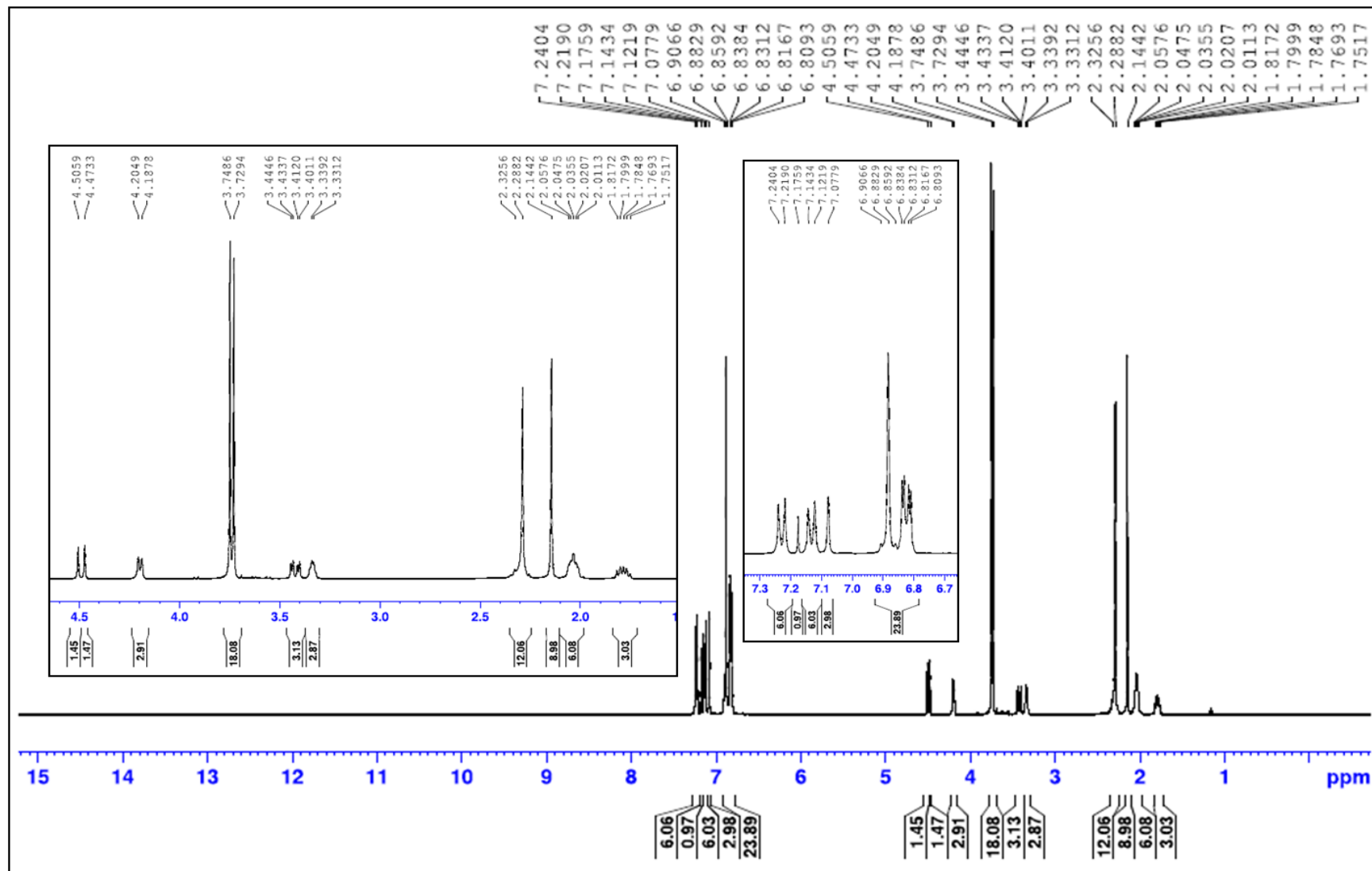


Fig. S58. ^1H -NMR spectrum of compound **14r** in CDCl_3 .

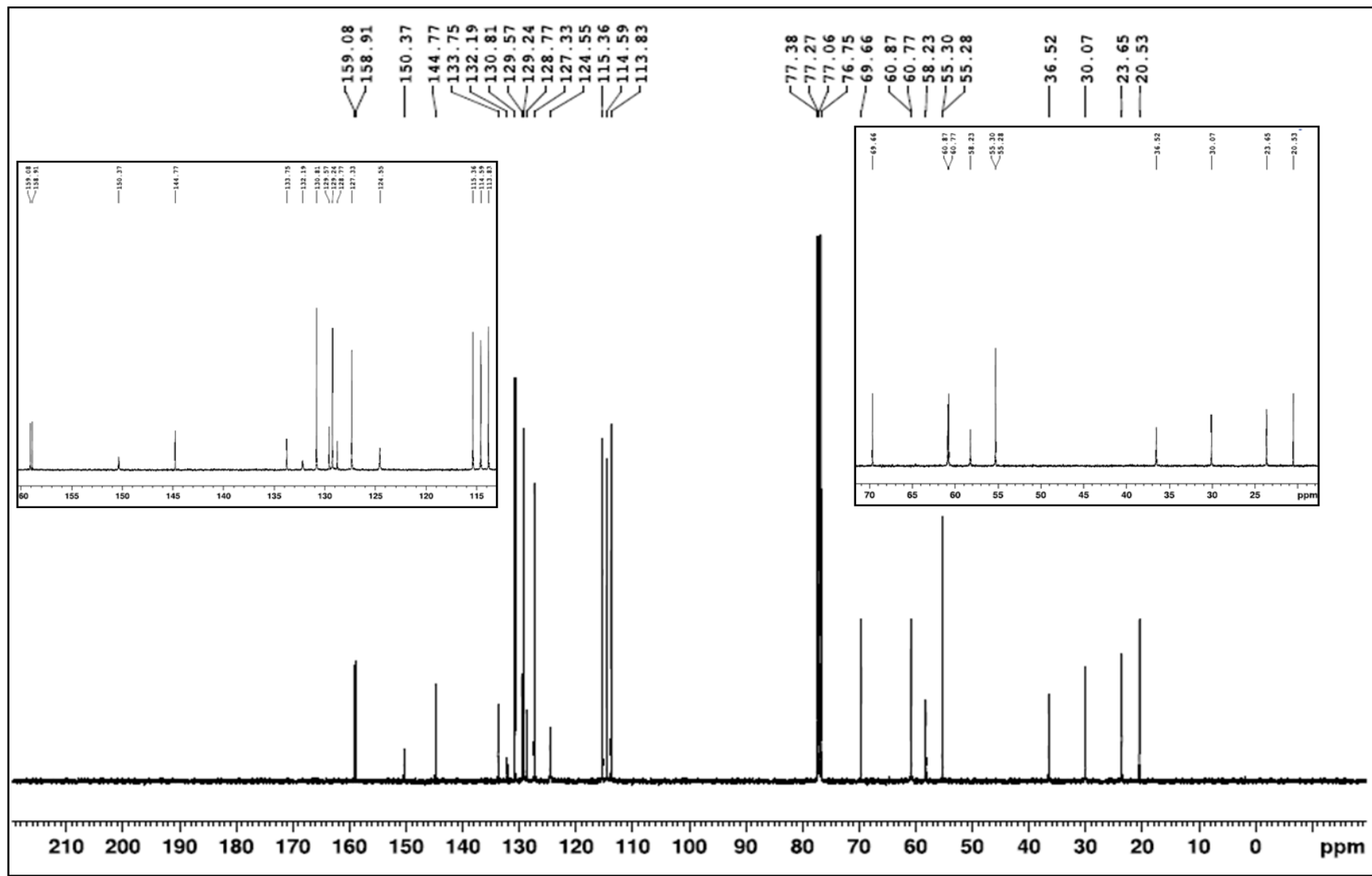


Fig. S59. ^{13}C -NMR spectrum of compound **14r** in CDCl_3 .

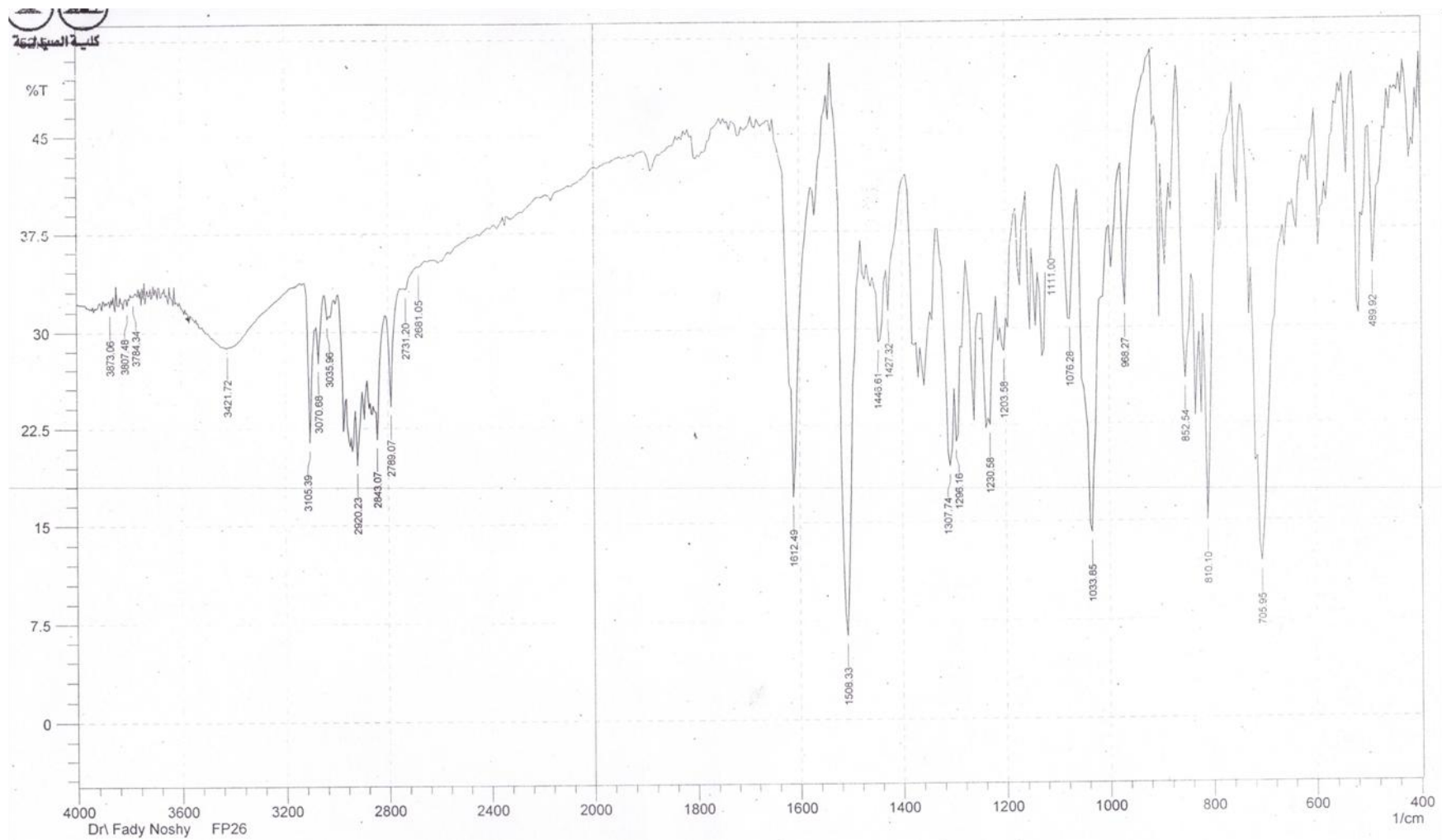


Fig. S60. IR spectrum of compound **14s** (KBr pellet).

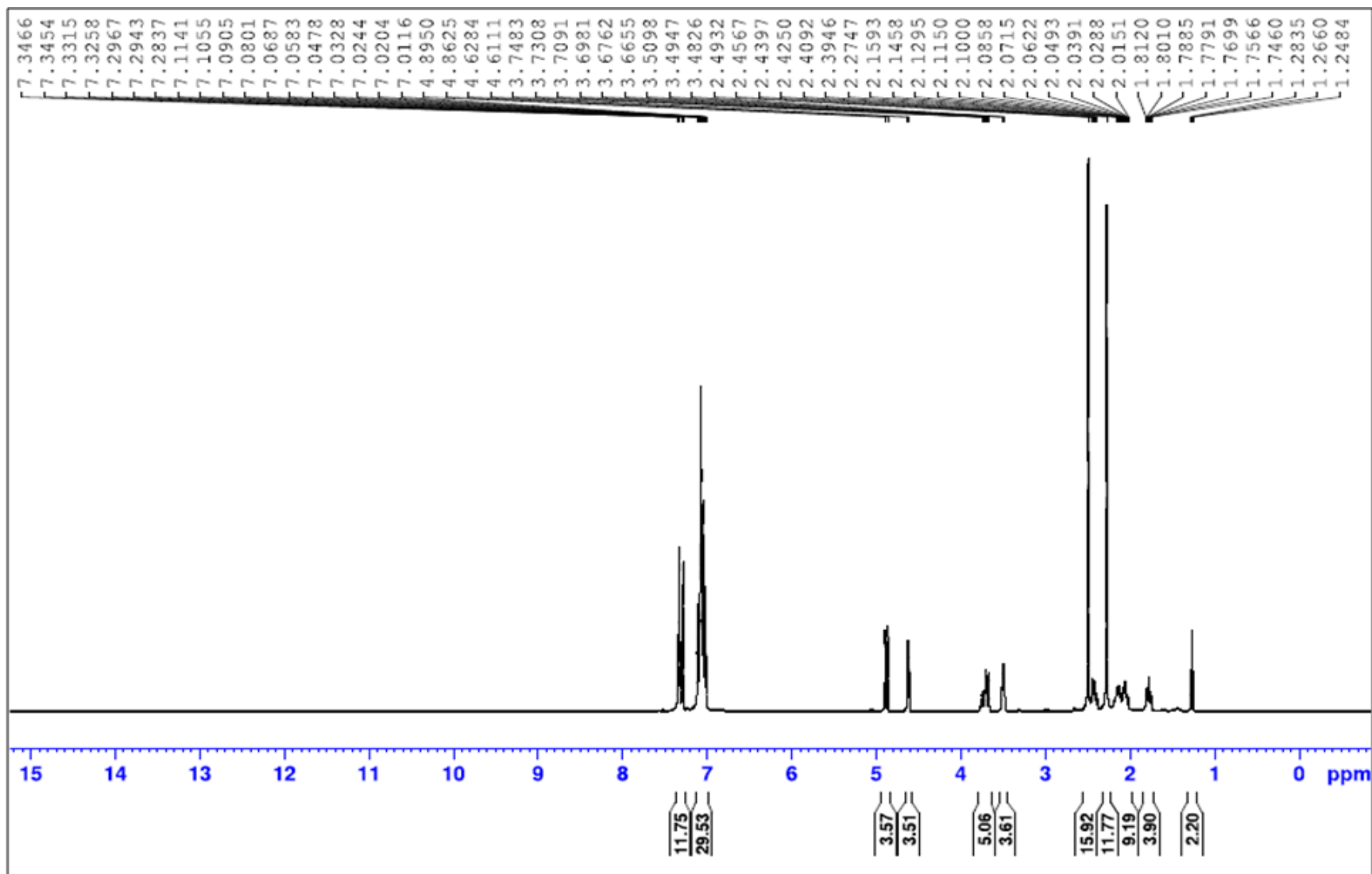


Fig. S61. ^1H -NMR spectrum of compound **14s** in CDCl_3 .

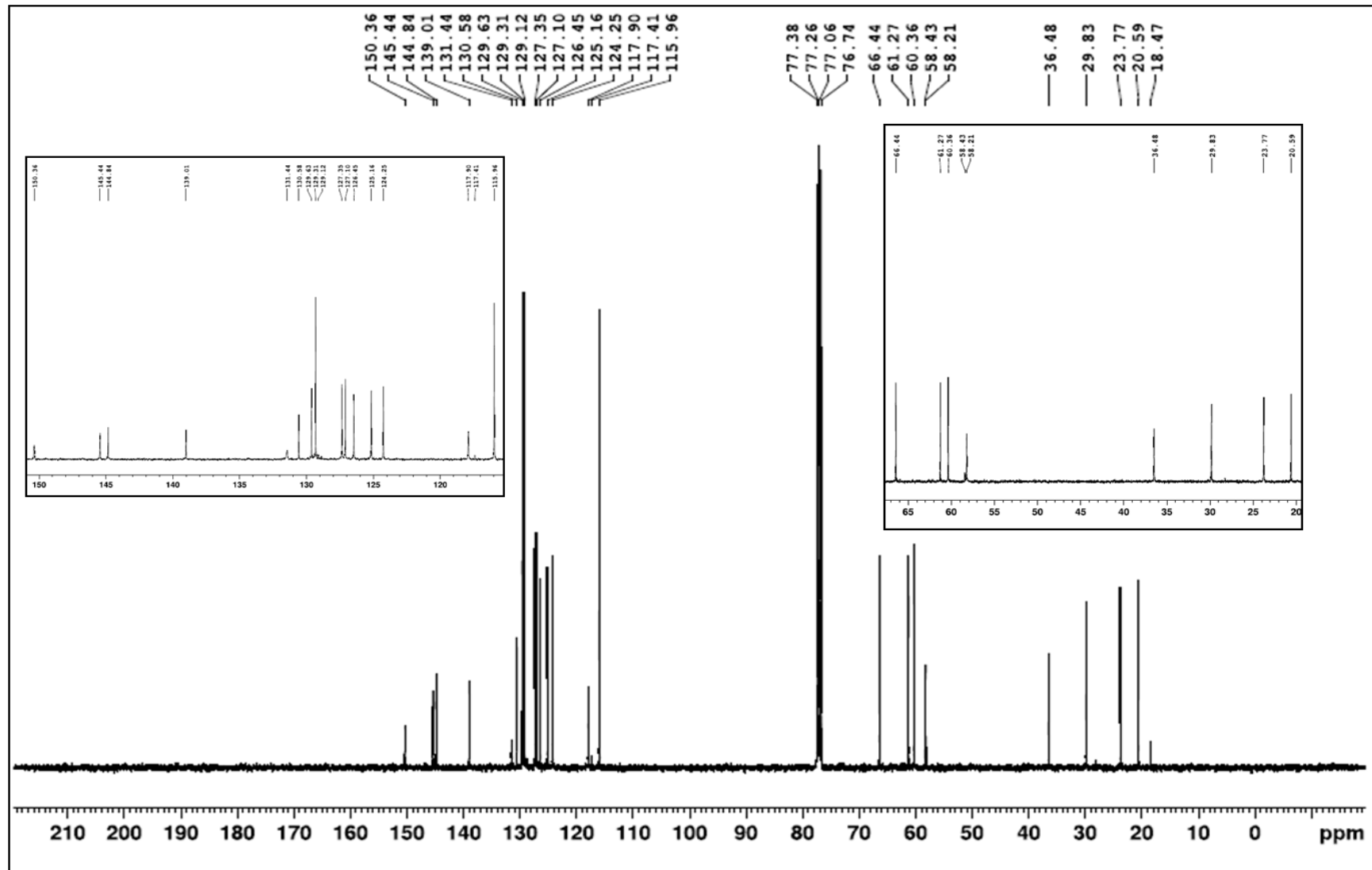


Fig. S62. ^{13}C -NMR spectrum of compound 14s in CDCl_3 .

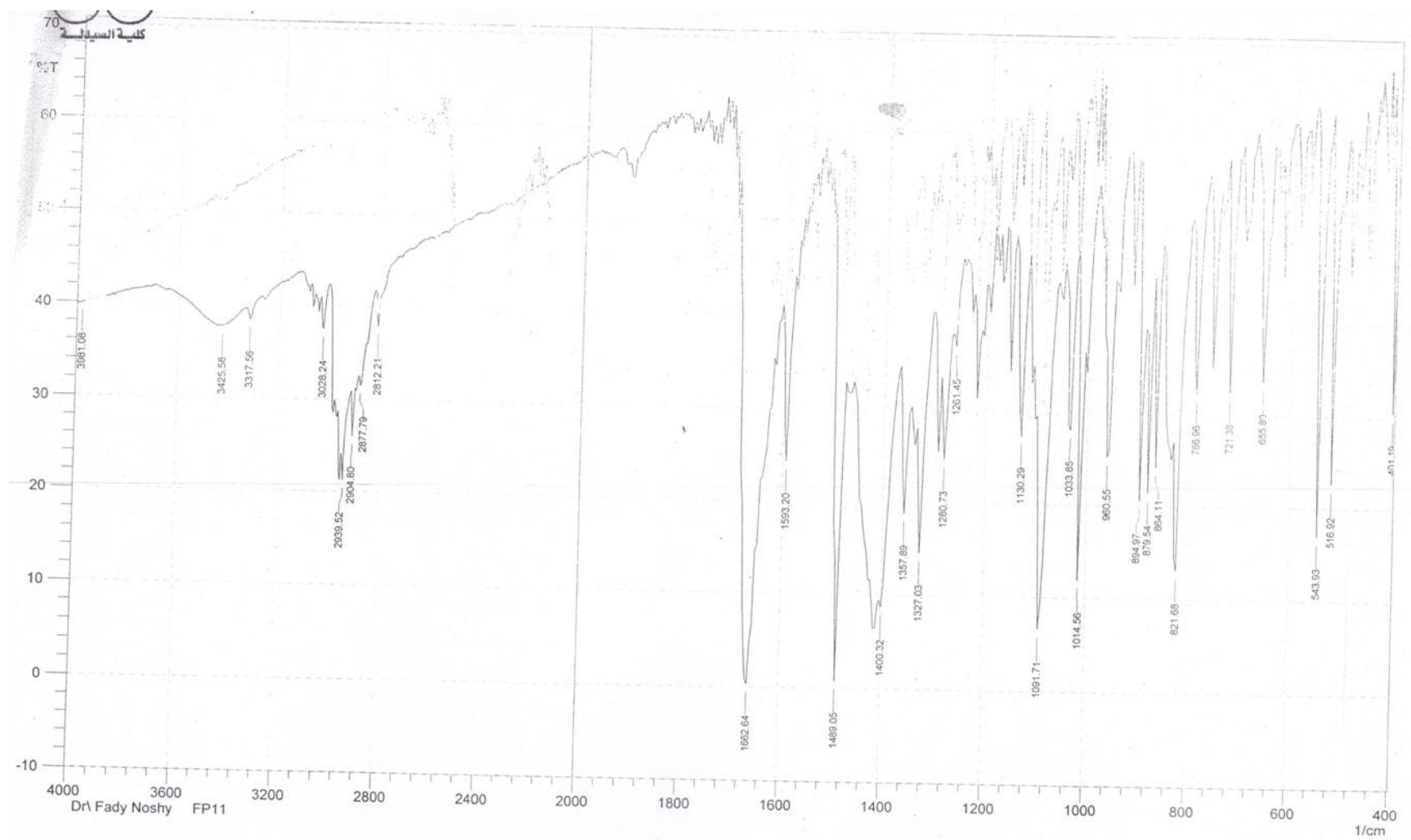


Fig. S63. IR spectrum of compound **16a** (KBr pellet).

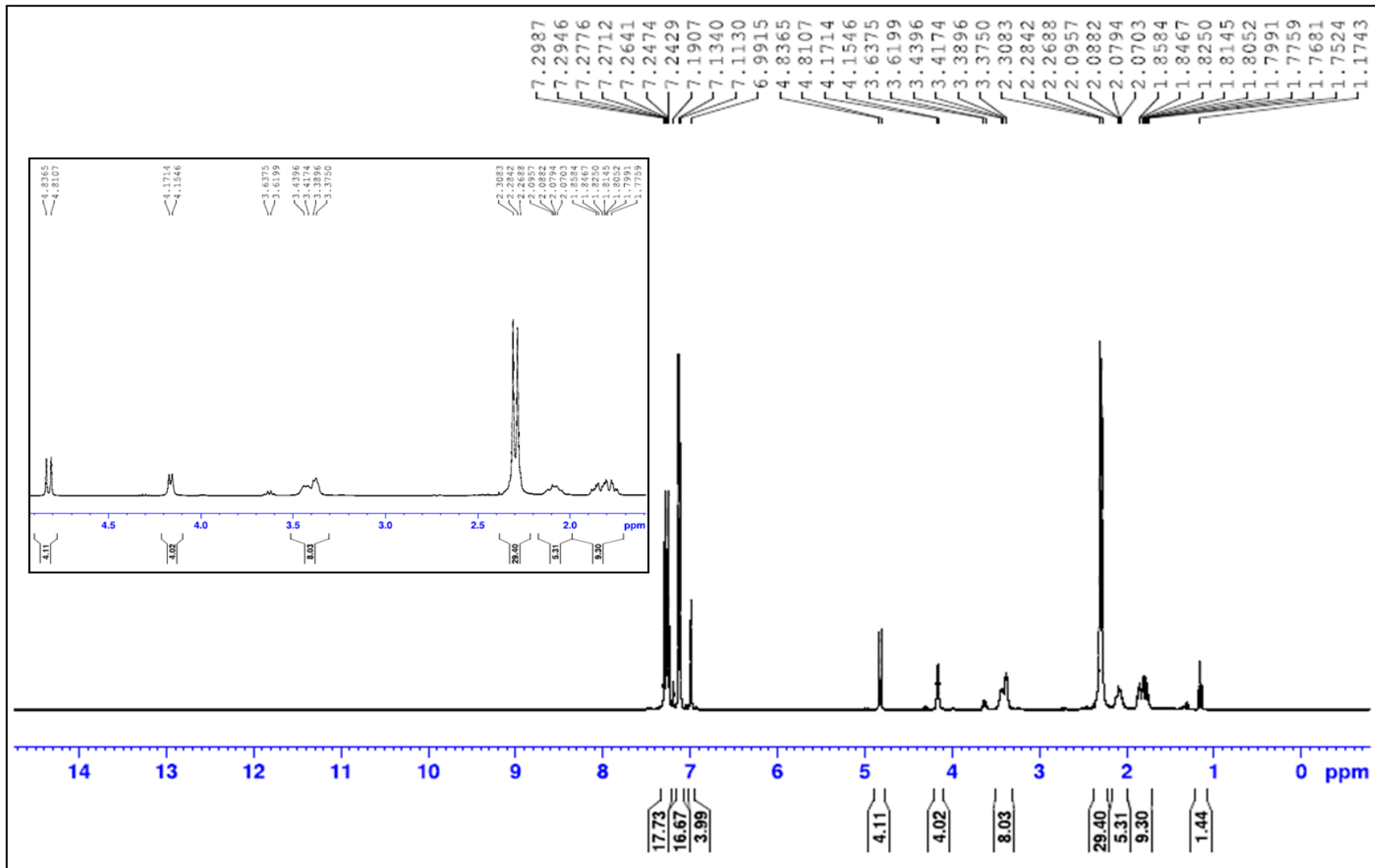


Fig. S64. ¹H-NMR spectrum of compound 16a in CDCl₃.

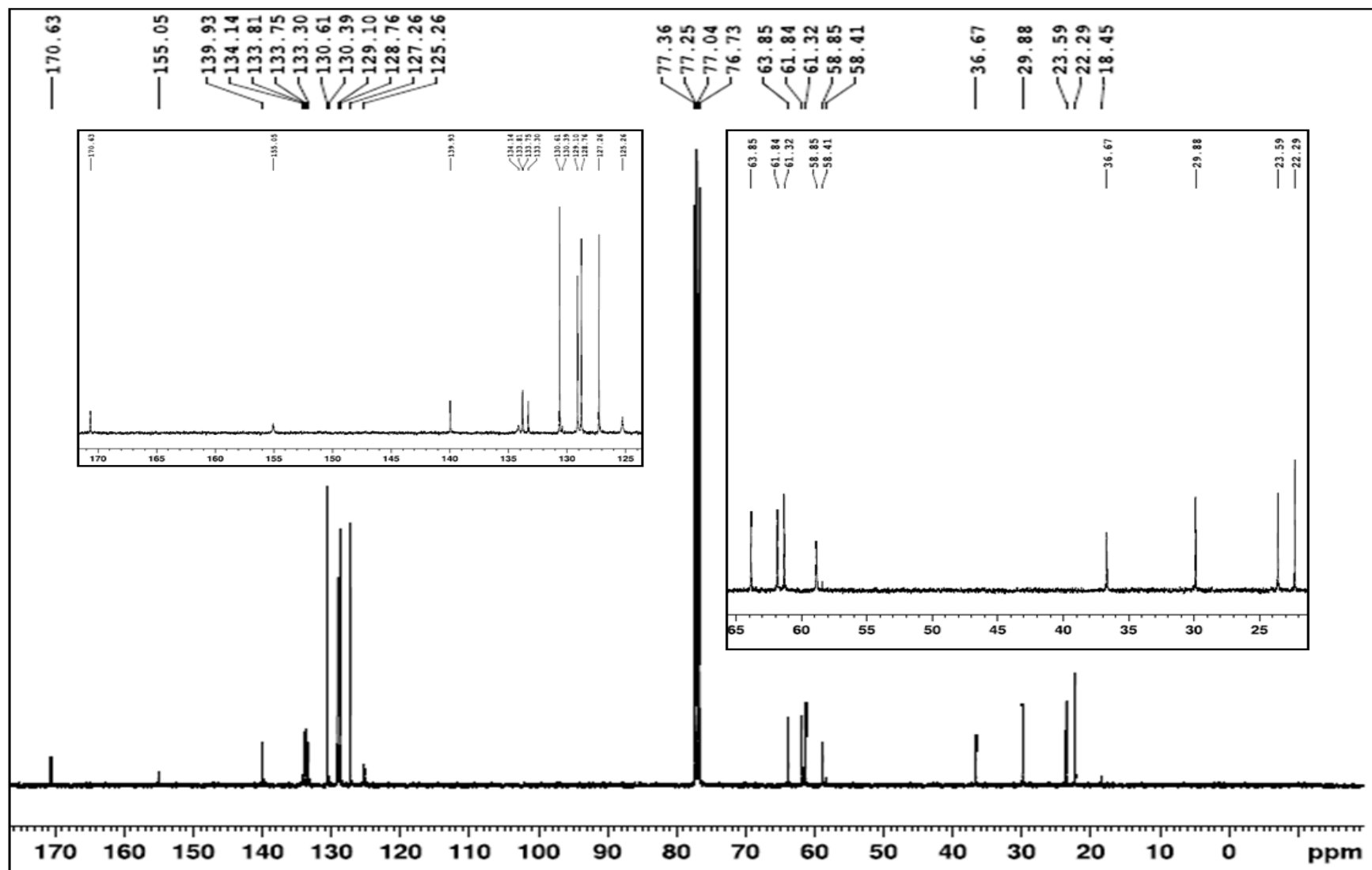


Fig. S65. ^{13}C -NMR spectrum of compound **16a** in CDCl_3 .

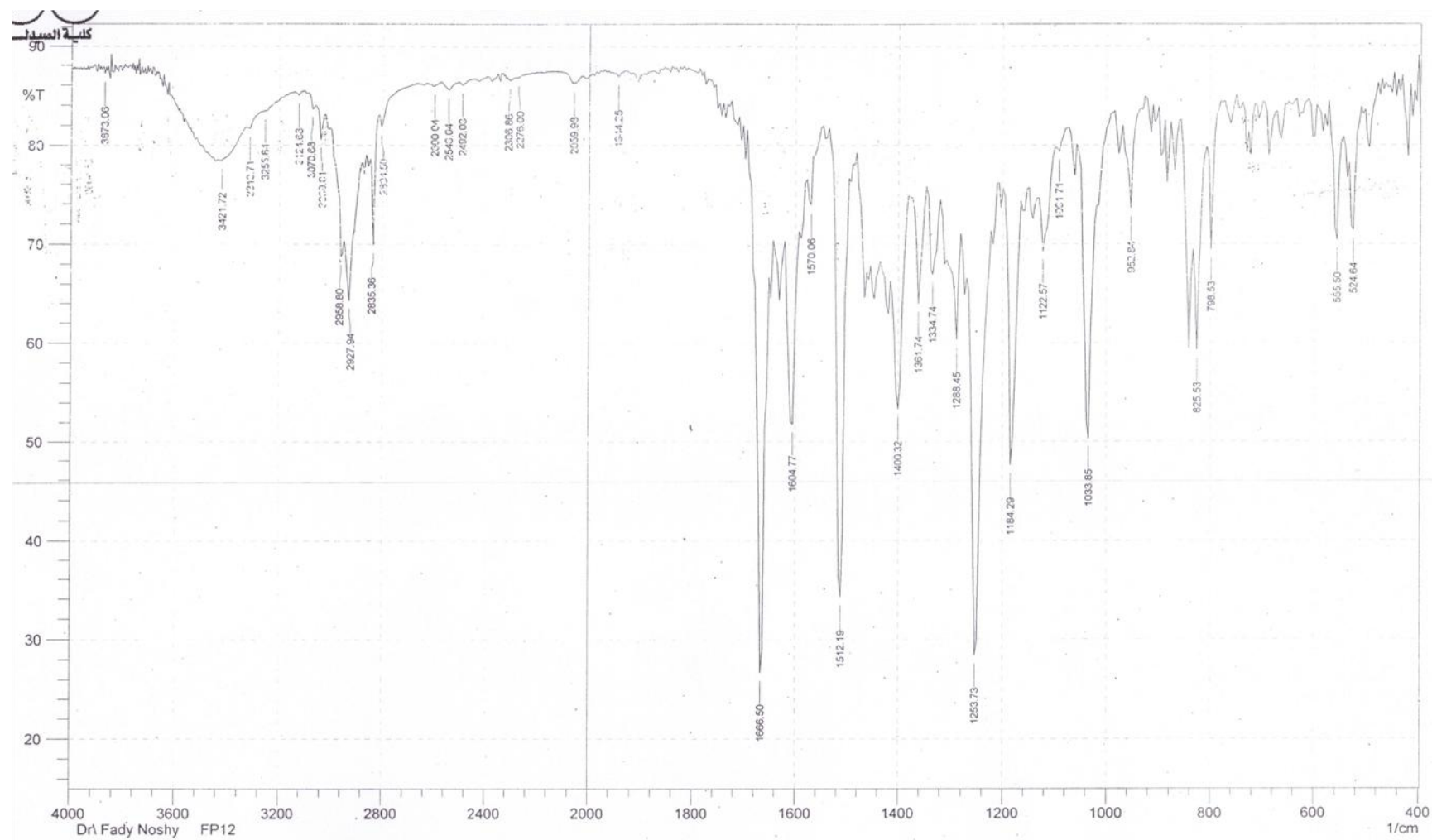


Fig. S66. ^1H -NMR spectrum of compound **16b** in CDCl_3 .

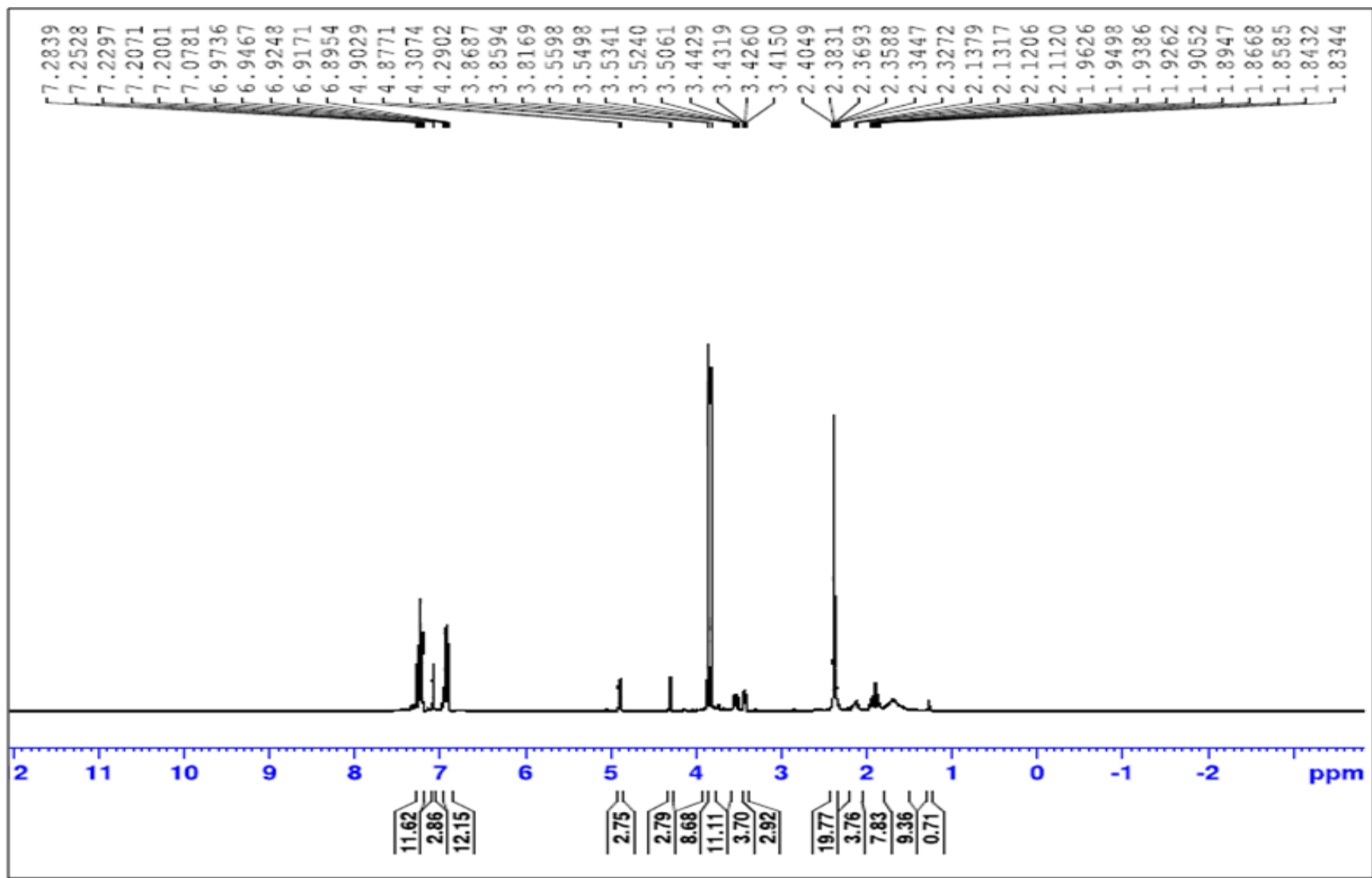


Fig. S67. ^1H -NMR spectrum of compound **16b** in CDCl_3 .

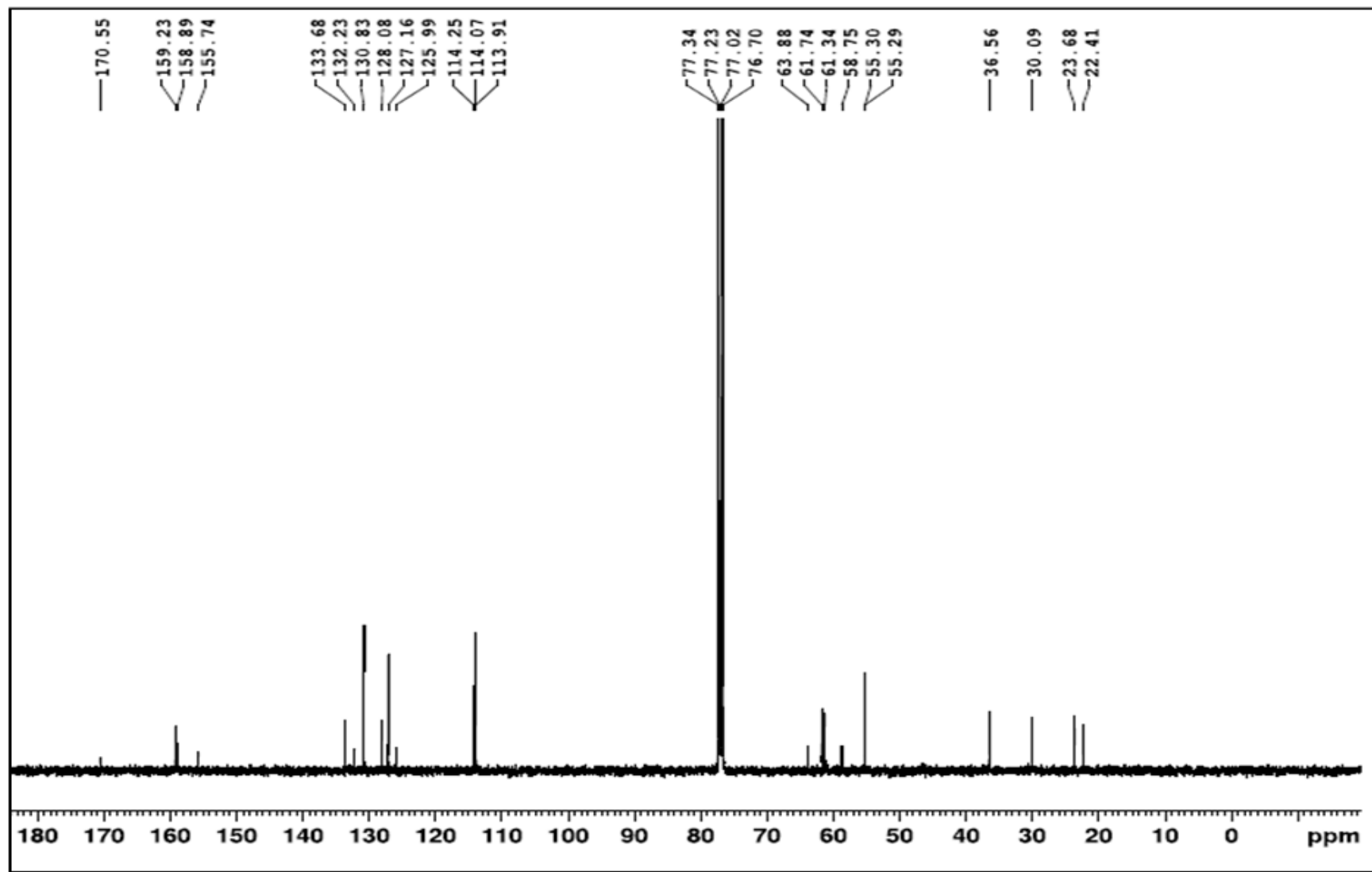


Fig. S68. ^{13}C -NMR spectrum of compound **16b** in CDCl_3 .

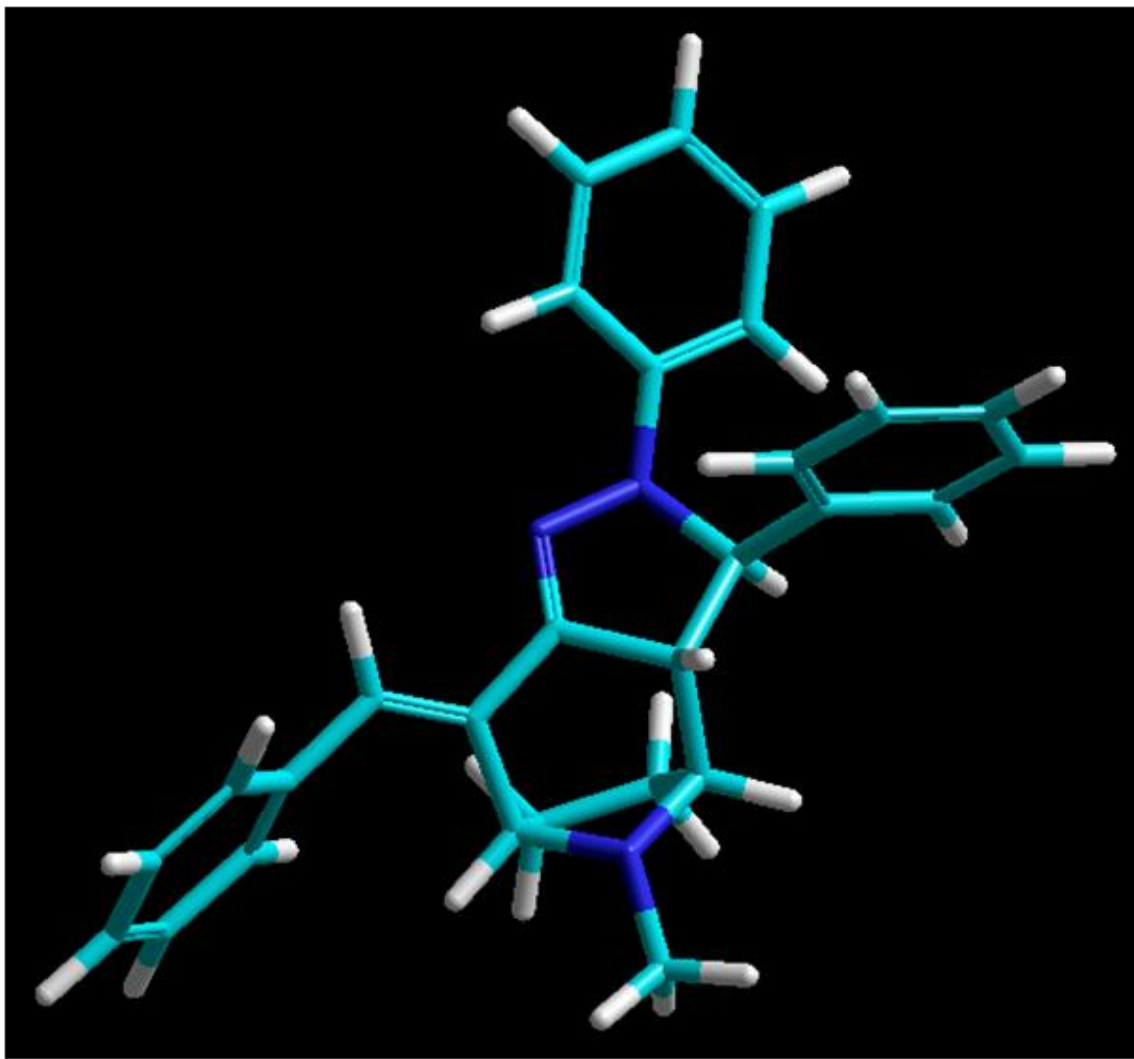


Fig. S69. A projection of the optimized structure of compound **14a** by semi-empirical AM1.

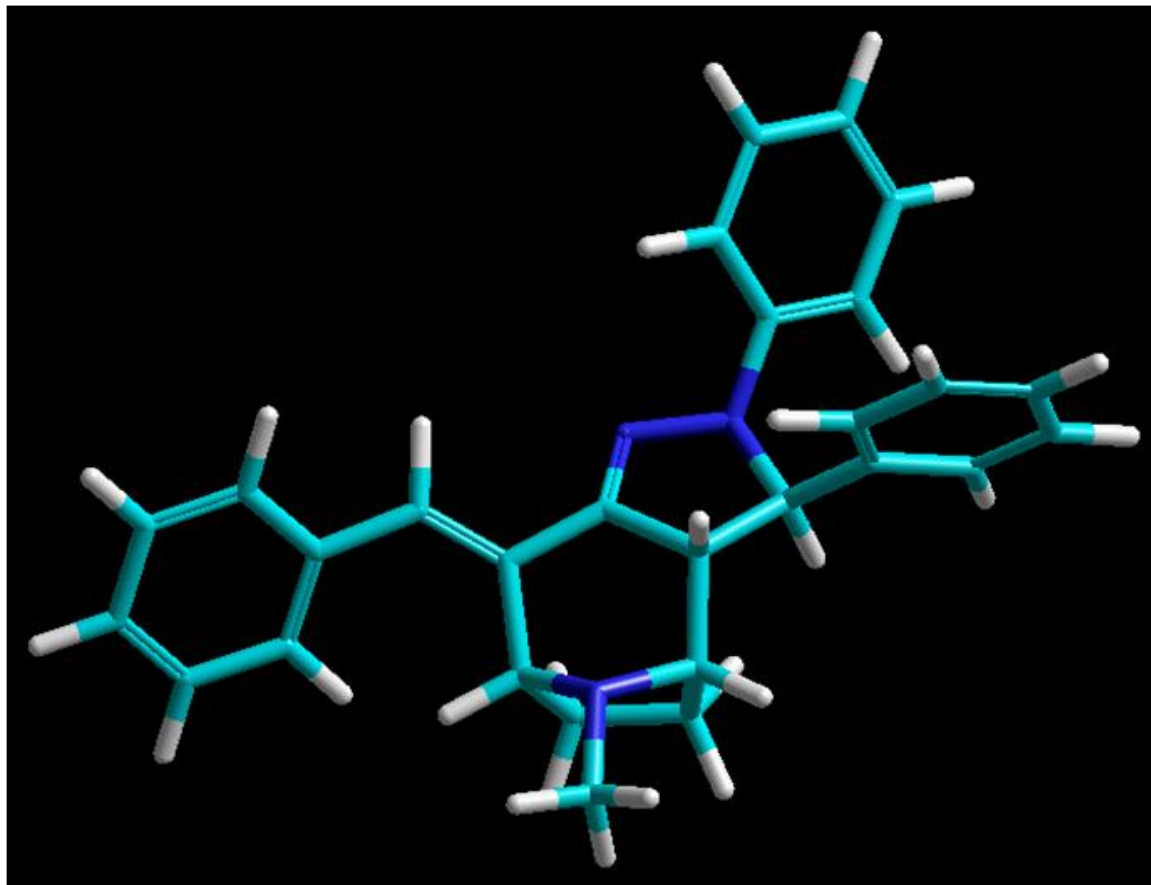


Fig. S70. A projection of the optimized structure of compound **14a** by semi-empirical PM3.

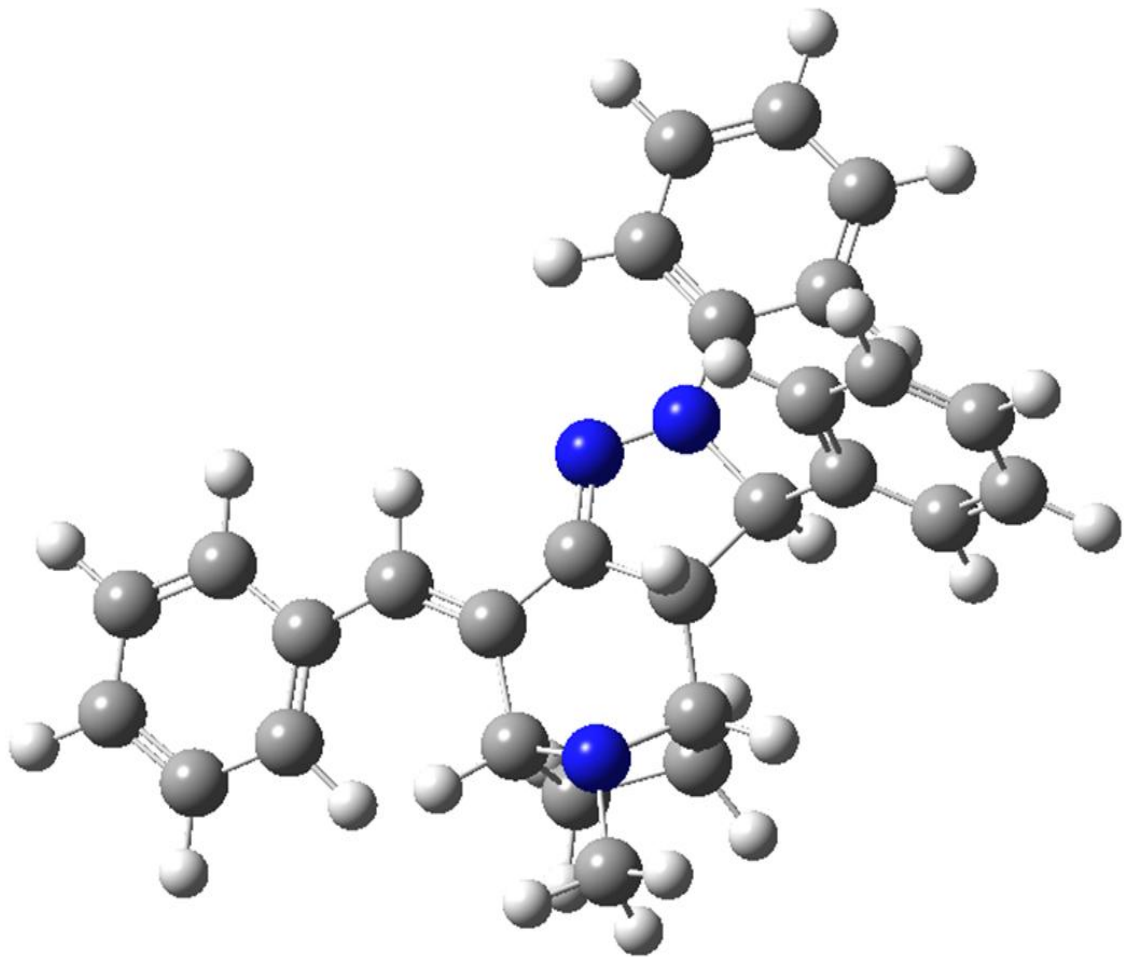


Fig. S71. A projection of the optimized structure of compound **14a** by DFT/B3LYP with 6-31G(d,p) level of theory.

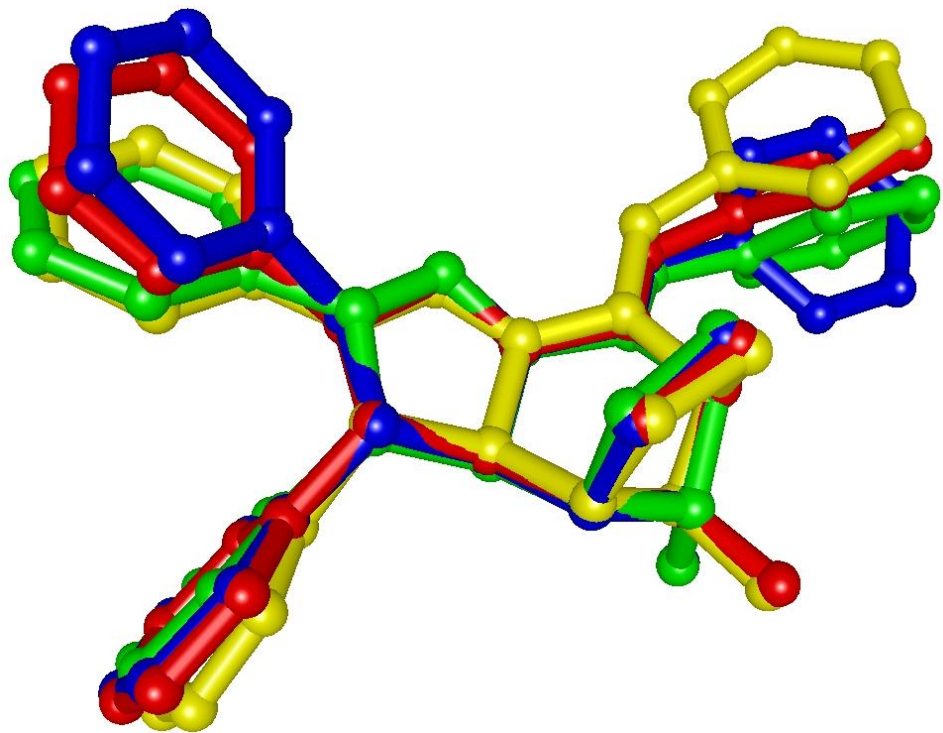
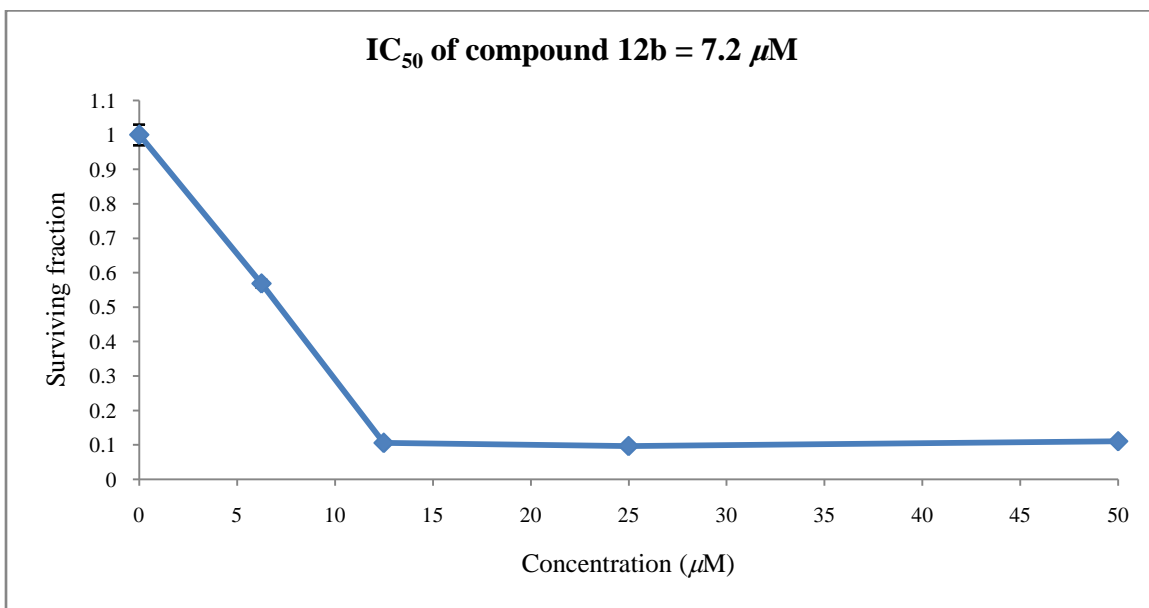
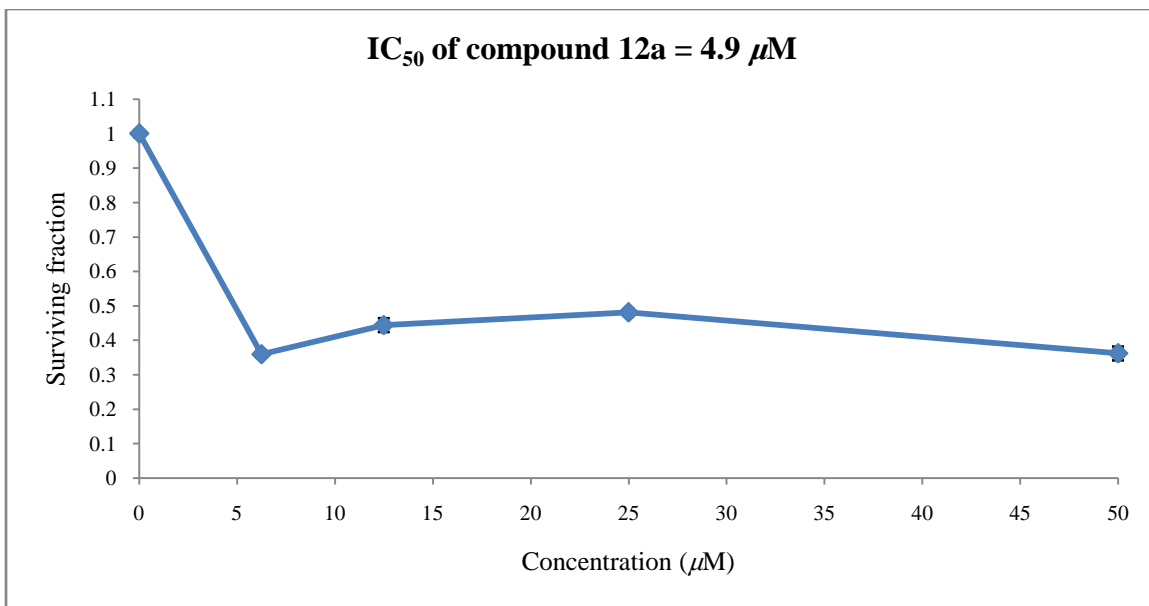
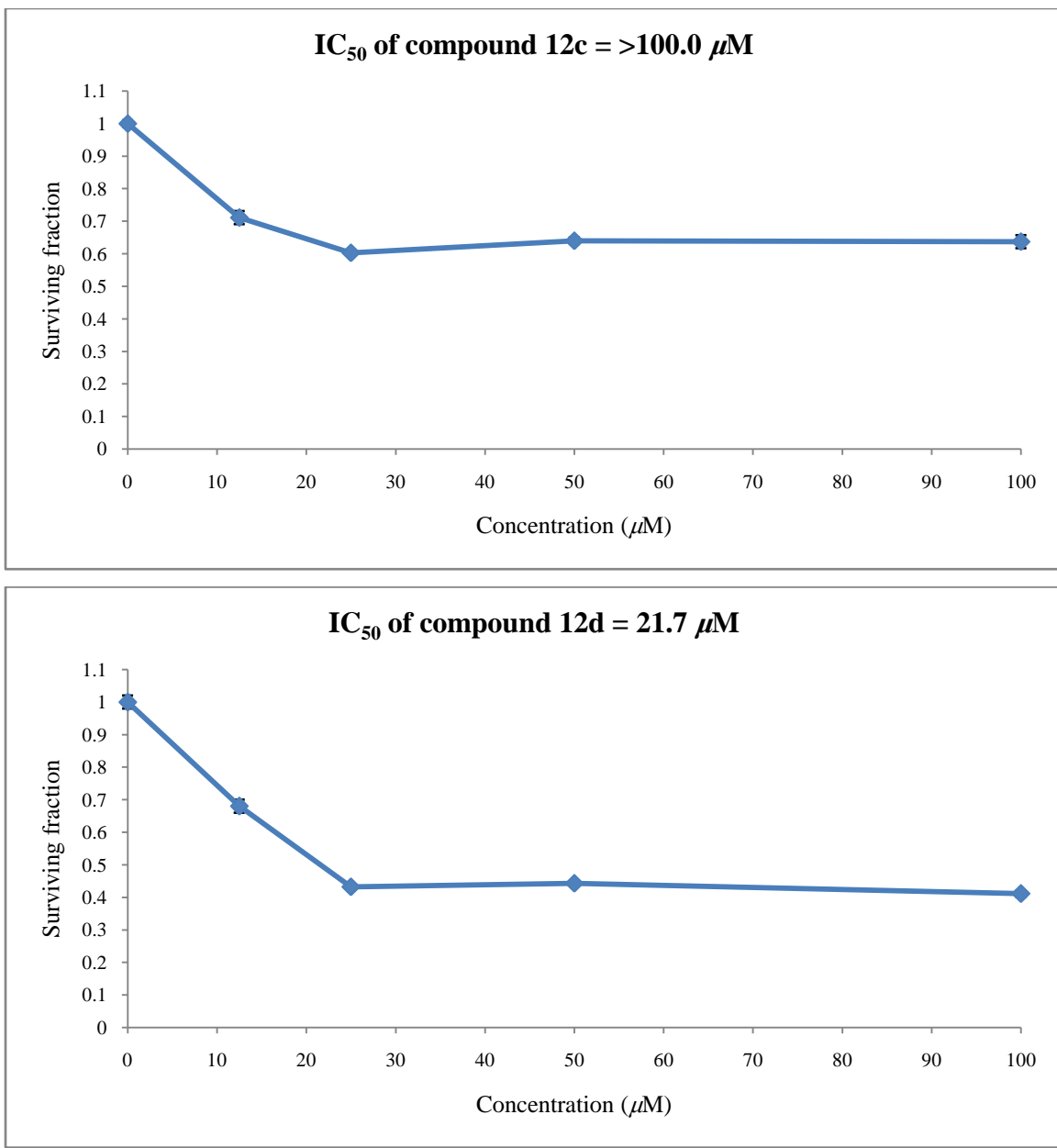
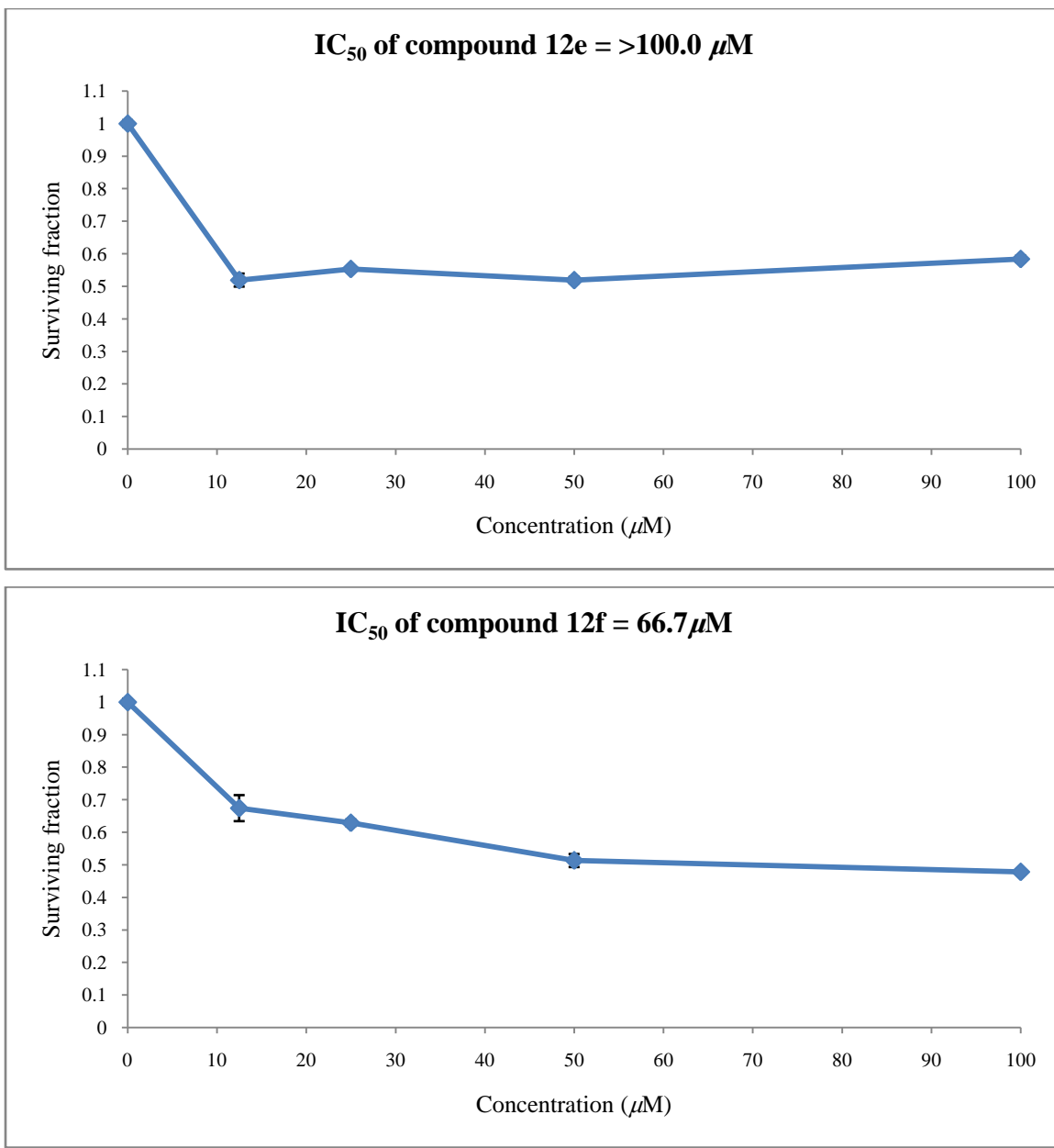
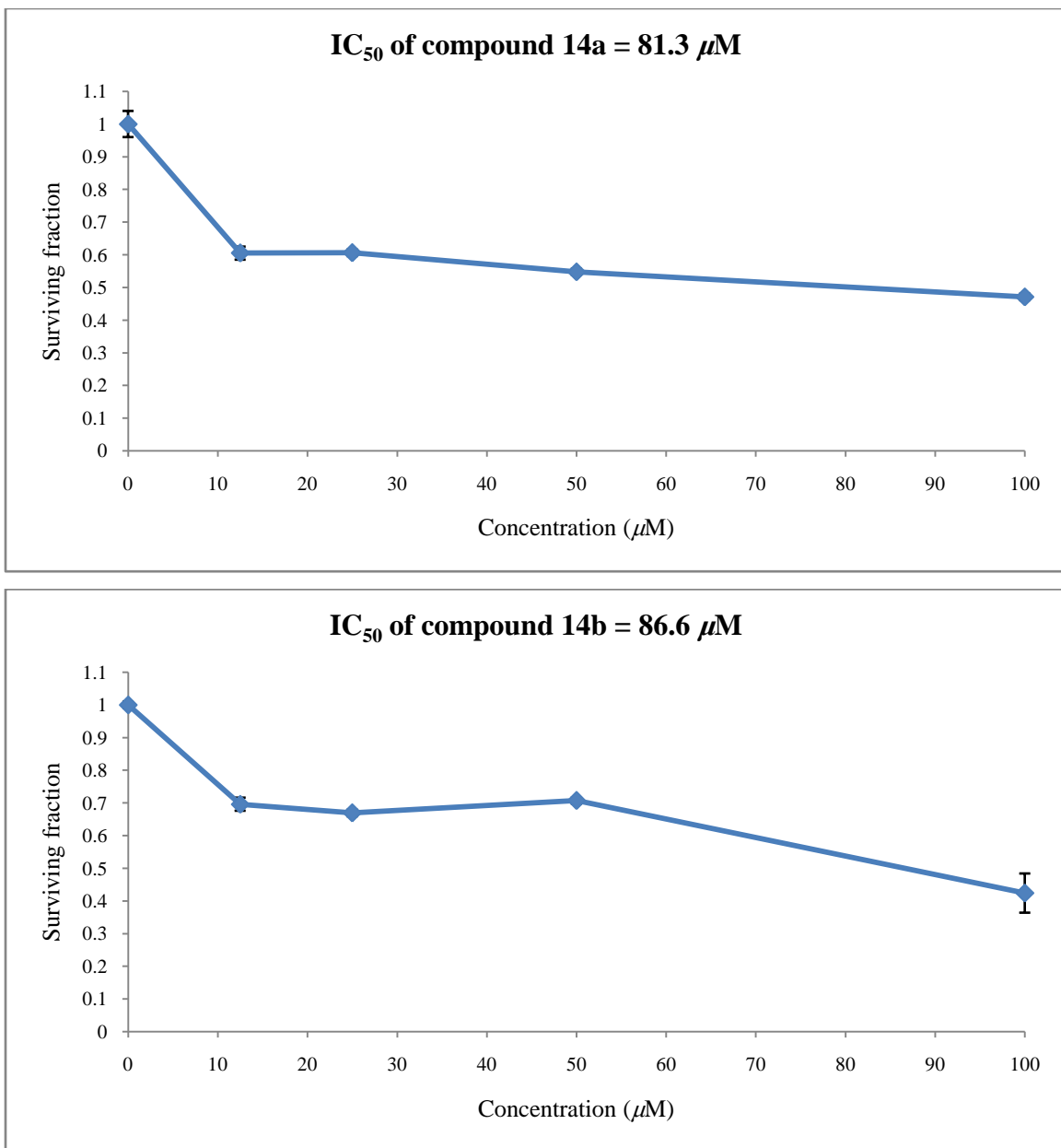


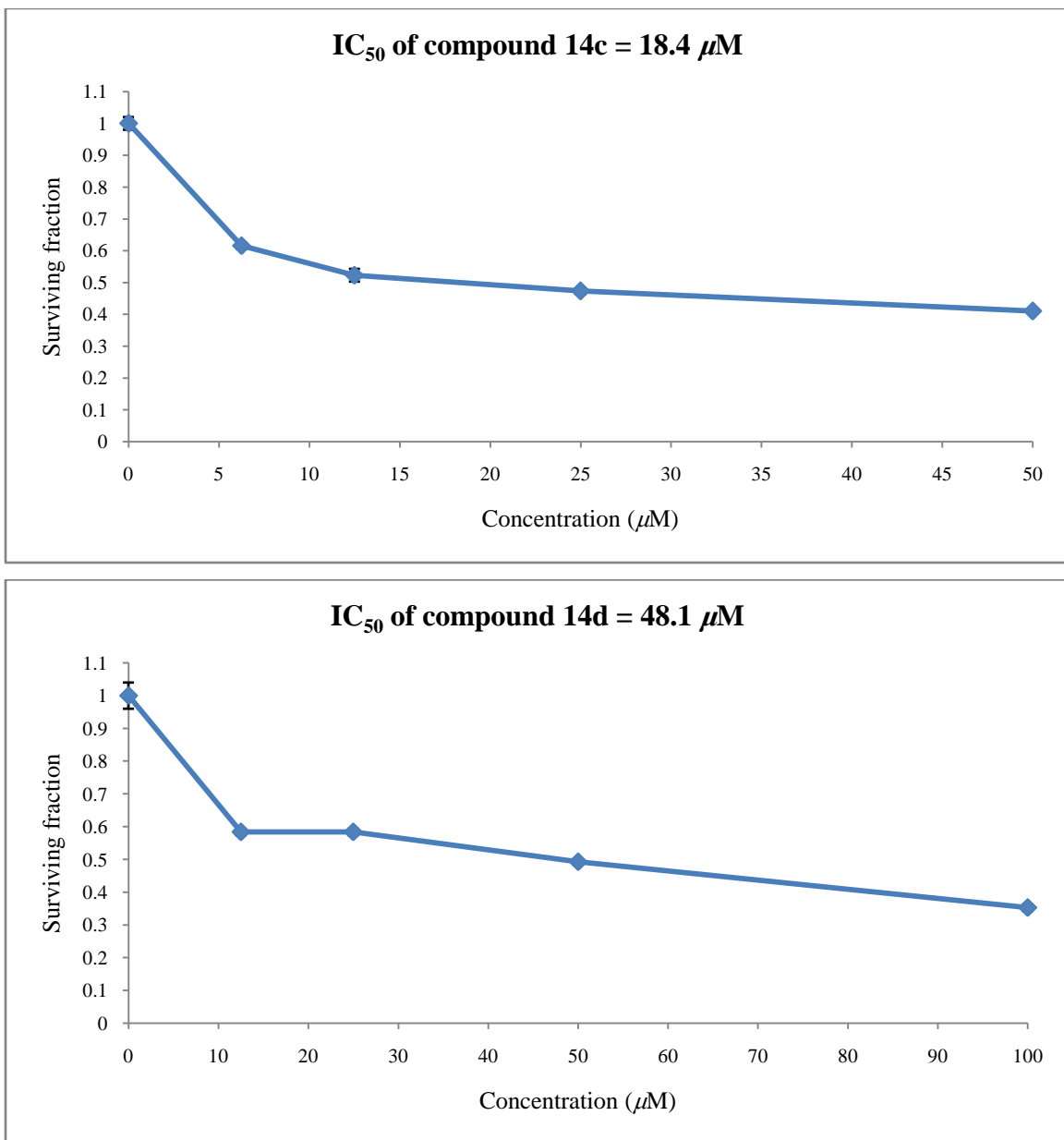
Fig. S72. Overlay diagram of **14a**; red (X-ray structure), green (AM1), blue (PM3) and yellow (DFT).

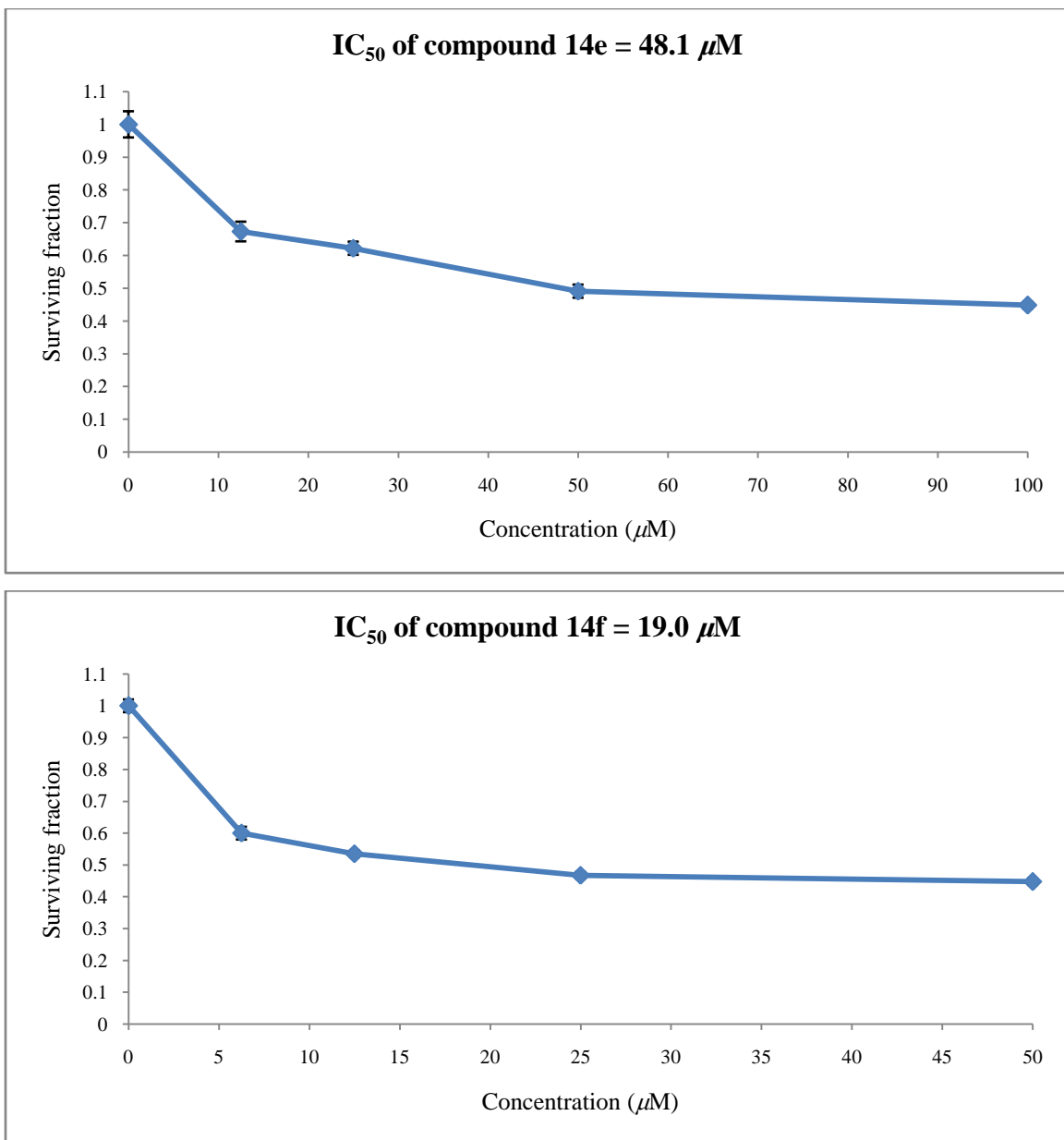




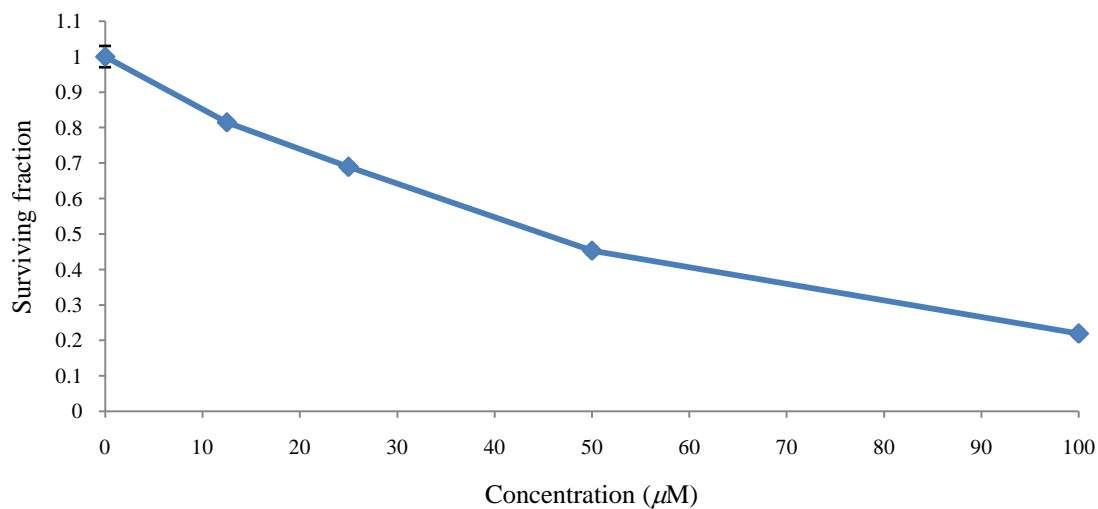




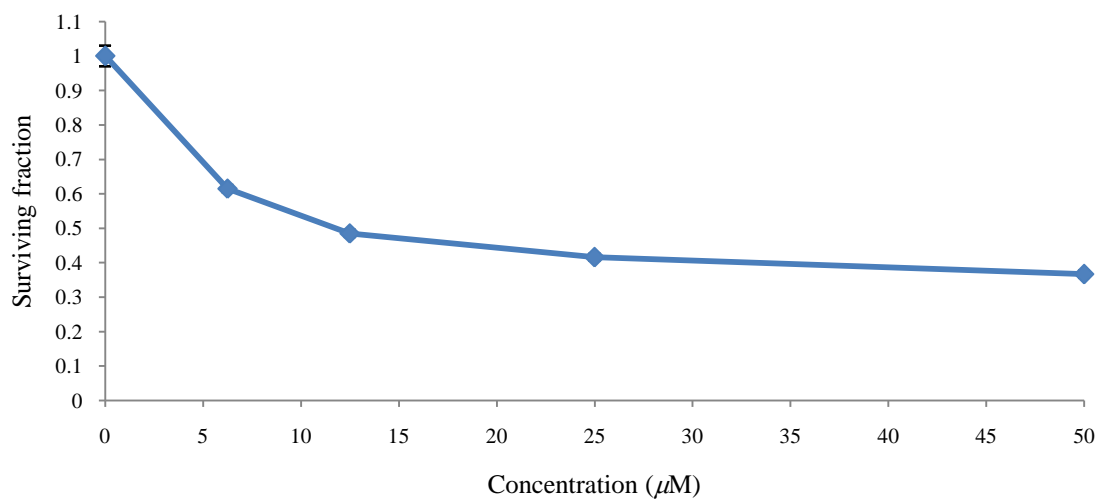


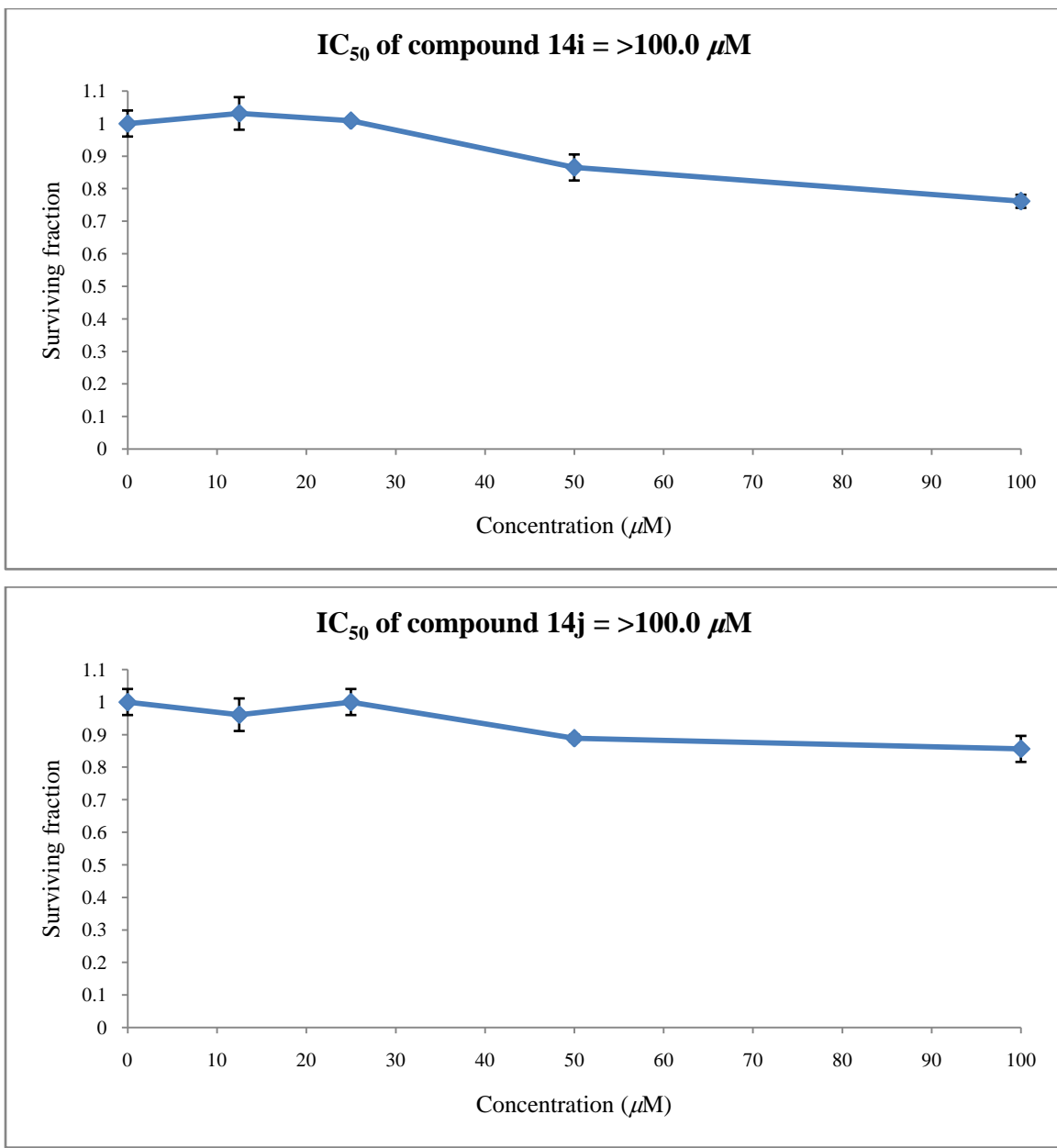


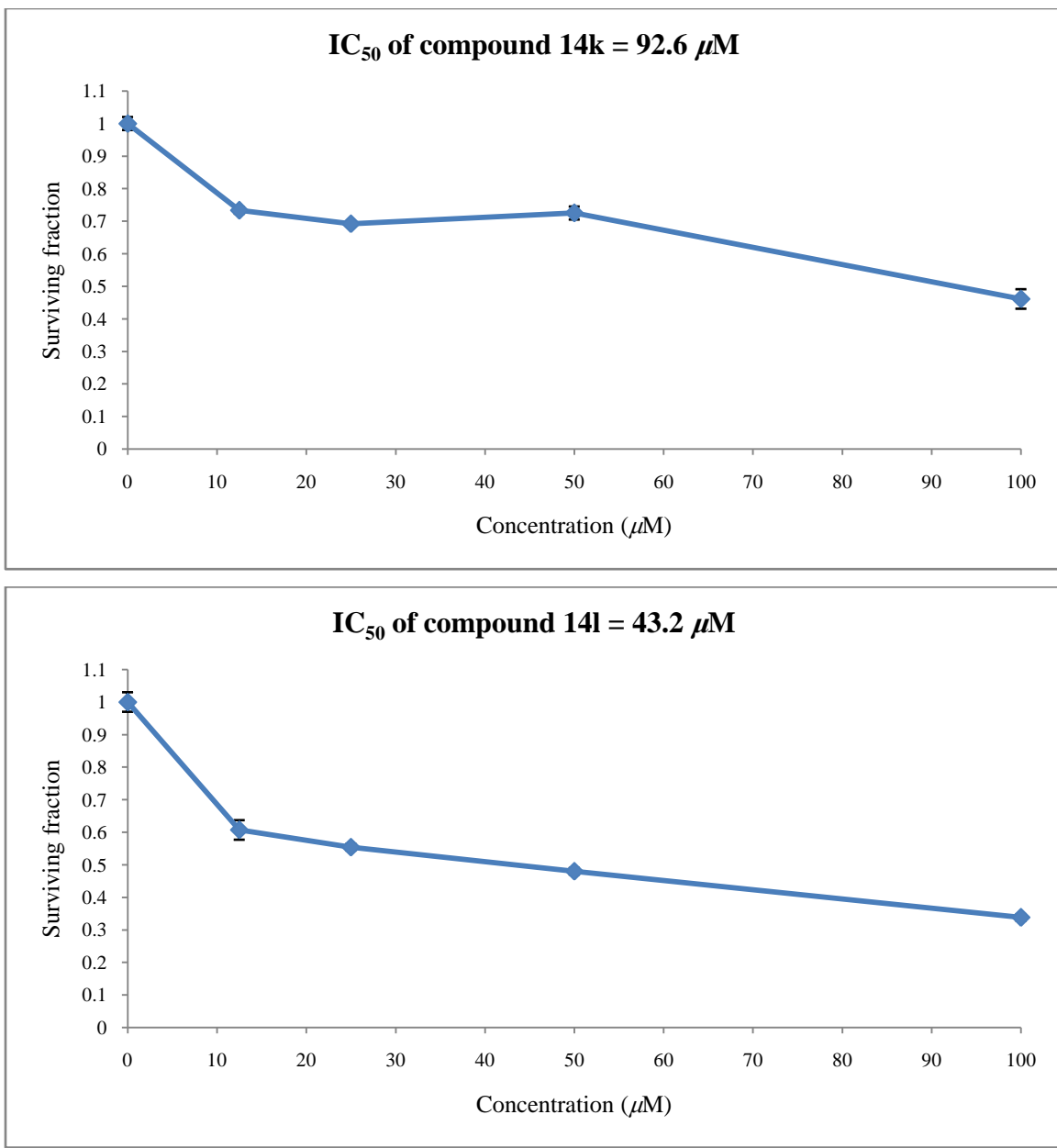
IC₅₀ of compound 14g = 44.9 μ M

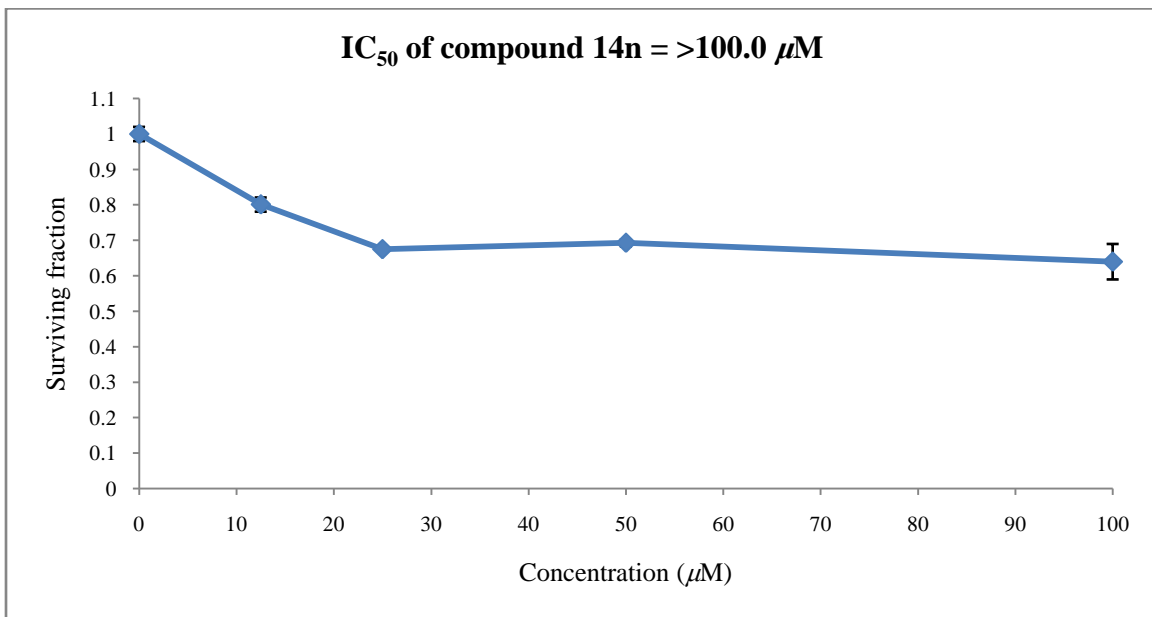
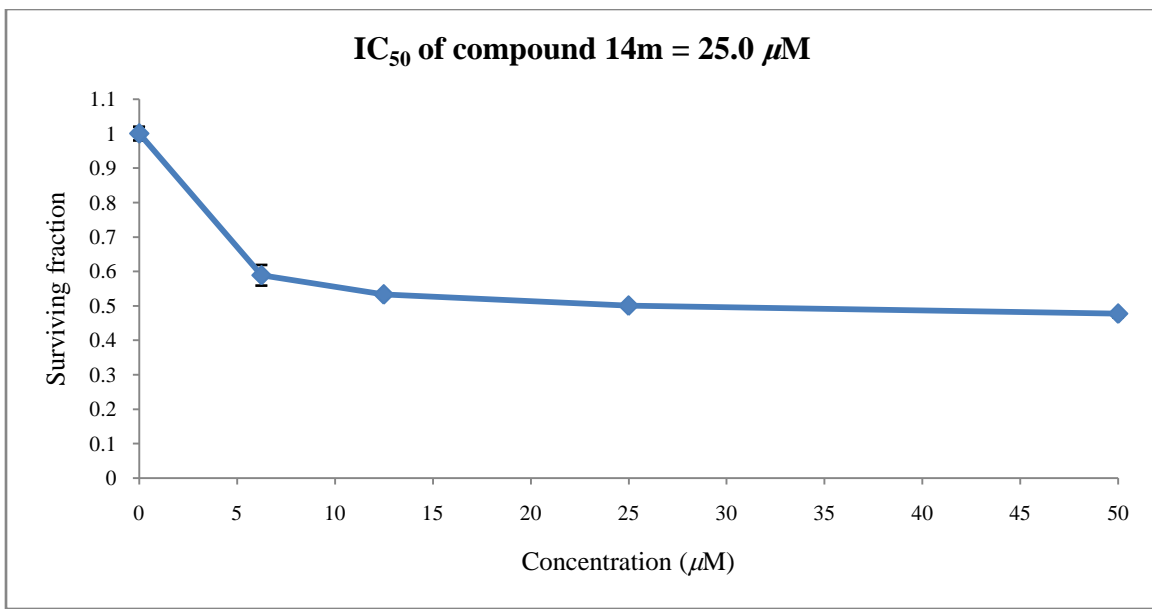


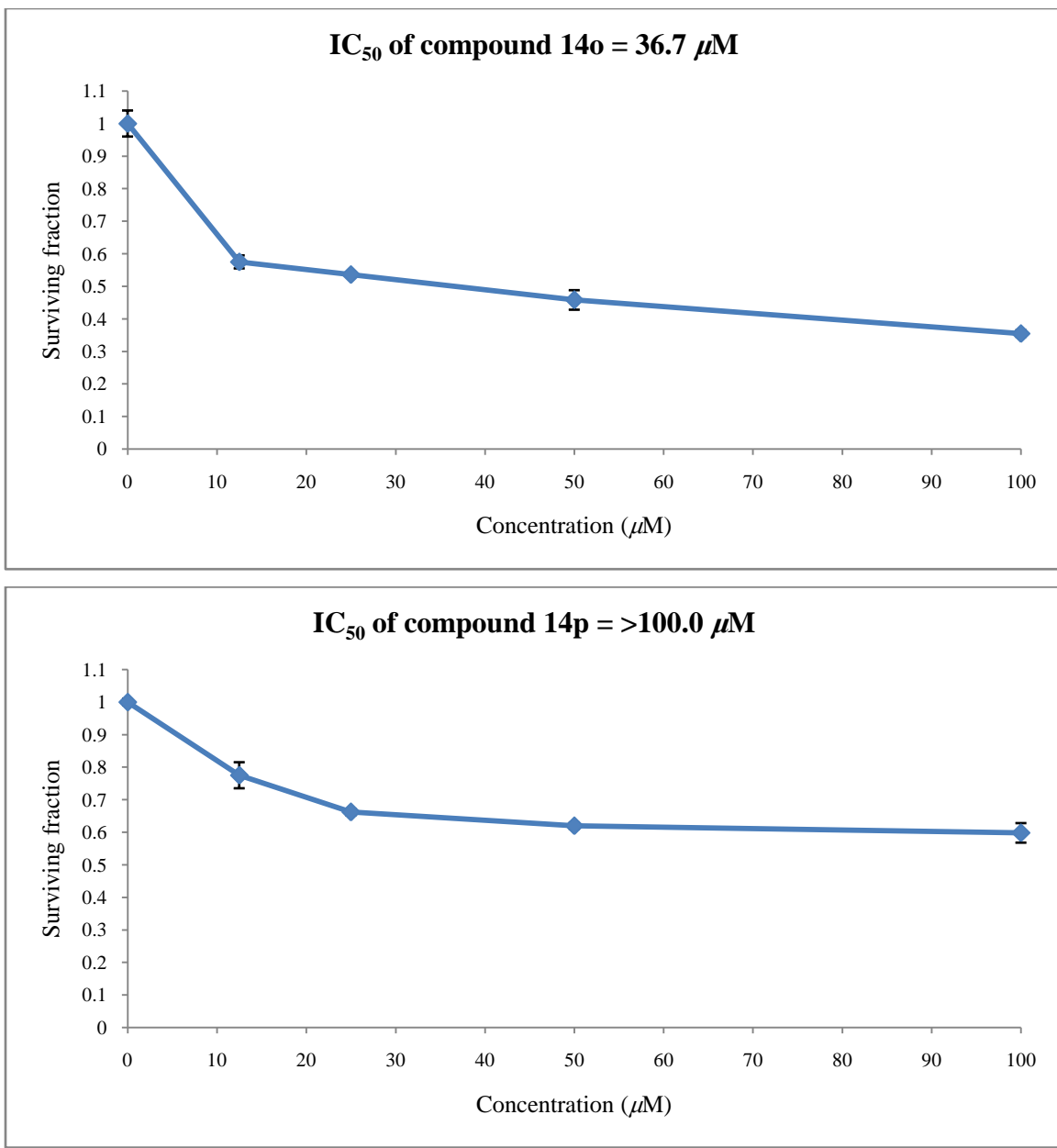
IC₅₀ of compound 14h = 11.9 μ M



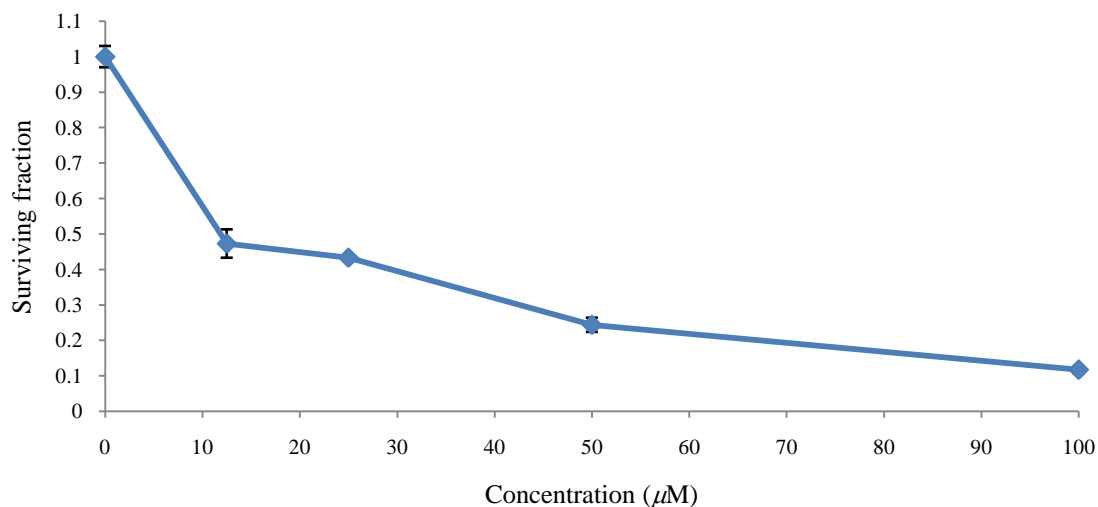




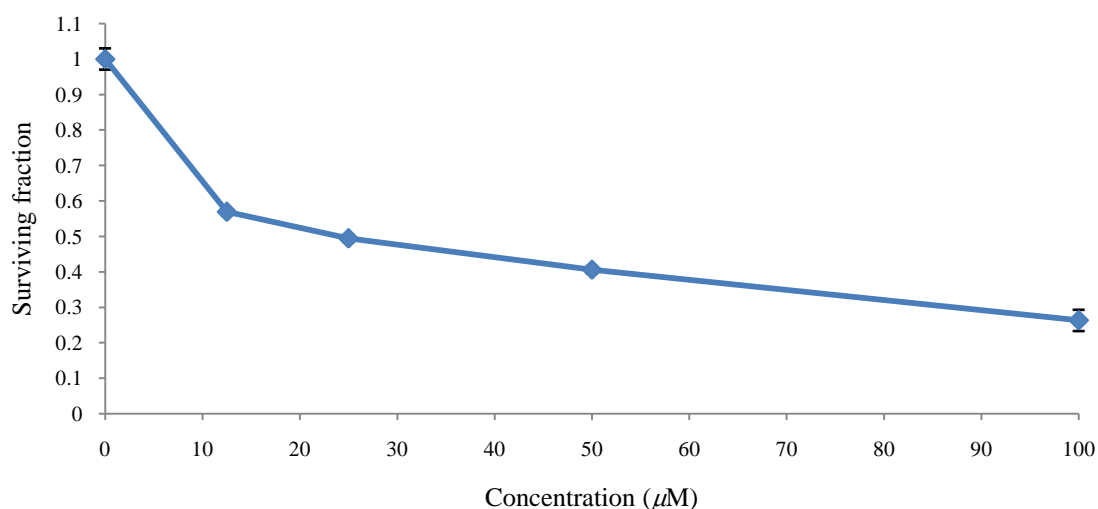


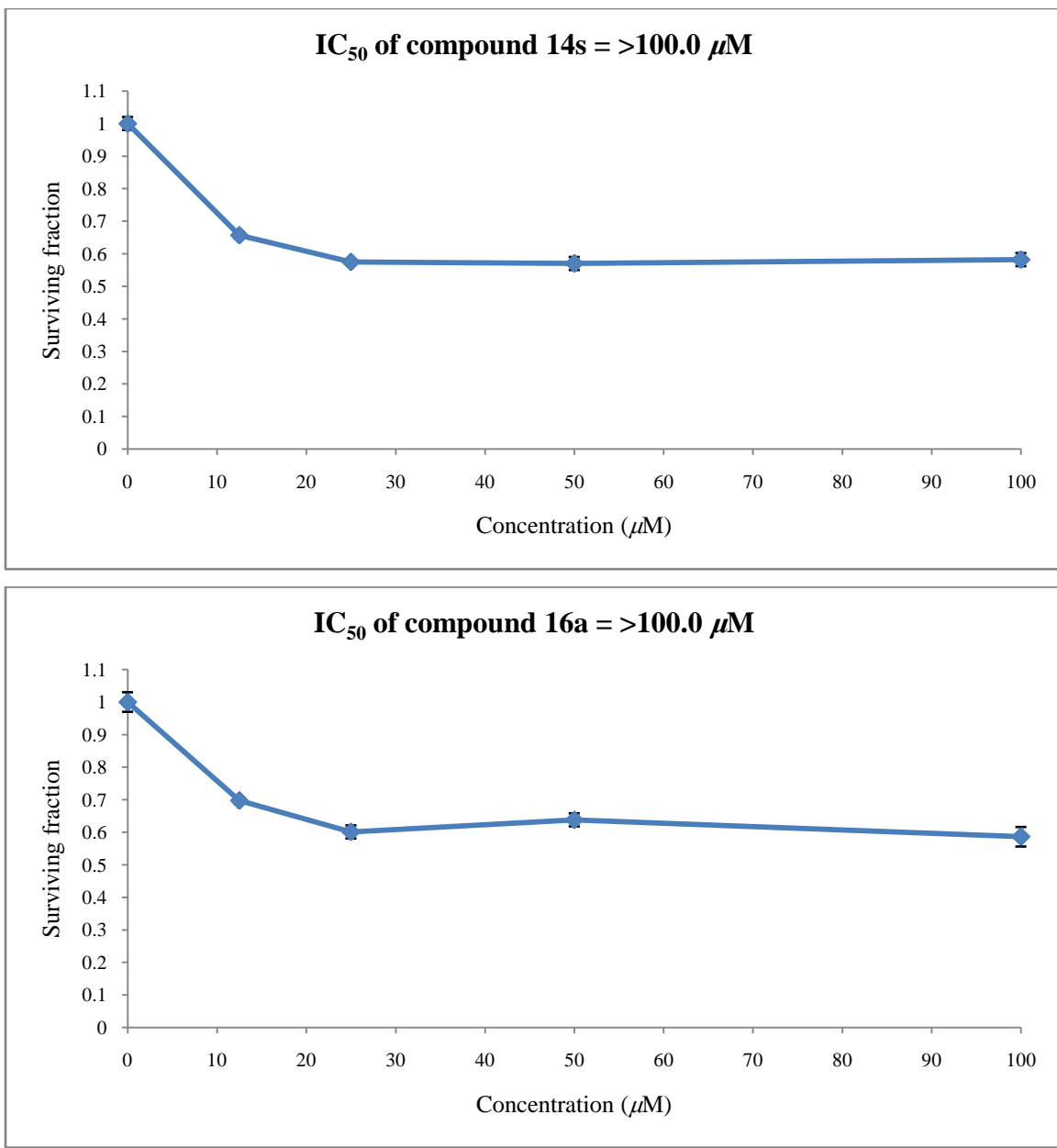


IC₅₀ of compound 14q = 11.9 μ M



IC₅₀ of compound 14r = 24.2 μ M





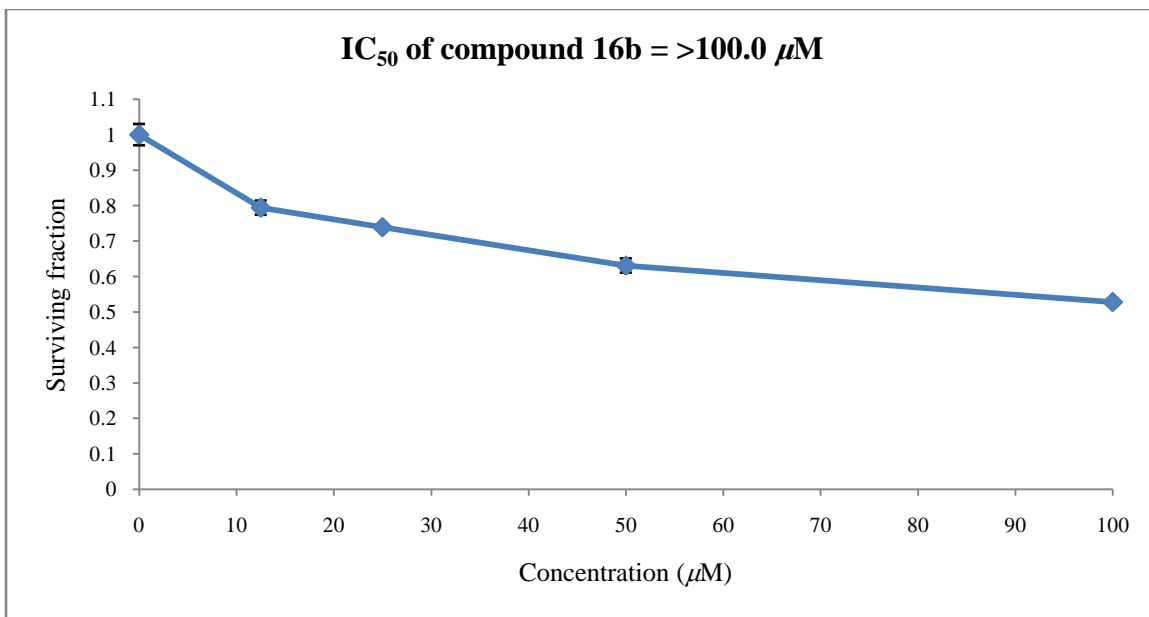
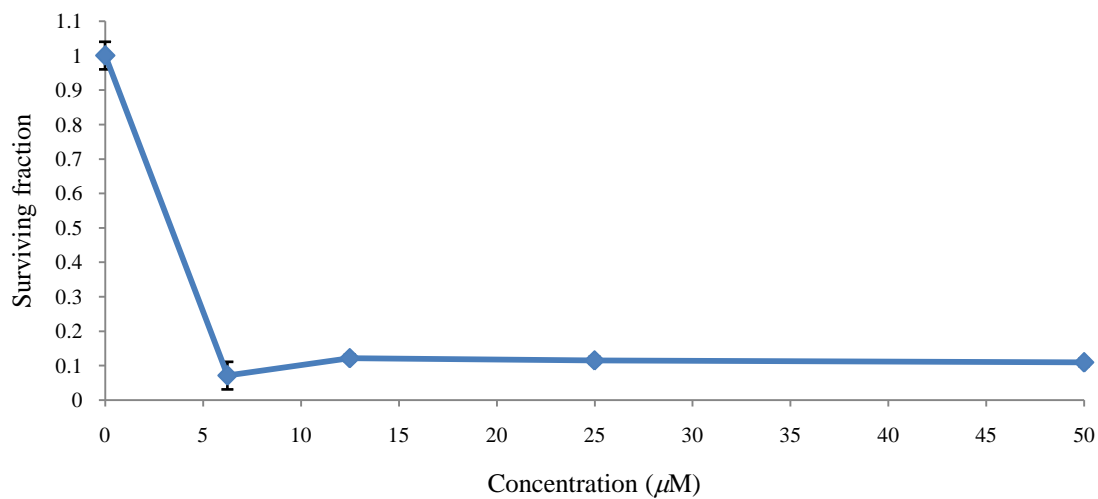
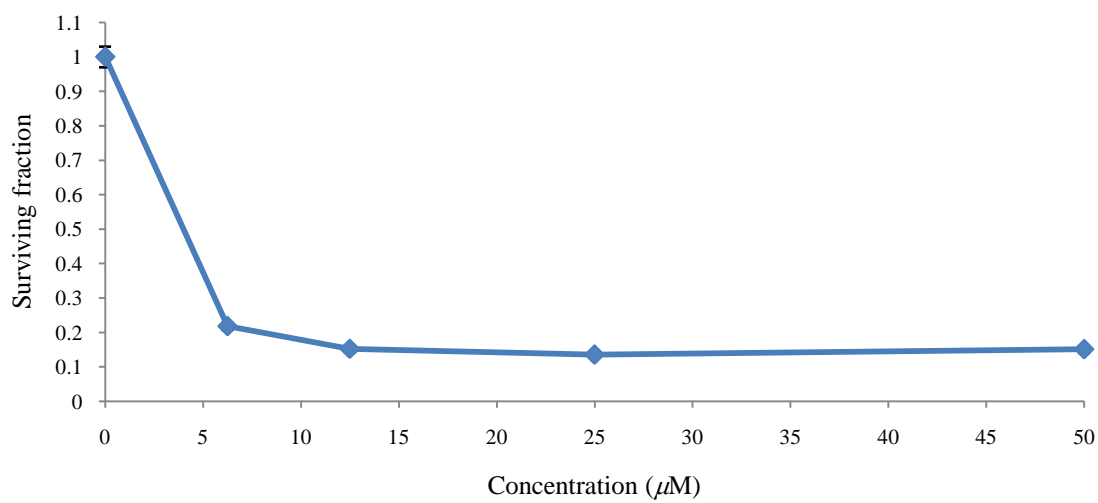


Fig. S73. Dose-response curve of the tropane containing-compounds against HepG2 (liver cancer) cell line.

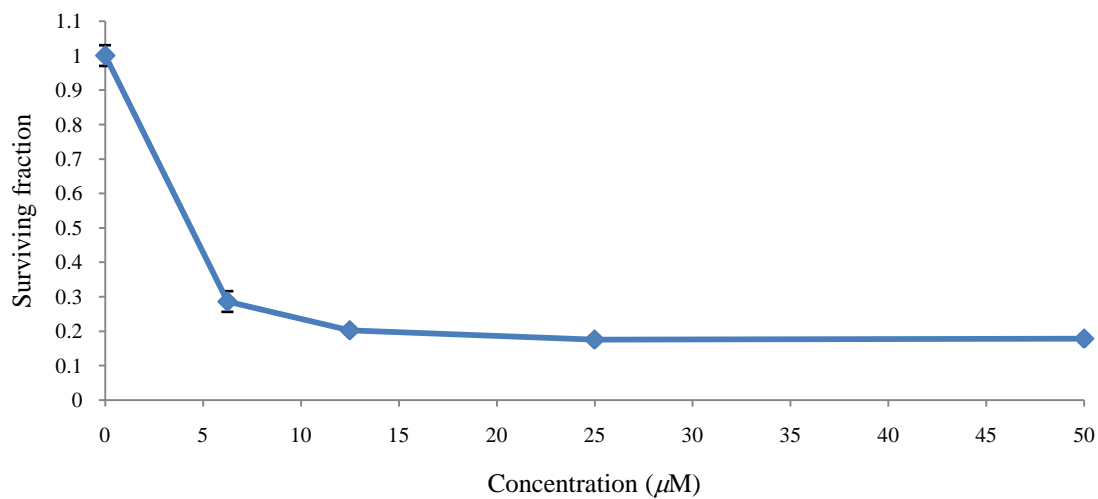
IC₅₀ of compound 12a = 3.4 μ M



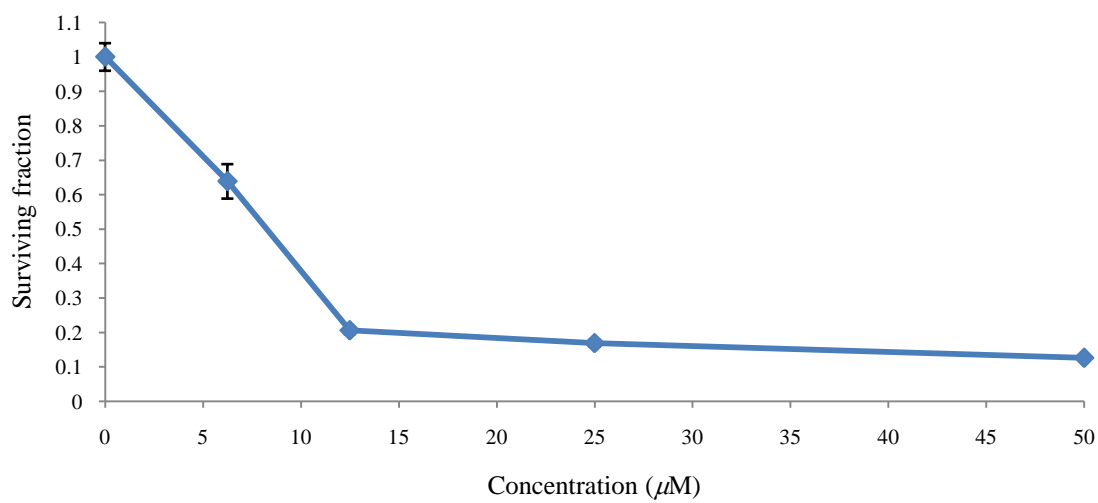
IC₅₀ of compound 12b = 4.0 μ M

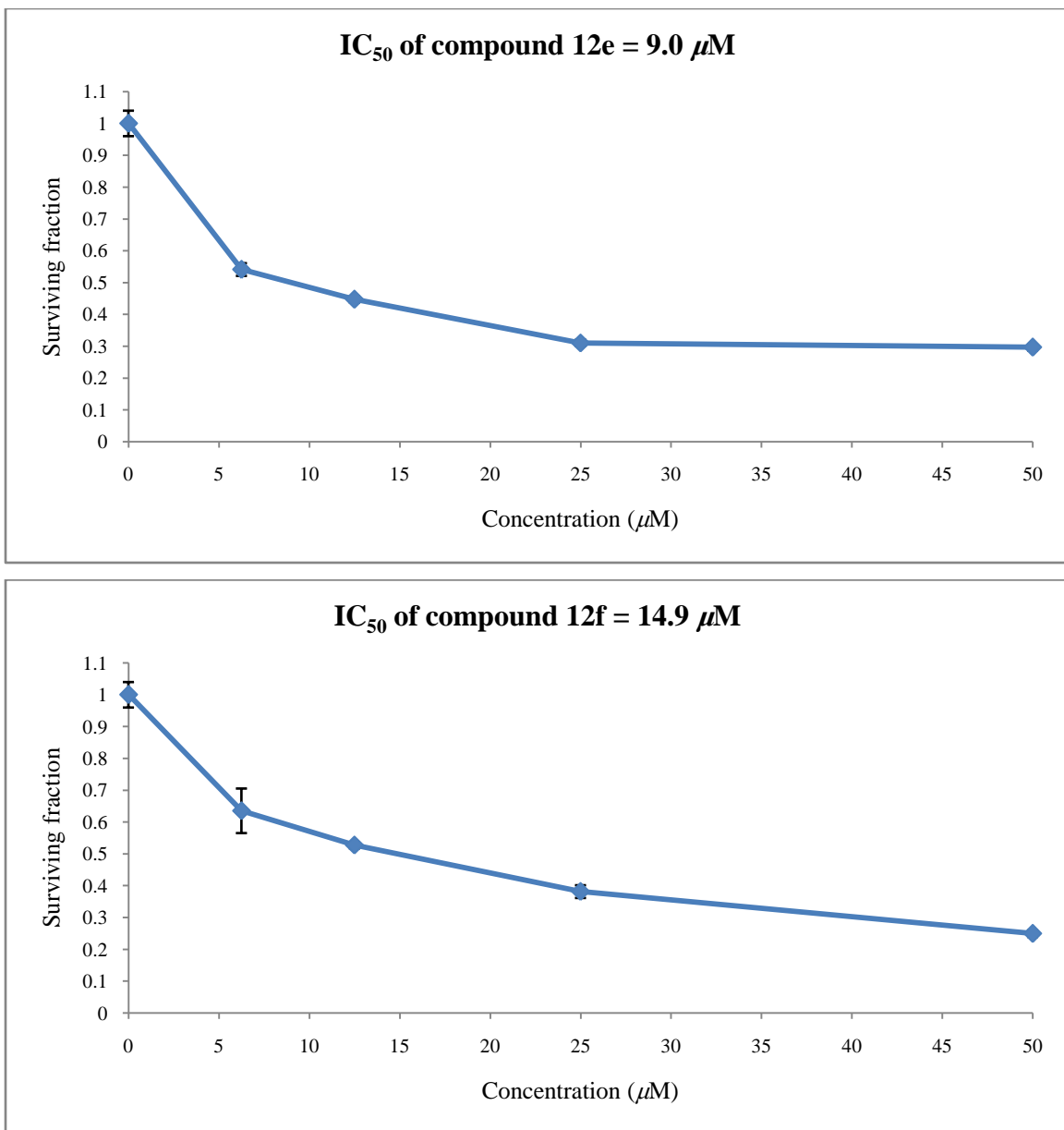


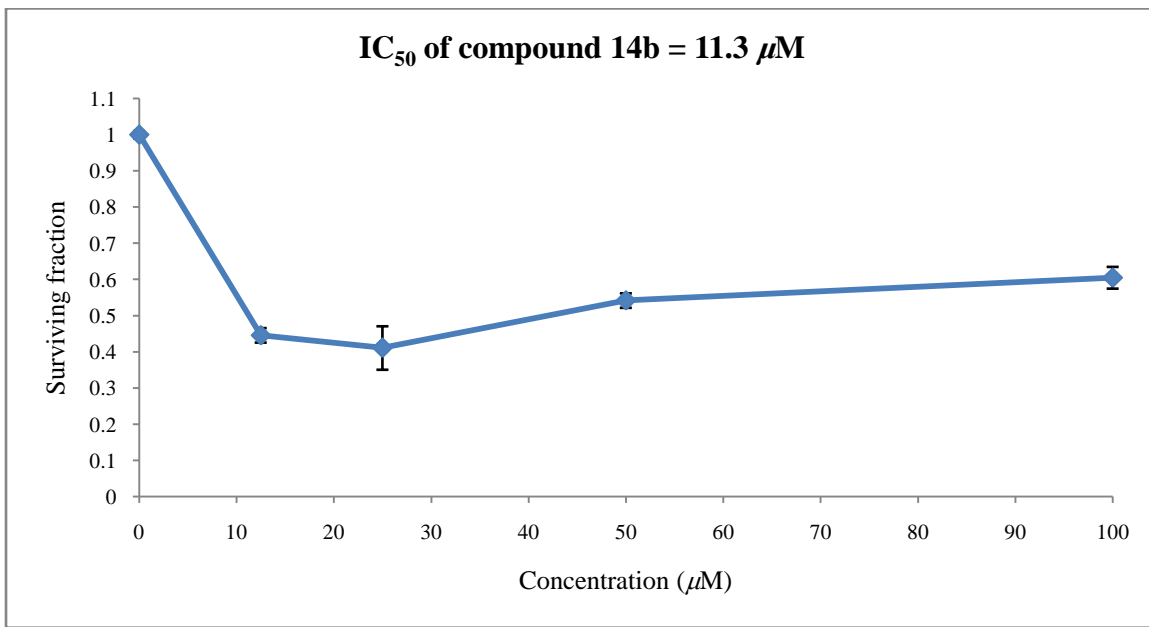
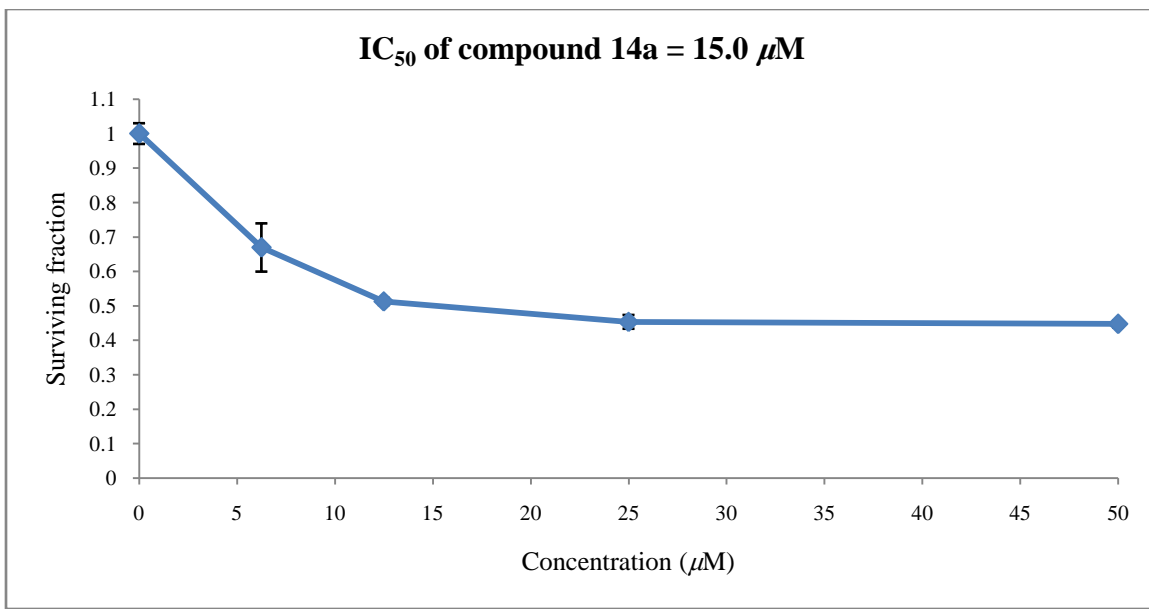
IC₅₀ of compound 12c = 4.4 μ M



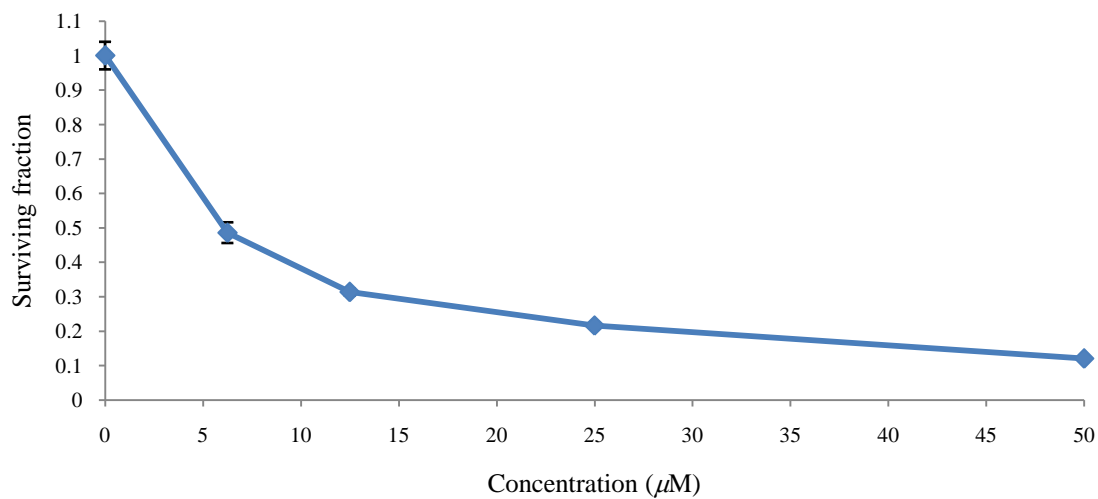
IC₅₀ of compound 12d = 8.3 μ M



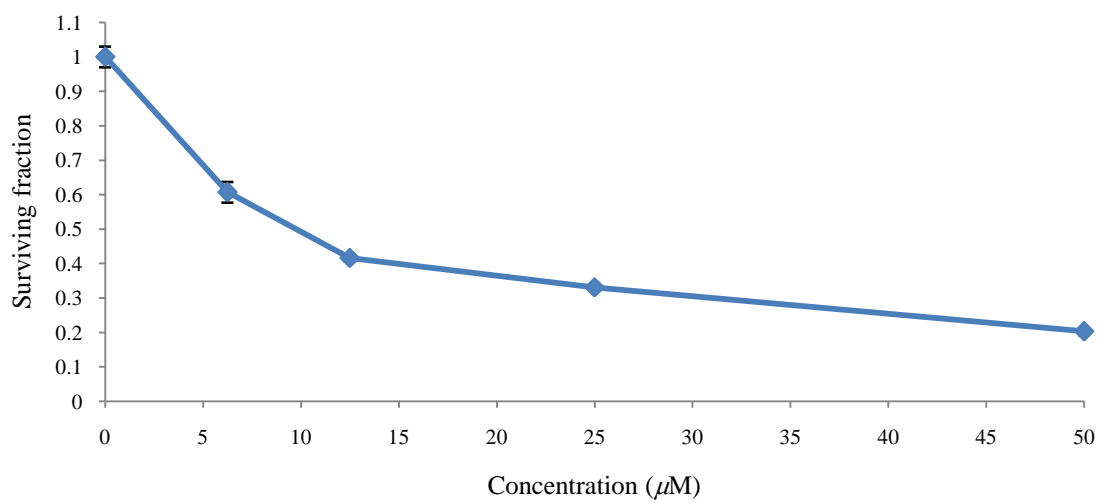


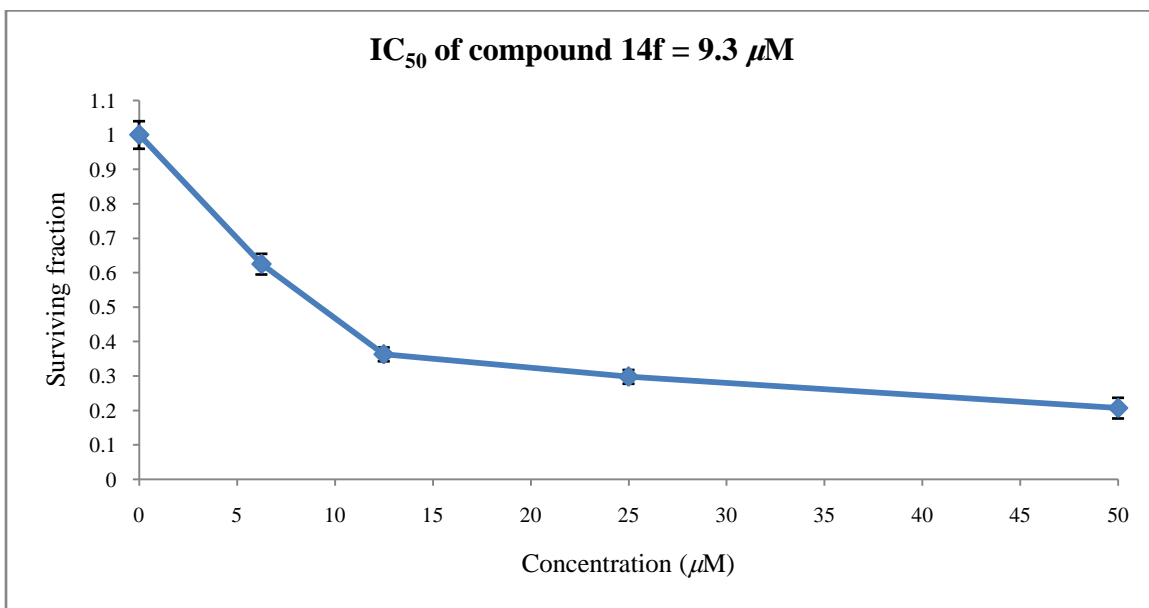
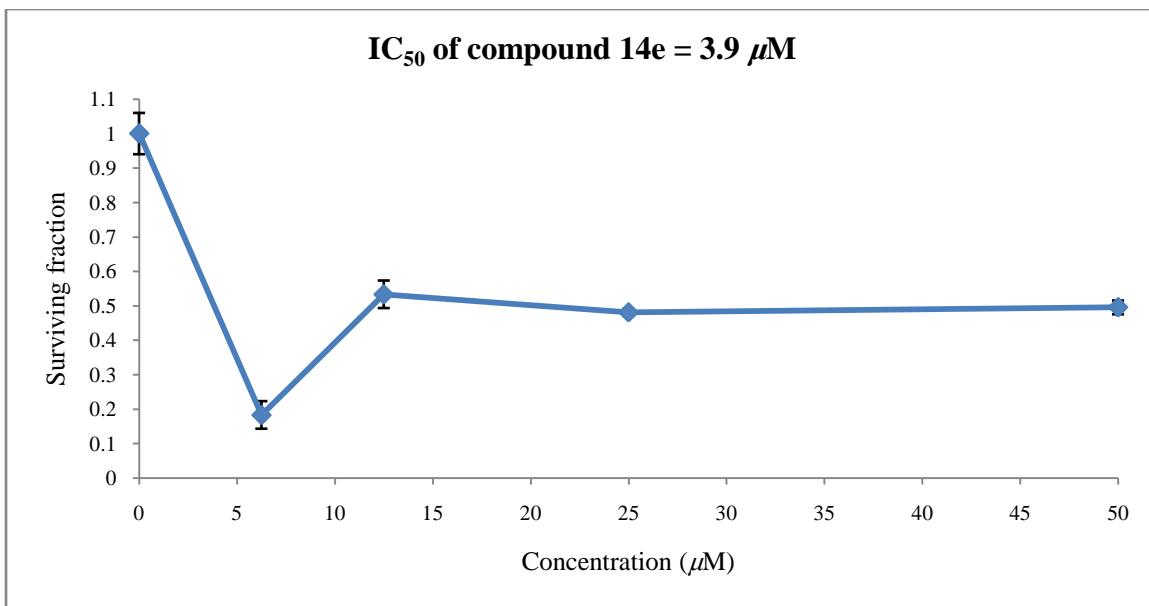


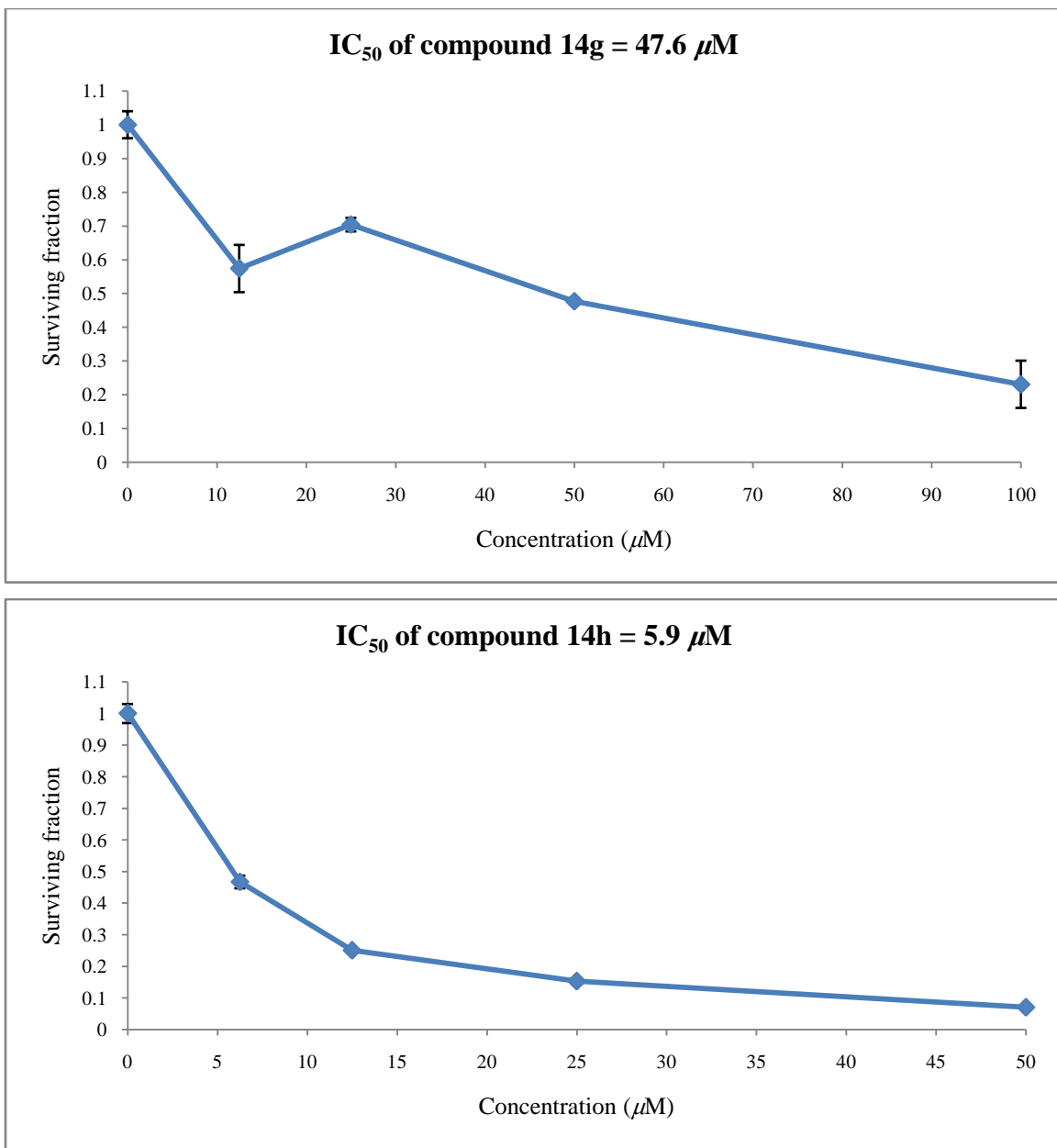
IC₅₀ of compound 14c = 6.1 μ M

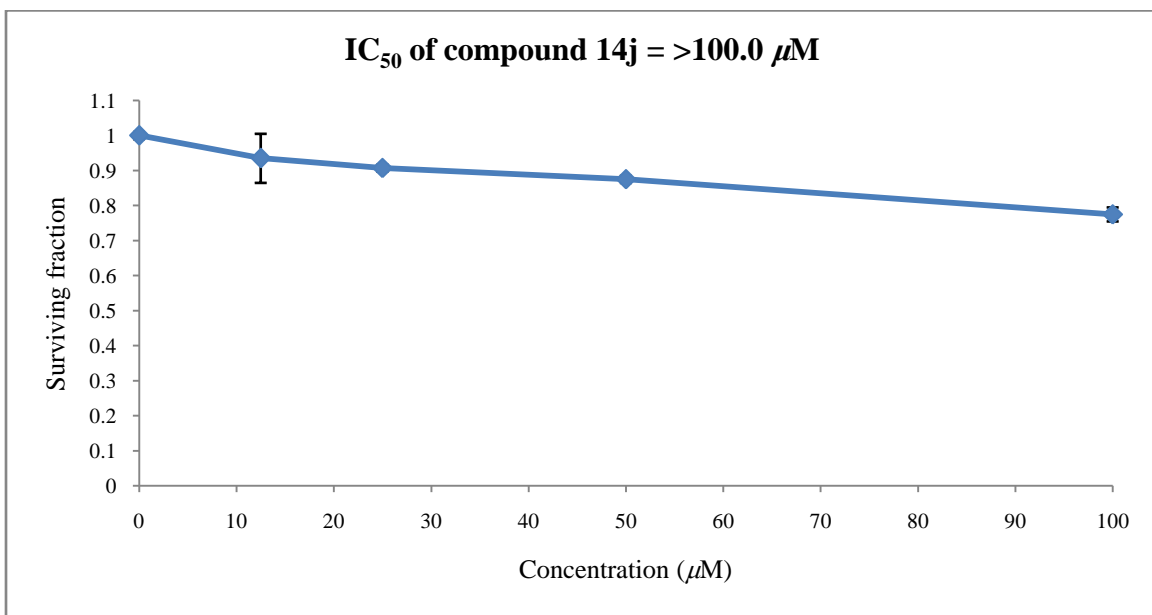
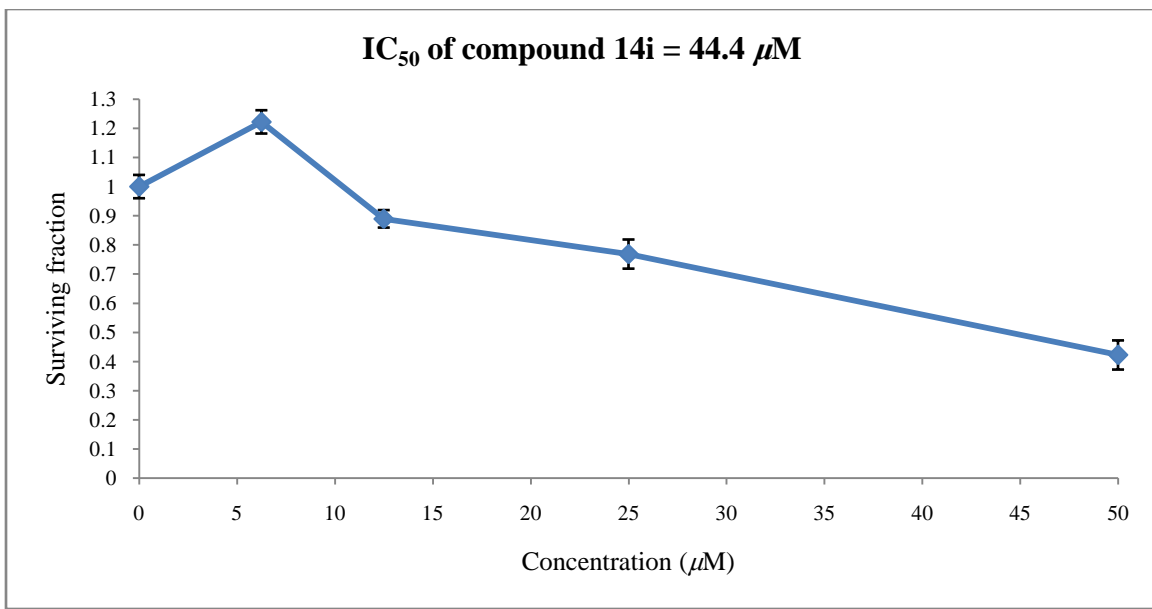


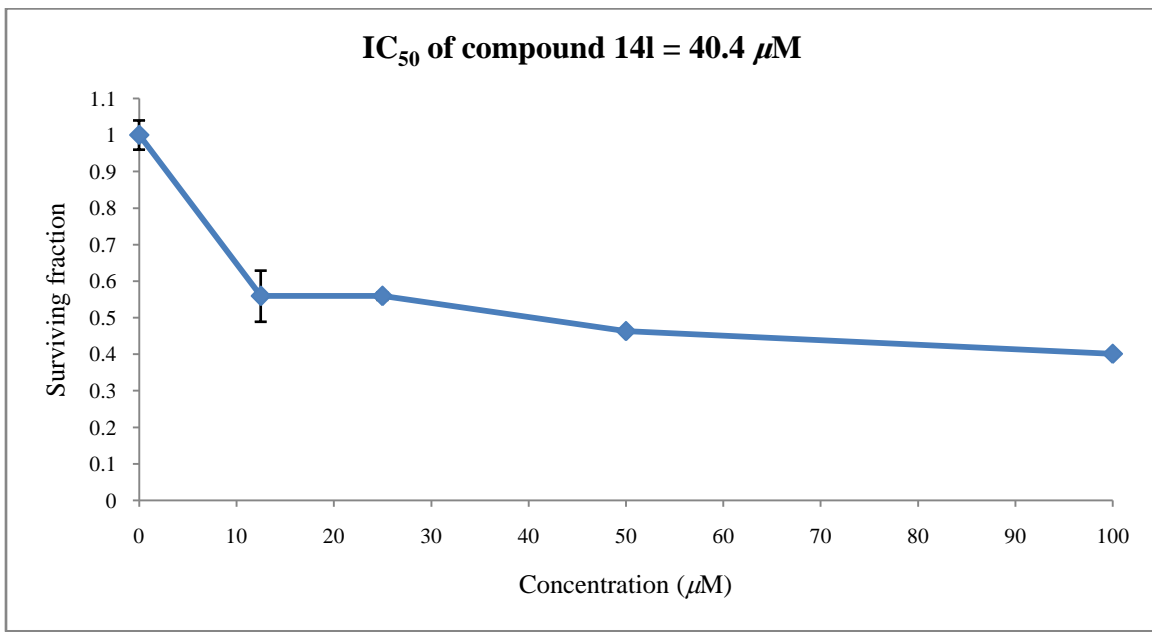
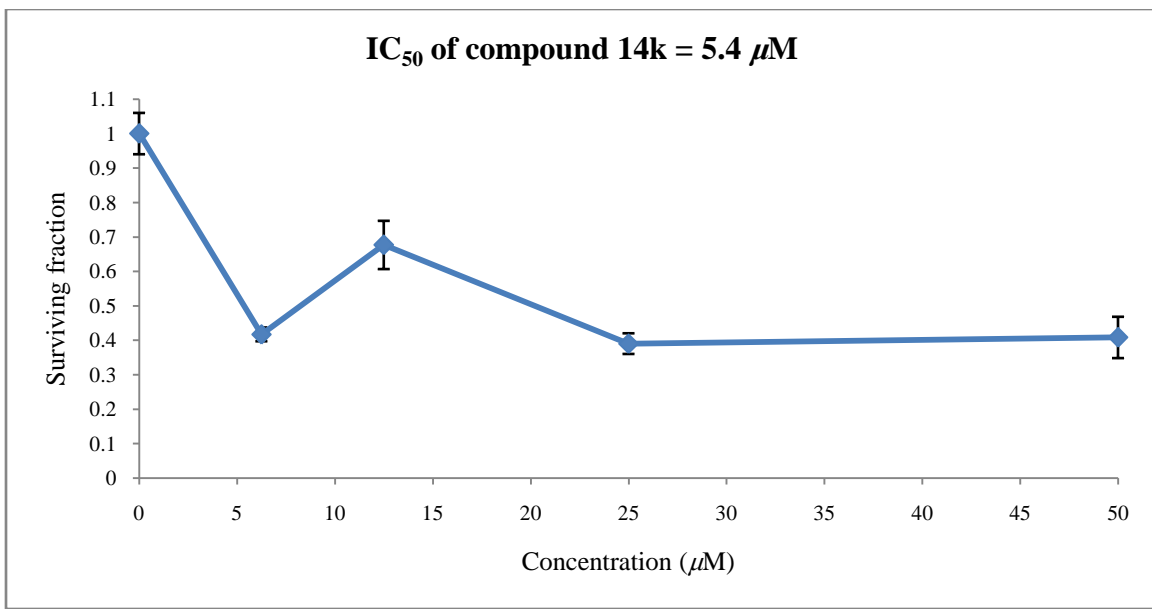
IC₅₀ of compound 16d = 9.9 μ M



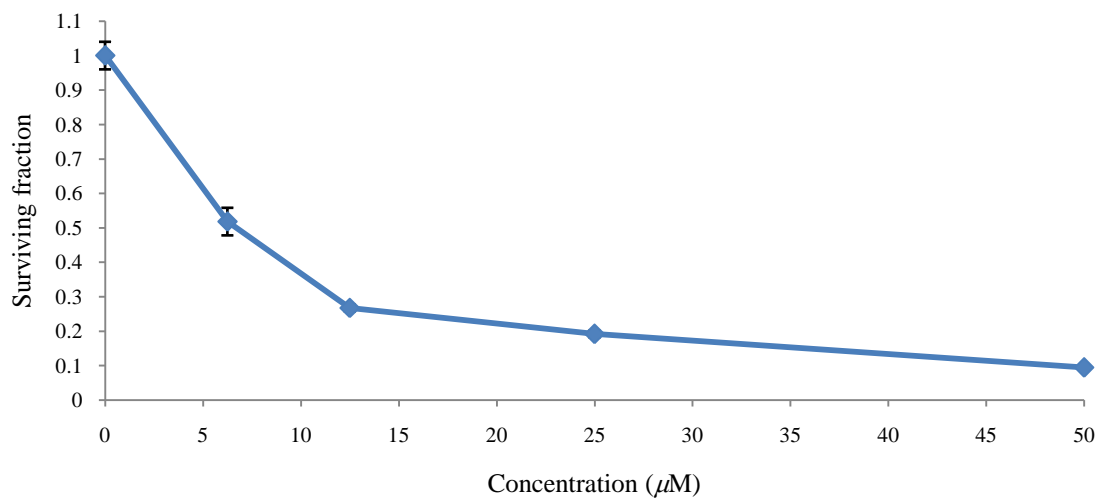




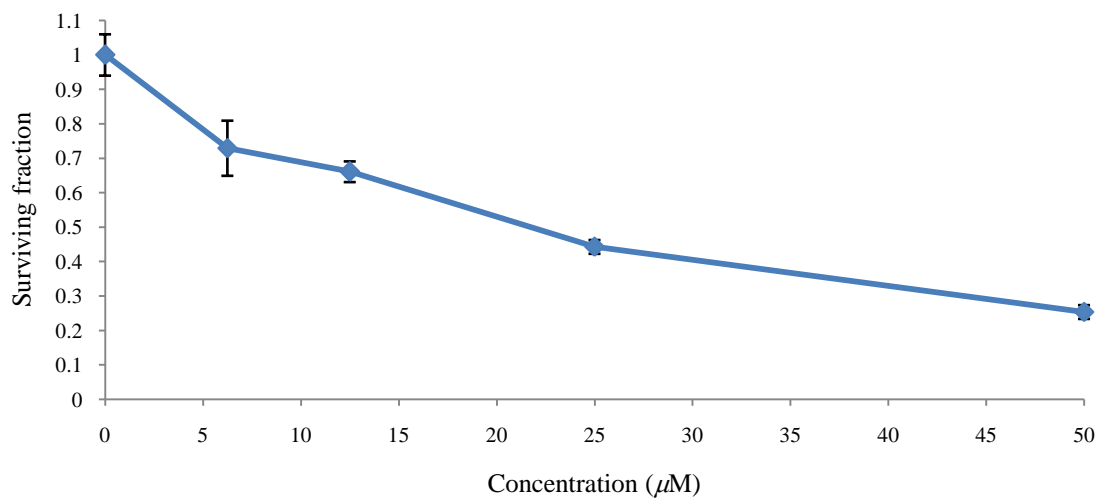


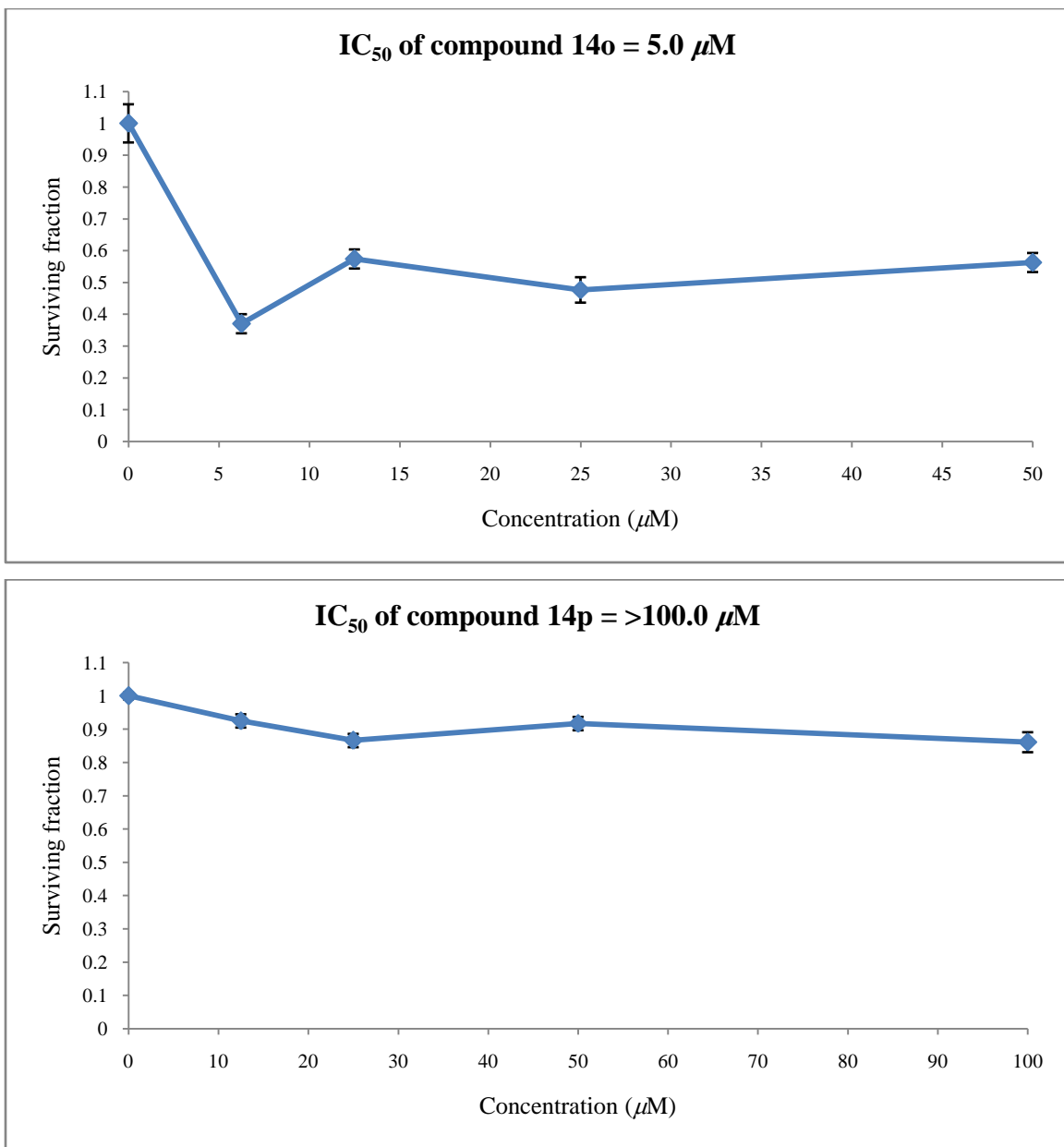


IC₅₀ of compound 14m = 6.8 μ M

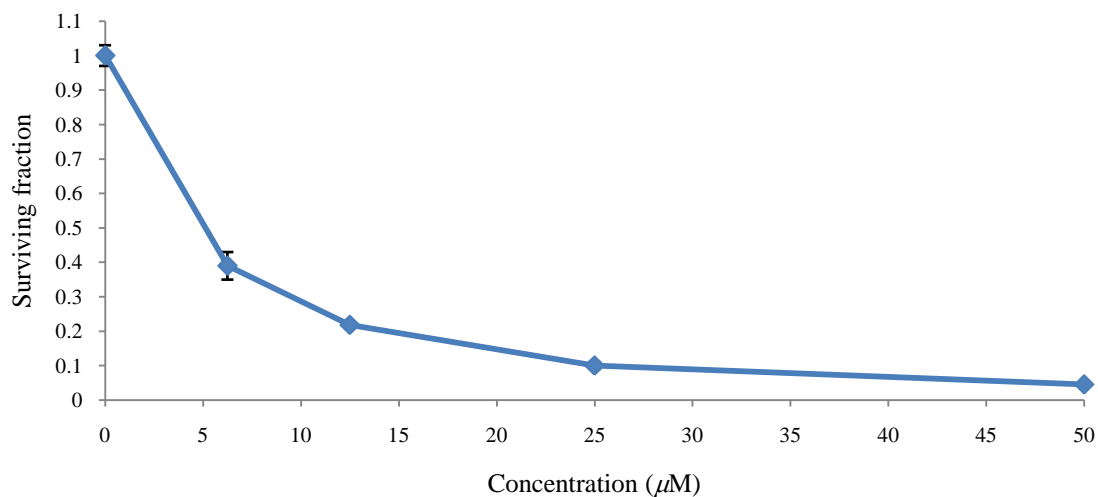


IC₅₀ of compound 14n = 21.8 μ M

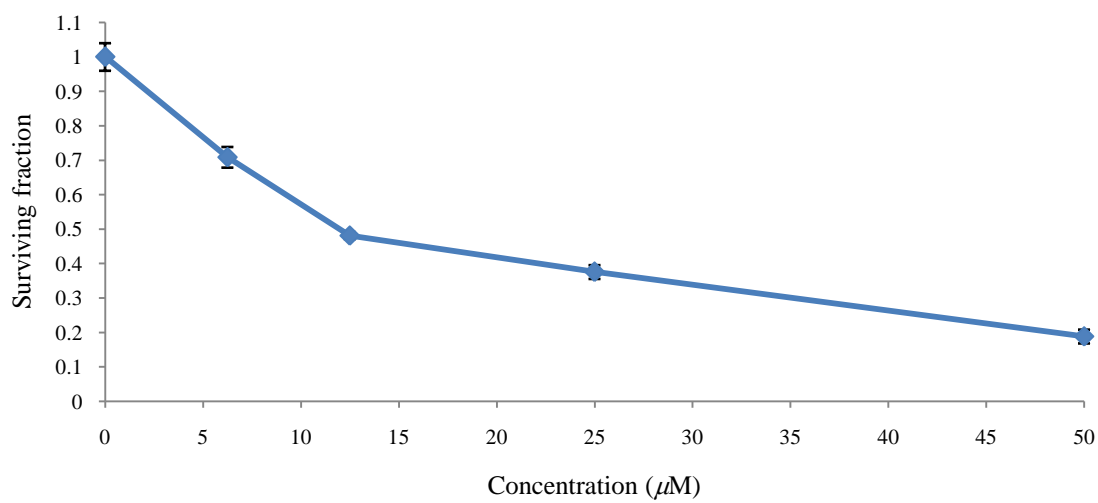


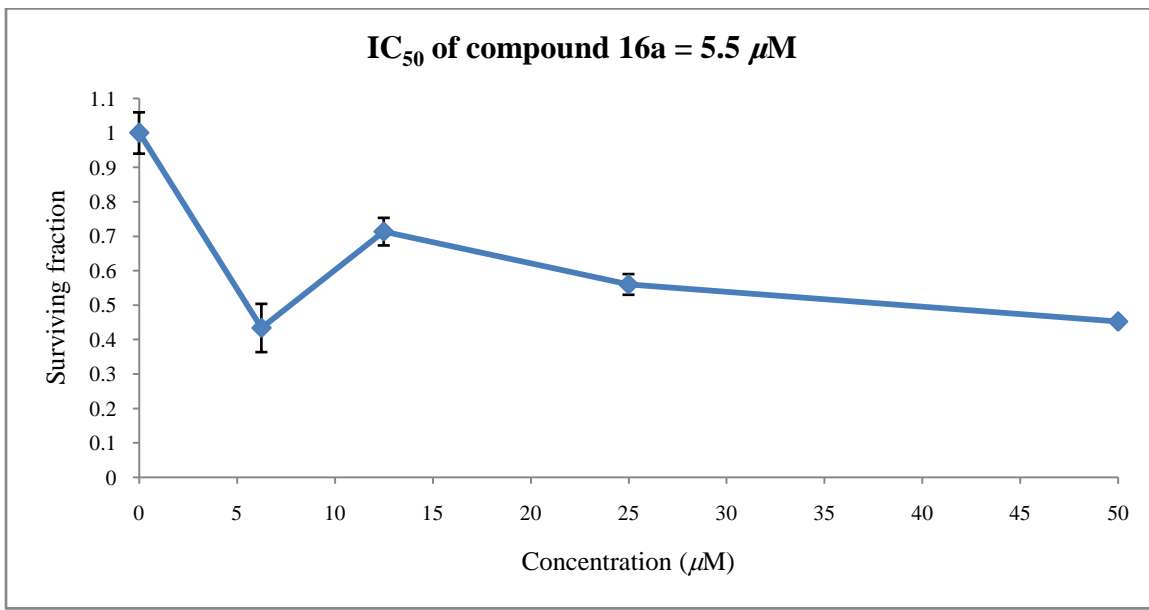
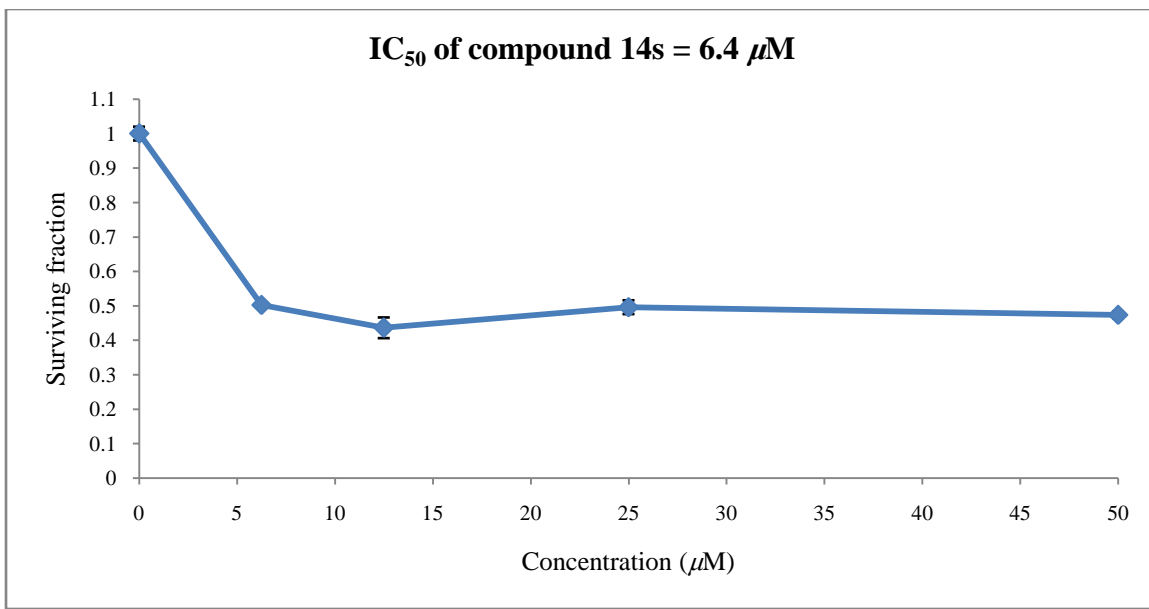


IC₅₀ of compound 14q = 5.1 μ M



IC₅₀ of compound 14r = 12.1 μ M





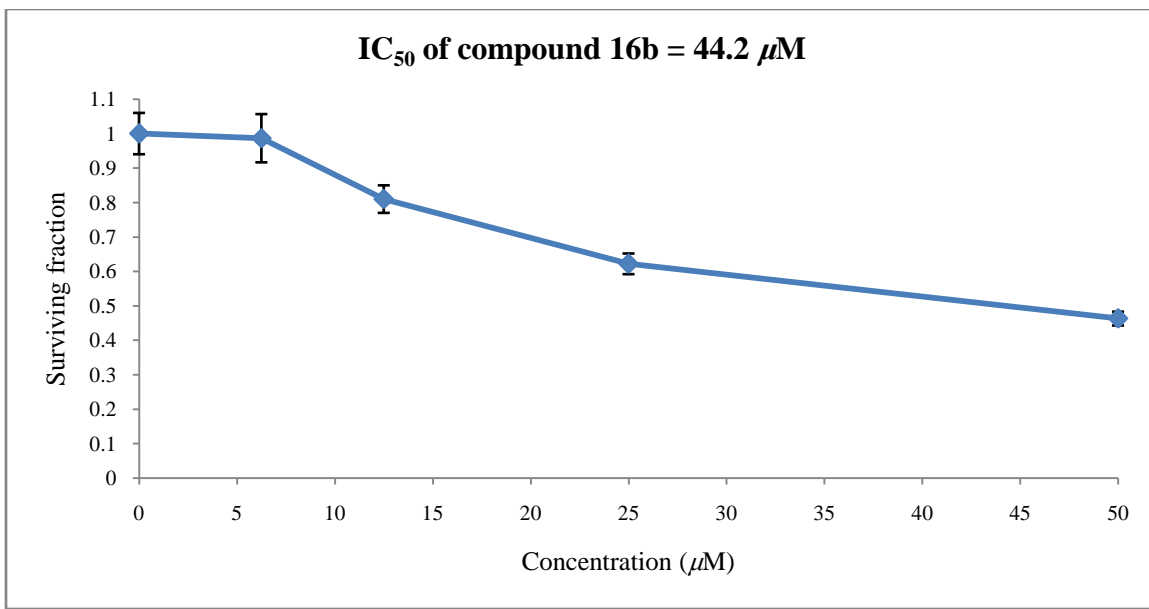


Fig. S74. Dose-response curve of the tropane containing-compounds against MCF7 (breast cancer) cell line.

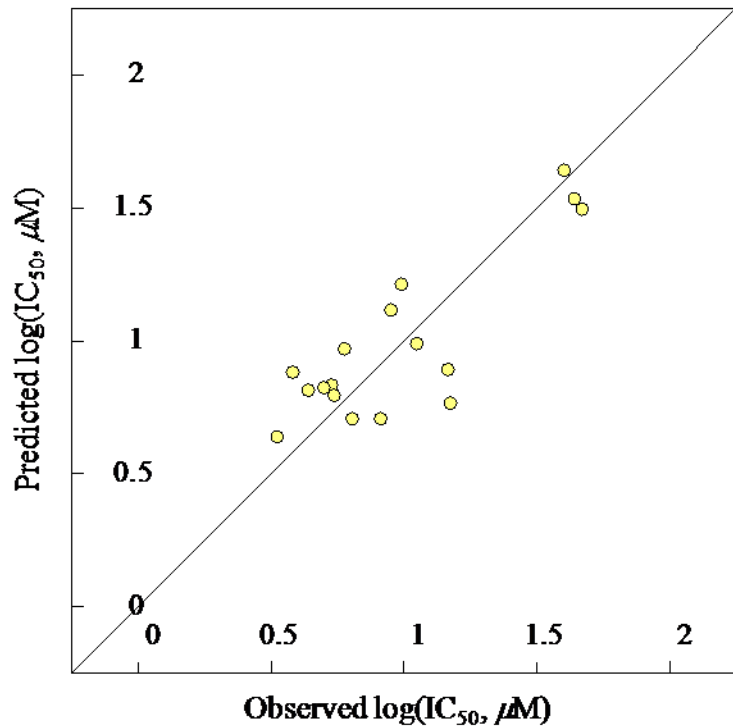


Fig. S75. BMLR-QSAR model plot of correlations representing the observed *versus* predicted $\log(\text{IC}_{50}, \mu\text{M})$ values for the subset group (A+B) against MCF7 (beast) carcinoma cell line.

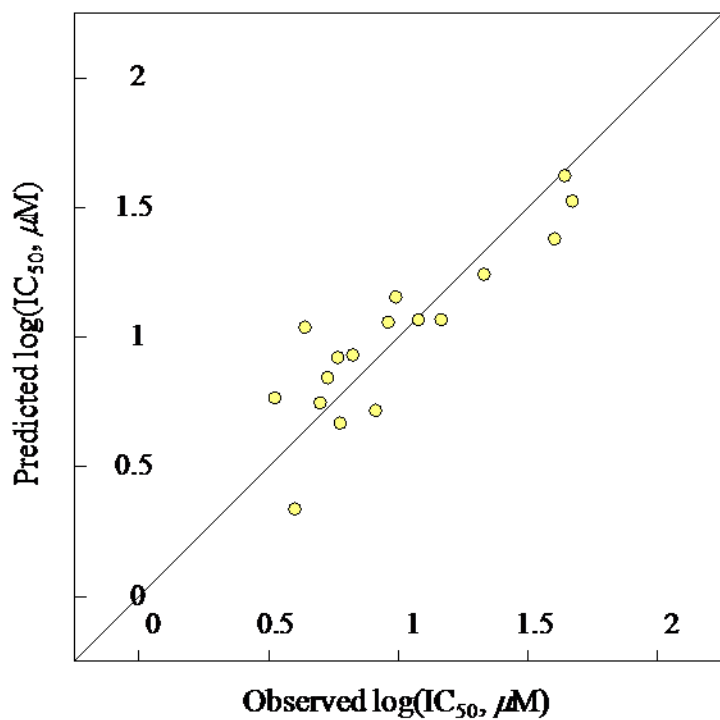


Fig. S76. BMLR-QSAR model plot of correlations representing the observed *versus* predicted log(IC₅₀, μM) values for the subset group (A+C) against MCF7 (beast) carcinoma cell line.

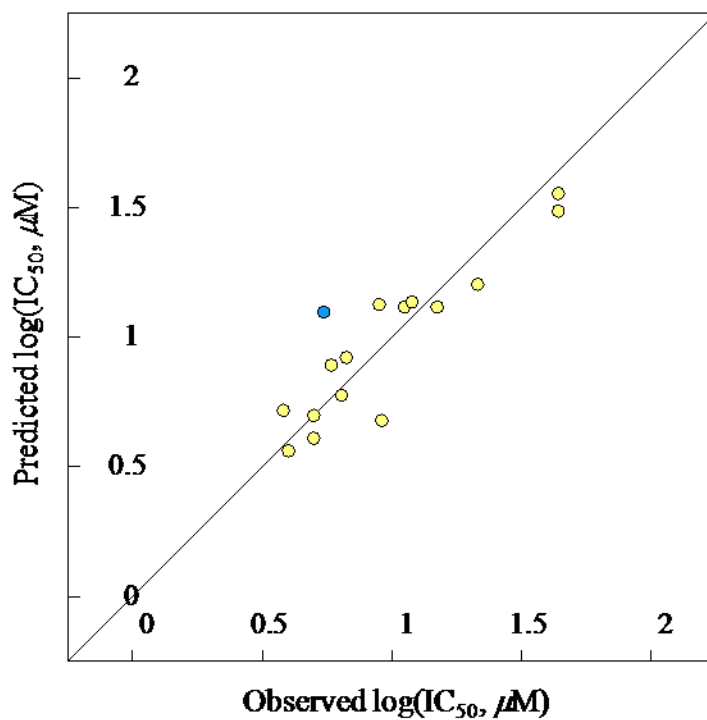


Fig. S77. BMLR-QSAR model plot of correlations representing the observed *versus* predicted $\log(\text{IC}_{50}, \mu\text{M})$ values for the subset group (B+C) against MCF7 (beast) carcinoma cell line (compound **16a** is an outlier).